

**QUANTITATIVE PERFORMANCE AND TRADEOFFS  
IN THE MAP KINASE SIGNALING MODULE**

Thesis by  
Stephen Chapman

In partial fulfillment of the requirements  
For the degree of  
Doctor of Philosophy

CALIFORNIA INSTITUTE OF TECHNOLOGY

Pasadena, California

2009

(Defended January 23, 2009)

© 2009

Stephen Chapman

All rights reserved

## ACKNOWLEDGEMENTS

First and foremost, I would like to acknowledge my advisor, Anand Asthagiri. His most inspirational qualities (in the scientific sense) are his deep curiosity, insightful guidance, and his conscientious scientific analysis. Navigating the everyday life of research, which can be characterized by extended bouts of frustration tied together by brief periods of euphoric success, requires diligence and focus. Anand's tireless patience, steady encouragement, and positive motivation were vital to my development and accomplishments here at Caltech.

To the members of the Asthagiri group, Nicholas Graham, Claudiu Giurumescu, Niki Galownia, Melissa Pope, Keiichiro Kushiro, Jin-Hong Kim, Paul Minor, and Ehsan Jabbarzadeh, I thank you for providing assistance, advice, and a welcoming work environment. I am particularly grateful to Claudiu for readily lending a helping hand with all things math, coding, and computers. And to Nick, thank you for helpful discussions, elder guidance, and weekly tacos from Ernie's.

I would also like to thank my thesis committee, Mark Davis, Christina Smolke, and Paul Sternberg, for their comments and advice. Caltech is a wonderful community in which to pursue science, encouraging seamless collaboration between labs and departments, in large part due to the generosity of the faculty that work here.

I am very grateful for the generosity of Ray Deshaies, who allowed me to pursue experiments in his lab, taking advantage of their expertise in yeast. Many Deshaies lab

members readily shared their time and knowledge to my benefit. I would like to thank Rusty Lipford for getting me started with yeast, Dane Mohl for tirelessly answering my many questions and supplementing my reagent stock, and Nathan Pierce for helpful discussions about my project. I would especially like to thank Geoff Smith and Heenam Park, who in addition to their assistance with experiments, gave me a home in the Deshaies lab by generously sharing their bench space with me.

Finally, I would like to thank my wife, Lizette Loya, for always encouraging me throughout my time at Caltech, and my daughter, Alexandra, for her energy, joy, and curiosity.

**ABSTRACT****QUANTITATIVE PERFORMANCE AND TRADEOFFS IN THE  
MAP KINASE SIGNALING MODULE**

January, 2009

Stephen Chapman, B.S. University of California, Berkeley

M.S., Chemical Engineering, California Institute of Technology

Ph.D., Chemical Engineering, California Institute of Technology

Intracellular signal transduction networks propagate and integrate the information that cells sense from environmental stimuli. The quantitative performance of signaling networks regulates cell decisions, and aberrations in network performance lead to pathologies such as cancer. The mitogen-activated protein (MAP) kinase cascade is a highly-conserved signaling module that regulates diverse cellular processes, such as proliferation, differentiation, and apoptosis in eukaryotic species ranging from yeast to human. While the principal components and mechanisms that define the MAP kinase module are well established, our understanding of and ability to tune its quantitative performance is limited. Here, we probe more deeply how the quantitative properties of the MAP kinase module may be affected by variations in the expression levels of the key constituents of the cascade—kinases, phosphatases and scaffolds.

Using a computational approach, we delineate how four quantitative properties—responsiveness to input, dynamic range of output, signal amplification, and signal

lifetime—depend on the relative abundances of the two core components of the MAPK module, kinases and phosphatases. We identify a reduced metric termed the ‘resistance to activation’ that predicts the quantitative properties of the module across a wide range of parameter values. Its predictive utility extends to dynamic properties such as signal lifetime, which often dictates the MAP kinase’s effect on cell function. Our analysis highlights tradeoffs in design, as not all quantitative attributes of the module can be simultaneously optimized. Thus, the resistance to activation captures the fundamental principles that determine cascade behavior and can be exploited to guide quantitative redesign of the MAP kinase module.

In addition to the expression levels of kinases and phosphatases, scaffolds play a key role in signal propagation through the MAP kinase module. Protein scaffolds bring together multiple components of a signaling pathway, thereby promoting signal flux along a common physical “backbone.” Scaffolds figure prominently in natural signaling pathways and are emerging as a promising platform for synthetic circuits. To better understand how scaffolding quantitatively affects signal transmission, we conducted an *in vivo* experimental sensitivity analysis of MAP kinase response to broad perturbations in the expression level of Ste5, an exemplar scaffold of the yeast mating pathway. Our results demonstrate that the expression level of Ste5 significantly affects several quantitative aspects of signal propagation, including signal throughput, pathway ultrasensitivity, and baseline leakage. These new insights into the quantitative role of scaffolding in MAP kinase signaling suggest advantages and limitations in designing synthetic scaffold-based regulatory networks.

## TABLE OF CONTENTS

|  |           |
|--|-----------|
| Acknowledgements .....   | iii       |
| Abstract.....  | v         |
| Table of Contents .....  | vii       |
| List of Figures .....  | x         |
| List of Tables .....   | xii       |
| <br>   |           |
| <b>CHAPTER I. Introduction .....</b>   | <b>1</b>  |
| 1. The canonical MAP kinase cascade .....  | 1         |
| 2. Quantitative attributes of MAP kinase pathways .....  | 5         |
| 2.1 Ultrasensitivity: The MAP kinase module as a biochemical switch.....   | 5         |
| 2.2 Bistability: Discrete transitions and biochemical ‘memory’ .....   | 8         |
| 2.3 Signal dynamics: Transient versus sustained MAP Kinase responses lead to<br>distinct cellular fates .....  | 9         |
| 2.4 Protein scaffolds quantitatively affect MAP kinase output.....   | 11        |
| 3. Current results: The effect of varying the expression levels of module components<br>on the quantitative performance of the MAP kinase cascade..... | 13        |
| 4. References.....   | 16        |
| <br>   |           |
| <b>CHAPTER II. Resistance to signal activation governs design features of<br/>the MAP Kinase signaling module .....</b>                                | <b>20</b> |
| 1. Abstract.....   | 20        |
| 2. Introduction.....   | 21        |
| 3. Model Development - Schematic and Equations .....   | 26        |
| 4. Results.....  | 30        |
| 4.1 Model construction identifies most tangible design opportunities .....   | 30        |
| 4.2 Sustained input and steady-state features.....   | 30        |
| 4.2-1 Potency .....  | 33        |
| 4.2-2 Range of output .....  | 35        |
| 4.2-3 Signal amplification.....  | 37        |
| 4.2-4 Transient input and module dynamics .....  | 39        |
| 4.3 Resistance to activation.....  | 43        |

|  |           |
|--|-----------|
| 4.4 Relaxation of resistance parameters.....   | 47        |
| 5. Discussion .....  | 53        |
| 6. Appendix.....   | 59        |
| 7. Acknowledgements .....  | 62        |
| 8. References.....   | 63        |
| <br>   |           |
| <b>CHAPTER III. Quantitative effect of scaffold abundance on signal propagation.....</b> | <b>67</b> |
| 1. Abstract.....   | 67        |
| 2. Introduction.....   | 68        |
| 3. Results and Discussion .....  | 71        |
| 3.1 Modulation of scaffold expression level.....   | 71        |
| 3.2 Effect of scaffold on signal throughput and pathway ultrasensitivity .....           | 72        |
| 3.3 Closer examination of the Ste5 module .....  | 75        |
| 3.4 Sensitivity of signal quality to scaffold abundance .....                            | 79        |
| 3.5 Potential implications for natural and synthetic scaffold-based modules.....         | 80        |
| 4. Materials and Methods.....  | 82        |
| 4.1 Strains.....   | 82        |
| 4.2 Plasmid constructs .....   | 82        |
| 4.3 Western blot.....  | 83        |
| 4.3-1 Cell growth and lysis .....  | 83        |
| 4.3-2 SDS-PAGE – quantitative Western blots only .....                                   | 84        |
| 4.3-3 Immuno-blotting.....   | 85        |
| 4.3-4 Analysis – quantitative Western blots only.....                                    | 86        |
| 4.4 Flow cytometry.....  | 86        |
| 4.5 Halo assays for $\alpha$ -factor sensitivity .....                                   | 87        |
| 5. Acknowledgements .....  | 88        |
| 6. Supplementary Data .....  | 89        |
| 6.1 Quantitative Western blot analysis .....   | 89        |
| 6.2 Dose-response properties as a function of Ste5 abundance .....                       | 90        |
| 6.3 Signal fidelity is robust to perturbation in Ste5 expression.....                    | 92        |
| 7. References.....   | 94        |
| <br>   |           |
| <b>CHAPTER IV. Future work.....</b>  | <b>97</b> |
| 1. Experimental sensitivity analysis of scaffold perturbation in the HOG pathway.....    | 97        |

|   |     |
|---|-----|
| 2. The effect of scaffold abundance on signal dynamics in the MAP kinase mating pathway ..... | 99  |
| 3. Extension of resistance metric to a scaffold-based MAP kinase cascade.....                 | 100 |
| 4. Investigation of MAP kinase design properties that result from scaffold dimerization ..... | 101 |
| 4.1 Robustness to perturbation in scaffold abundance .....                                    | 102 |
| 4.2 Dimerization may augment the scaffold's contribution to signal fidelity.....              | 104 |
| 5. References.....  | 108 |

## LIST OF FIGURES

|   |    |
|---|----|
| Figure I-1. MAP kinase model schematic. ....  | 2  |
| Figure I-2. MAP kinase scaffolds direct signal flow.....  | 5  |
| Figure I-3. Hill equation characterizes MAP kinase ultrasensitivity. ....   | 6  |
| Figure I-4. MAP kinase signal duration controls cell behavior. ....   | 10 |
| Figure I-5. MAP kinase signal propagation biphasically depends on scaffold concentration. ....  | 12 |
| Figure II-1. Model schematic.....   | 22 |
| Figure II-2. Temporal profile of module output in response to a step input: the effect of varying the relative amount of phosphatase versus kinase. ....                        | 31 |
| Figure II-3. Module dose-response to changes in the relative amount of phosphatase versus kinase.....   | 32 |
| Figure II-4. Input potency.....   | 34 |
| Figure II-5. Dynamic range of module output. ....   | 36 |
| Figure II-6. Signal amplification versus attenuation.....   | 38 |
| Figure II-7. Temporal profile of module output following instantaneous loss of input....  | 41 |
| Figure II-8. Output decay in semi-log format.....   | 42 |
| Figure II-9. Half-life of Erk signal in response to an exponential decay in input. ....   | 43 |
| Figure II-10. The dependence of half-life of Erk signal on the resistance to activation for wide range of perturbations in $\pi_s$ and $\kappa_s$ .....                         | 45 |
| Figure II-11. The dependence of dynamic range of module output on resistance to activation for wide range of perturbations in $\pi_s$ and $\kappa_s$ .....                      | 46 |
| Figure II-12. The dependence of input potency on resistance to activation for wide range of perturbations in $\pi_s$ and $\kappa_s$ .....                                       | 47 |
| Figure II-13. Dynamic range as a function of single stage resistances. ....   | 51 |
| Figure II-14. Potency as a function of single stage resistances. ....   | 52 |
| Figure II-15. Sensitivity analysis of the ability of module resistance to predict half-life due to changes in $\pi_s$ and $\kappa_s$ for perturbations in $\tau_i$ .....        | 59 |
| Figure II-16. Sensitivity analysis of the ability of module resistance to predict half-life due to changes in $\pi_s$ and $\kappa_s$ for perturbations in $\varepsilon_i$ ..... | 60 |

|  |     |
|--|-----|
| Figure II-17. Sensitivity analysis of the ability of module resistance to predict half-life due to changes in $\pi_s$ and $\kappa_s$ for perturbations in $\alpha_i$ ..... | 61  |
| Figure III-1. The Ste5 scaffold and the pheromone MAP kinase pathway in <i>S. cerevisiae</i> . .....   | 69  |
| Figure III-2. Modulating the expression level of the scaffold Ste5. ....   | 71  |
| Figure III-3. Sensitivity analysis of mating pathway response to perturbation in scaffold abundance.....   | 73  |
| Figure III-4. Perturbation of scaffold abundance quantitatively alters phenotypic response.....  | 75  |
| Figure III-5. Phospho-MAPK response to perturbation in Ste5 expression.....  | 76  |
| Figure III-6. Quantitative measurements of phospho-MAP kinase and pFUS1-GFP responses. ....  | 76  |
| Figure III-7. Scaffold-limited and Ste7-limited regimes of signaling.....  | 78  |
| Figure III-8. Quantitative Western blot of Ste5myc abundance. ....   | 89  |
| Figure III-9. Dose-response curves of pFUS1-GFP as a function of Ste5 abundance.....   | 91  |
| Figure III-10. Signal fidelity is robust to perturbations in Ste5 abundance.....   | 93  |
| Figure IV-1. Scaffold dimerization permits signal activation for incompletely bound complexes via <i>trans</i> -phosphorylation. ....                                      | 103 |
| Figure IV-2. A shared signaling intermediate can facilitate signal leakage. ....   | 105 |
| Figure IV-3. Model schematic of scaffold dimerization with signal crosstalk.....   | 106 |

**LIST OF TABLES**

|   |    |
|---|----|
| Table II-1. Five classes of dimensionless parameters specify module attributes..... | 29 |
| Table III-1. Yeast strains used in this study.....                                  | 82 |
| Table III-2. Plasmids used in this study.....                                       | 83 |
| Table III-3. Quantitative characteristics of dose-response profiles.....            | 90 |

## CHAPTER I. INTRODUCTION

Intracellular signal transduction networks propagate and integrate the information that cells sense from environmental stimuli (Asthagiri and Lauffenburger, 2000). The quantitative performance of signaling networks regulates cell decisions in complex microenvironments, and aberrations in network performance lead to pathologies, such as cancer (Hanahan and Weinberg, 2000). It has been proposed that signaling networks are composed of modular sub-networks and that a quantitative understanding of these modular building blocks would provide deeper insights into cellular decision-making (Asthagiri and Lauffenburger, 2000; Hartwell et al., 1999). One such prominent signaling module is the Mitogen-Activated Protein (MAP) kinase cascade. This signaling cascade controls diverse cellular processes, such as proliferation, differentiation, and apoptosis in eukaryotic species ranging from *S. pombe* to *H. sapiens* (Lewis et al., 1998). While the principal molecular components and mechanisms that define the MAP kinase module are well established, how these components and mechanisms work together to determine the quantitative performance of the module remains an area of intense research. A better understanding of this relationship between individual module components and the integrated behavior of the module would provide design strategies for re-engineering module performance by targeting critical components within the module.

### ***1. The canonical MAP kinase cascade***

The canonical MAP kinase cascade consists of three serially activating kinases: the MAPK kinase kinase (MAPKKK) phosphorylates and activates MAPK kinase

(MAPKK), which in turn phosphorylates and activates MAPK (Figure I-1). This structure is a widely recurring motif in intracellular signaling pathways across a range of species and has, therefore, garnered the label of a “signaling module.”

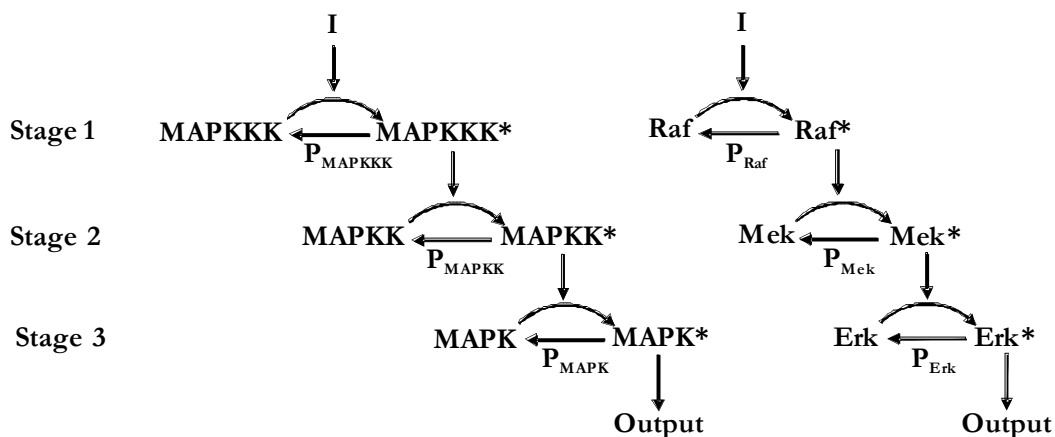


**Figure I-1. MAP kinase model schematic.**

The canonical MAP kinase cascade is depicted above as three serially-activated kinases ( $K_s$ ), balanced at each stage of the cascade by a deactivating phosphatase ( $P_s$ ). On the right, the Erk subfamily is shown.

In mammalian cells, MAP kinase cascades are categorized into one of three subfamilies: Erk, JNK, and p38. The best-characterized subfamily is the Erk module (Figure I-1), which contains the kinases Raf (MAPKKK), Mek (MAPKK), and Erk (MAPK). Commonly stimulated by growth factors, the output of the Erk module, active Erk, proceeds to activate transcription factors and other proteins ultimately influencing important cellular processes such as proliferation and differentiation (Lewis et al., 1998; Pearson et al., 2001; Widmann et al., 1999).

MAP kinase modules play a key role in many non-mammalian eukaryotic species as well. In *Saccharomyces cerevisiae*, multiple MAP kinase modules regulate diverse responses such as mating, invasive growth, and the high-osmolarity glycerol (HOG) stress response (Gustin et al., 1998). Consistent with the conserved architecture, the yeast mating pathway consists of three serially-activating kinases: Ste11 (MAPKKK), Ste7 (MAPKK), and Fus3 (MAPK). Pheromone-mediated stimulation of this pathway culminates in Fus3 activation, which precipitates cell cycle arrest and morphological changes associated with mating (Gustin et al., 1998; Widmann et al., 1999).

The activation and deactivation of MAP kinases is driven by the opposing actions of upstream kinases and protein phosphatases, respectively. Generally, signaling pathways require the constitutive action of protein phosphatases in order to dampen kinase activity when stimulus is absent or has been removed, restoring kinases to their inactive state (Keyse, 2000). Protein phosphatases also contribute to the quantitative performance of MAP kinase modules. By altering their expression level, protein phosphatases modulate MAP kinase signal properties, ultimately influencing cell behavior (Bhalla et al., 2002; Keyse, 2000).

In addition to the core kinases and phosphatases, protein scaffolds play a prominent role in MAP kinase signal propagation. By definition, scaffold proteins bind multiple members of the MAP kinase module, bringing together various kinases onto a single, physical backbone. Protein scaffolds have been associated with virtually all MAP kinase cascades ranging from yeast to humans (Dard and Peter, 2006). Despite their

widespread prevalence (and in contrast to the kinases of the MAP kinase cascade), MAP kinase scaffolds share little structural homology between orthologous pathways, leaving only functional similarities to define and guide our understanding of signaling scaffolds.

The role that scaffolds play in signal transduction is a current area of intense research. Scaffolding proteins confer signal specificity by assembling the appropriate group of upstream activators in order to selectively direct activation of a target MAP kinase. For example, the yeast scaffold Ste5 recruits Ste11 (MAPKKK), Ste7 (MAPKK) and Fus3 (MAPK) (Bardwell, 2006). Meanwhile, another yeast scaffold, Pbs2, recruits Ste11 and Hog1 (MAPK); Pbs2 itself possesses the MAPKK functionality. Thus, Ste5 provides a route for Ste11  $\rightarrow$  Fus3 signal transfer, while Pbs2 provides an alternative route: Ste11  $\rightarrow$  Hog1 (Figure I-2). By providing specific routes to activate Fus3 and Hog1, the scaffolds encode the appropriate cellular response, mating or osmolarity response, respectively. Moreover, the stimulus-response identity can be reassigned by simple concatenation of scaffold binding domains (Park et al., 2003), highlighting the potential for re-directing signal flow through molecular engineering of scaffolds.

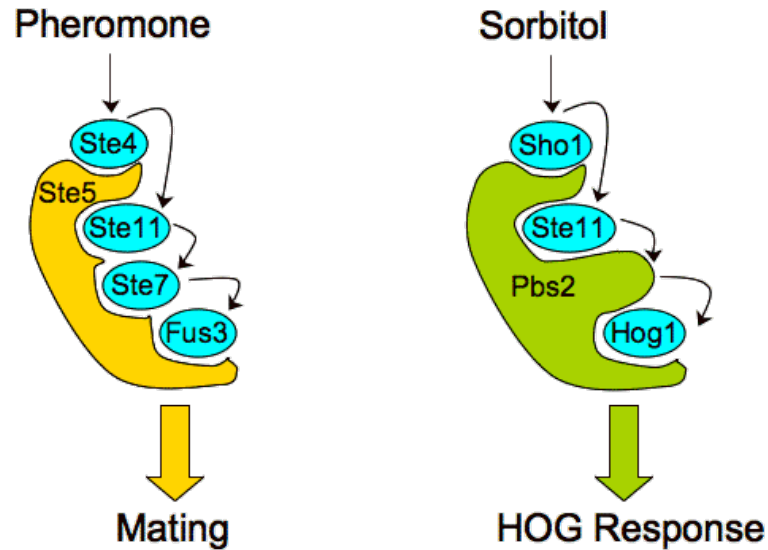


**Figure I-2. MAP kinase scaffolds direct signal flow.**

## ***2. Quantitative attributes of MAP kinase pathways***

### ***2.1 Ultrasensitivity: The MAP kinase module as a biochemical switch***

The conserved architecture of the MAP kinase cascade has raised questions regarding what signaling attributes such a structure might confer. One phenomenon that has been investigated extensively is the role of cascade structure in generating a steep steady-state stimulus/response curve, a property termed ultrasensitivity (Figure I-3). As originally defined, ultrasensitive responses are those that achieve a steeper output response with respect to stimulus than a hyperbolic reference curve, described by the Michaelis-Menten equation (Goldbeter and Koshland, 1981). Typically, the Hill

coefficient ( $n_H$ )<sup>1</sup> is used to quantify the sharpness of the curve, and has been generalized to describe the degree of the ultrasensitive response (Huang and Ferrell, 1996).

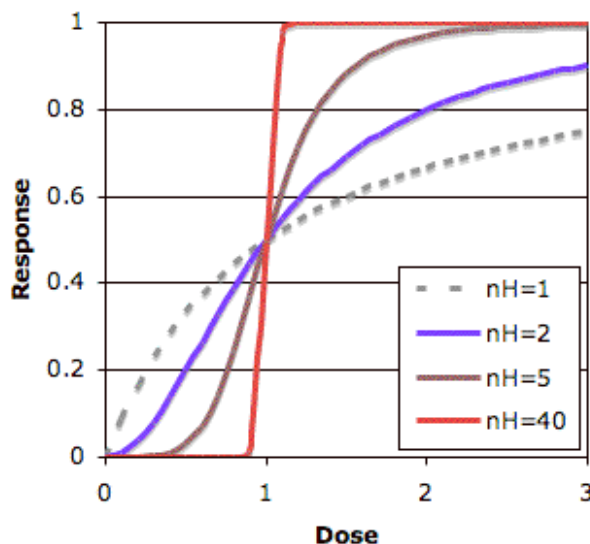


**Figure I-3. Hill equation characterizes MAP kinase ultrasensitivity.**

As the Hill coefficient increases, the dose-response curve becomes more switch-like. The non-sigmoidal Michaelis-Menten curve ( $n_H=1$ ) serves as a reference for comparison.

In Huang and Ferrell's model of the MAP kinase cascade, a particular form of multi-step activation that results in an ultrasensitive response is identified. In the model, the activation of MAPKK and MAPK by MAPKKK and MAPKK, respectively, proceeds through a distributive, two-collision mechanism rather than through a processive, one-collision mechanism. Experimental studies in *Xenopus* oocytes confirmed that the

---

<sup>1</sup> The Hill coefficient compares the 'steepness' of a stimulus/response curve to that of the Michaelis-Menten reference curve – the greater the Hill coefficient, the steeper the response. Responses characterized by Hill coefficients  $< 1$  are not ultrasensitive.

activation of p42 MAP kinase by Mek indeed occurs by a distributive, two-collision mechanism (Ferrell and Bhatt, 1997; Huang and Ferrell, 1996). Furthermore, the multi-level cascade structure itself contributes to the overall ultrasensitive response through multiplicative amplification of the individual responses at each stage (Brown et al., 1997; Ferrell, 1997; Kholodenko et al., 1997). The model predicts that the distributive activation mechanism, in concert with the combinatorial effect of the cascade structure, can result in an ultrasensitive response characterized by a Hill coefficient of 4.9. These predictions are in excellent agreement with experiments performed in *Xenopus* oocyte extracts (Huang and Ferrell, 1996).

However, experimental analysis of MAP kinase activation in intact *Xenopus* oocytes revealed that the ultrasensitive response in single cells was characterized by a Hill coefficient of 42, far exceeding the Hill coefficient of 4.9 observed in protein extracts and predicted by the model (Ferrell and Machleder, 1998). This discrepancy was attributed to the fact that the MAP kinase cascade is embedded in a positive feedback loop *in vivo*, where p42 MAP kinase activation promotes the accumulation of Mos (MAPKKK), thereby strengthening signal throughput (Matten et al., 1996). Indeed, positive feedback is yet another mechanism by which to generate ultrasensitivity. The intrinsic ultrasensitivity of the cascade together with the positive feedback loop results in a biochemical switch, where a graded stimulus is converted into a binary output (Ferrell, 1999).

## ***2.2 Bistability: Discrete transitions and biochemical ‘memory’***

Bistability in signaling networks has generated particular interest due to its ability to explain discrete, often irreversible, transitions that are commonly observed in biology (Sible, 2003). The maturation of *Xenopus* oocytes is an excellent example of a cellular event that progresses through distinct, stable phases. The ultrasensitive MAP kinase response has been placed at the center of the biochemical network that controls the irreversible transition inherent in *Xenopus* oocyte maturation (Ferrell, 2002). By adjusting the gains of the positive and negative feedback loops, a monostable, switch-like response can bifurcate into a bistable, hysteretic response (Ferrell and Xiong, 2001). Experimental analysis has provided abundant evidence confirming that the Mos/Mek/p42 MAP kinase cascade indeed controls and stably maintains the irreversible oocyte maturation decision (Ferrell and Machleder, 1998; Xiong and Ferrell, 2003).

In addition to its role in *Xenopus* oocytes, the MAP kinase cascade is prevalent in other signaling networks that have been found to exhibit bistability, such as the Epidermal Growth Factor (EGF) Receptor signaling pathway (Bhalla and Iyengar, 1999; Bhalla and Iyengar, 2001; Bhalla et al., 2002). The most notable of these studies identifies MAP Kinase Phosphatase-1 (MKP) as the “locus of flexibility” that can toggle the network between bistable and monostable regimes (Bhalla et al., 2002). Initial activation of the network by a transient stimulus elicits a sustained, supra-basal response that is maintained by positive feedback. The sustained activation of the cascade is eventually attenuated through slow-acting, negative feedback actuated by the up-regulation of MKP expression. The phosphatase serves two functions: (1) increased MKP

expression leads to signal adaptation<sup>2</sup>, and (2) the continued presence of MKP after adaptation serves to attenuate any subsequent stimulation of the network. Thus, MKP not only precipitates signal adaptation, but also confers a ‘memory’ function by temporally preventing re-activation of the network.

### ***2.3 Signal dynamics: Transient versus sustained MAP Kinase responses lead to distinct cellular fates***

In addition to ultrasensitivity and bistability, the MAP kinase cascade is known to communicate biochemical information via its dynamic response. The MAP kinase response in PC12 cells serves as a paradigm that demonstrates the relevance of signal duration (Figure I-4): stimulation with EGF leads to a transient response that promotes proliferation, while stimulation with Nerve Growth Factor (NGF) leads to a sustained response that induces neuronal differentiation (Marshall, 1995). A similar transient versus sustained response occurs in *S. cerevisiae*, where a common MAP kinase cascade mediates two developmental options—invasive growth and mating. Yeast grows invasively when Kss1 activation is sustained, while when activated in a transient manner, Kss1 helps support the mating response (Sabbagh et al., 2001).

---

<sup>2</sup> Adaptation refers to the re-setting of signal output to pre-stimulus levels.

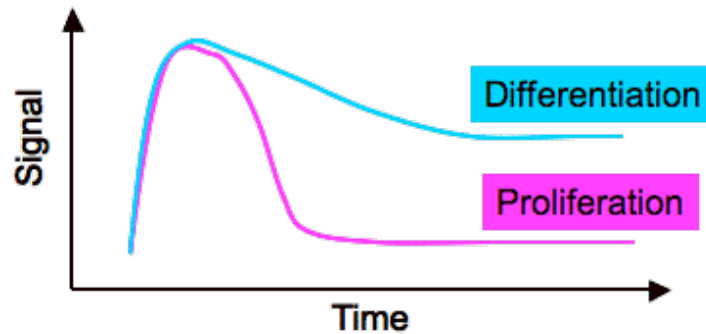


**Figure I-4. MAP kinase signal duration controls cell behavior.**

To examine more deeply the mechanisms that determine transient versus sustained signaling, a model of the MAP kinase signaling pathway that focused on signal adaptation as a function of multiple forms of negative feedback was developed (Asthağiri and Lauffenburger, 2001). An important conclusion reached by this model analysis was that two forms of negative feedback—decoupling deactivation and constitutive deactivation—were required to achieve full signal adaptation. Although negative feedback could mitigate continued stimulation of the cascade, constitutive deactivators were required for the specific deactivation of the accumulated output.

An ancillary effect of the decoupling negative feedback was that of ultra-desensitization of the network. Ultra-desensitization describes a situation in which the signal output decays, and continues to decay, even in the presence of an *increasing* stimulus. Thus, for sufficiently strong decoupling deactivation, it is possible to sever signal throughput completely, effectively ignoring any further change in stimulus. As a result of signal decoupling, then, the output was free to decay via constitutive deactivation (Asthağiri and Lauffenburger, 2001).

#### ***2.4 Protein scaffolds quantitatively affect MAP kinase output***

In addition to their role in determining signal specificity, scaffolds quantitatively contribute to signal output. Scaffolds are not simply passive platforms for binding signaling components. Rather, many functionalities of scaffolds, both hypothesized and verified, suggest that they actively participate in signal transduction. For example, scaffolds may orient bound kinases for optimal interaction, thereby providing a catalytic advantage for signal activation (Dard and Peter, 2006). Some scaffolds form dimers, permitting both a *cis*- and a *trans*-phosphorylation mechanism for facilitating signal activation (Yablonski et al., 1996; Yasuda et al., 1999). Finally, recruitment of pathway effectors to scaffold complexes can quantitatively influence signaling output, a property that has been recently exploited to synthetically tune network behavior (Bashor et al., 2008).

Since scaffolds bind to multiple components of a signaling pathway, the stoichiometric relation of the scaffold to its binding partners will affect signal propagation. The effect of scaffold expression level on MAP kinase module performance was explored through computational analysis (Levchenko et al., 2000). In the model, protein scaffolds promote signaling by recruiting pathway components and localizing them onto a single complex. Thus, the scaffold provides a kinetic advantage by reducing the diffusional limitation of kinase activation; the model assumes no catalytic advantage. This model predicts a biphasic relationship between the scaffold concentration and the MAP kinase output, and is not sensitive to binding constants or cooperative binding of the kinases to the scaffold. The mechanism responsible for the decrease in signal

throughput at high scaffold concentration is combinatorial inhibition, an effect that arises when too much scaffold interferes with the optimal formation of competent signaling complexes (Figure I-5).

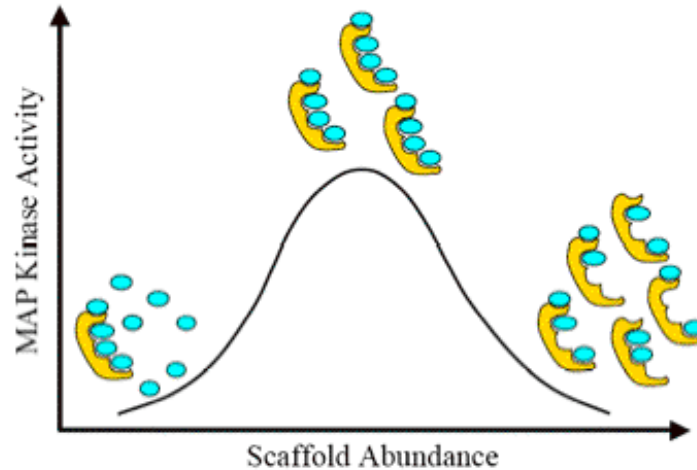


**Figure I-5. MAP kinase signal propagation biphasically depends on scaffold concentration.**

In addition to the biphasic effect on signal propagation, scaffolding can also influence the ultrasensitivity of MAP kinase signal propagation (Levchenko et al., 2000). Scaffold-bound kinases may be activated processively, while unbound kinases can be activated in a distributive, two-collision fashion. As a consequence, a reduction in module threshold properties may result from scaffold-mediated activation. Conversely, because they can dimerize, scaffolds may contribute to the ultrasensitivity of the MAP kinase response (Ferrell, 2000). Thus, how scaffolds quantitatively influence pathway ultrasensitivity remains to be determined.

### ***3. Current results: The effect of varying the expression levels of module components on the quantitative performance of the MAP kinase cascade***

Previous studies have identified many biologically-relevant quantitative features of MAP kinase pathways, including ultrasensitivity, bistability, and signal lifetime. Here, we probe more deeply how these quantitative properties may be affected by variations in the expression levels of the key constituents of the MAP kinase module—kinases, phosphatases and scaffolds. There are three principal reasons to focus on module sensitivity to expression level of its components. First, the expression levels of proteins vary from cell-to-cell even among genetically identical cells, i.e., cells are not quantitative clones even if they are genetic clones. Thus, understanding how sensitive the MAP kinase module is to perturbations in the expression level of its protein components will provide insights into cell population heterogeneity in MAP kinase signal propagation. Second, protein expression levels are not static. Cells dynamically alter protein expression levels to modulate cascade performance (Bhalla et al., 2002; Brondello et al., 1997; Matten et al., 1996). Understanding quantitatively how module performance is affected by these changes in protein expression would shed insight on the regulatory schemes that control MAP kinase-dependent cell processes. Finally, varying protein expression levels is a tractable design strategy that can be implemented using current molecular biology tools. Thus, it would be useful from an engineering perspective to better understand how such manipulations would affect the quantitative performance of the MAP kinase module.

In Chapter II, we use a computational approach to delineate how four quantitative properties of the MAP kinase module—responsiveness to input, dynamic range of output, signal amplification, and signal lifetime—depend on the relative abundances of the two core components, kinases and phosphatases. We uncover a reduced metric termed the ‘resistance to activation’ that predicts the quantitative properties of the MAP kinase module across a wide range of parameter values. This resistance metric successfully predicted signal lifetime, revealing two distinct regimes of signal decay: (1) stimulus limited decay and, (2) resistance limited decay. The resistance also captured other module properties such as the dynamic range and the responsiveness to input. Our analysis shows that all module attributes cannot be simultaneously optimized, revealing tradeoffs in module design. Thus, the resistance to activation captures the fundamental principles that determine cascade behavior and can be exploited to guide quantitative redesign of the MAP kinase module.

In addition to the expression levels of kinases and phosphatases, scaffold abundance will quantitatively affect MAP kinase signaling properties. In Chapter III we present an experimental sensitivity analysis that quantifies how MAP kinase module performance is affected by systematic variations in scaffold abundance. Our results show that scaffold abundance significantly affects several quantitative aspects of signal propagation, including signal throughput, pathway ultrasensitivity and baseline leakage. We demonstrate that tuning scaffold abundance comes with trade-offs in module performance: while changes in scaffold expression do not compromise signal specificity, it increases baseline leakage when no stimulus is present. These new insights into the

quantitative role of scaffolding in MAP kinase signaling suggest advantages and limitations in designing synthetic scaffold-based regulatory and metabolic circuits.

#### 4. References

- Asthagiri, A.R., and D.A. Lauffenburger. 2000. Bioengineering models of cell signaling. *Annu Rev Biomed Eng.* 2:31-53.
- Asthagiri, A.R., and D.A. Lauffenburger. 2001. A computational study of feedback effects on signal dynamics in a mitogen-activated protein kinase (MAPK) pathway model. *Biotechnol Prog.* 17:227-39.
- Bardwell, L. 2006. Mechanisms of MAPK signalling specificity. *Biochem Soc Trans.* 34:837-41.
- Bashor, C.J., N.C. Helman, S. Yan, and W.A. Lim. 2008. Using engineered scaffold interactions to reshape MAP kinase pathway signaling dynamics. *Science.* 319:1539-43.
- Bhalla, U.S., and R. Iyengar. 1999. Emergent properties of networks of biological signaling pathways. *Science.* 283:381-7.
- Bhalla, U.S., and R. Iyengar. 2001. Robustness of the bistable behavior of a biological signaling feedback loop. *Chaos.* 11:221-226.
- Bhalla, U.S., P.T. Ram, and R. Iyengar. 2002. MAP kinase phosphatase as a locus of flexibility in a mitogen-activated protein kinase signaling network. *Science.* 297:1018-23.
- Brondello, J.M., A. Brunet, J. Pouyssegur, and F.R. McKenzie. 1997. The dual specificity mitogen-activated protein kinase phosphatase-1 and -2 are induced by the p42/p44MAPK cascade. *J Biol Chem.* 272:1368-76.
- Brown, G.C., J.B. Hoek, and B.N. Kholodenko. 1997. Why do protein kinase cascades have more than one level? *Trends Biochem Sci.* 22:288.

- Dard, N., and M. Peter. 2006. Scaffold proteins in MAP kinase signaling: more than simple passive activating platforms. *Bioessays*. 28:146-56.
- Ferrell, J.E., Jr. 1997. How responses get more switch-like as you move down a protein kinase cascade. *Trends Biochem Sci*. 22:288-9.
- Ferrell, J.E., Jr. 1999. Building a cellular switch: more lessons from a good egg. *Bioessays*. 21:866-70.
- Ferrell, J.E., Jr. 2000. What do scaffold proteins really do? *Sci STKE*. 2000:PE1.
- Ferrell, J.E., Jr. 2002. Self-perpetuating states in signal transduction: positive feedback, double-negative feedback and bistability. *Curr Opin Cell Biol*. 14:140-8.
- Ferrell, J.E., Jr., and R.R. Bhatt. 1997. Mechanistic studies of the dual phosphorylation of mitogen-activated protein kinase. *J Biol Chem*. 272:19008-16.
- Ferrell, J.E., Jr., and E.M. Machleder. 1998. The biochemical basis of an all-or-none cell fate switch in *Xenopus* oocytes. *Science*. 280:895-8.
- Ferrell, J.E., and W. Xiong. 2001. Bistability in cell signaling: How to make continuous processes discontinuous, and reversible processes irreversible. *Chaos*. 11:227-236.
- Goldbeter, A., and D.E. Koshland, Jr. 1981. An amplified sensitivity arising from covalent modification in biological systems. *Proc Natl Acad Sci U S A*. 78:6840-4.
- Gustin, M.C., J. Albertyn, M. Alexander, and K. Davenport. 1998. MAP kinase pathways in the yeast *Saccharomyces cerevisiae*. *Microbiol Mol Biol Rev*. 62:1264-300.
- Hanahan, D., and R.A. Weinberg. 2000. The hallmarks of cancer. *Cell*. 100:57-70.

- Hartwell, L.H., J.J. Hopfield, S. Leibler, and A.W. Murray. 1999. From molecular to modular cell biology. *Nature*. 402:C47-52.
- Huang, C.Y., and J.E. Ferrell, Jr. 1996. Ultrasensitivity in the mitogen-activated protein kinase cascade. *Proc Natl Acad Sci U S A*. 93:10078-83.
- Keyse, S.M. 2000. Protein phosphatases and the regulation of mitogen-activated protein kinase signalling. *Curr Opin Cell Biol*. 12:186-92.
- Kholodenko, B.N., J.B. Hoek, H.V. Westerhoff, and G.C. Brown. 1997. Quantification of information transfer via cellular signal transduction pathways. *FEBS Lett*. 414:430-4.
- Levchenko, A., J. Bruck, and P.W. Sternberg. 2000. Scaffold proteins may biphasically affect the levels of mitogen-activated protein kinase signaling and reduce its threshold properties. *Proc Natl Acad Sci U S A*. 97:5818-23.
- Lewis, T.S., P.S. Shapiro, and N.G. Ahn. 1998. Signal transduction through MAP kinase cascades. *Adv Cancer Res*. 74:49-139.
- Marshall, C.J. 1995. Specificity of receptor tyrosine kinase signaling: transient versus sustained extracellular signal-regulated kinase activation. *Cell*. 80:179-85.
- Matten, W.T., T.D. Copeland, N.G. Ahn, and G.F. Vande Woude. 1996. Positive feedback between MAP kinase and Mos during *Xenopus* oocyte maturation. *Dev Biol*. 179:485-92.
- Park, S.H., A. Zarrinpar, and W.A. Lim. 2003. Rewiring MAP kinase pathways using alternative scaffold assembly mechanisms. *Science*. 299:1061-4.

- Pearson, G., F. Robinson, T. Gibson, B.-E. Xu, M. Karandikar, K. Berman, and M. Cobb. 2001. Mitogen-activated protein (MAP) kinase pathways: Regulation and physiological functions. *Endocrine Reviews*. 22:153-183.
- Sabbagh, W., Jr., L.J. Flatauer, A.J. Bardwell, and L. Bardwell. 2001. Specificity of MAP kinase signaling in yeast differentiation involves transient versus sustained MAPK activation. *Mol Cell*. 8:683-91.
- Sible, J.C. 2003. Cell biology: thanks for the memory. *Nature*. 426:392-3.
- Widmann, C., S. Gibson, M.B. Jarpe, and G.L. Johnson. 1999. Mitogen-activated protein kinase: conservation of a three-kinase module from yeast to human. *Physiol Rev*. 79:143-80.
- Xiong, W., and J.E. Ferrell, Jr. 2003. A positive-feedback-based bistable 'memory module' that governs a cell fate decision. *Nature*. 426:460-5.
- Yablonski, D., I. Marbach, and A. Levitzki. 1996. Dimerization of Ste5, a mitogen-activated protein kinase cascade scaffold protein, is required for signal transduction. *Proc Natl Acad Sci U S A*. 93:13864-9.
- Yasuda, J., A.J. Whitmarsh, J. Cavanagh, M. Sharma, and R.J. Davis. 1999. The JIP group of mitogen-activated protein kinase scaffold proteins. *Mol Cell Biol*. 19:7245-54.

## CHAPTER II. RESISTANCE TO SIGNAL ACTIVATION GOVERNS DESIGN FEATURES OF THE MAP KINASE SIGNALING MODULE

### *1. Abstract*

Given its broad influence over numerous cell functions, redesigning the mitogen-activated protein (MAP) kinase signaling module would offer powerful means to engineer cell behavior. Early challenges include identifying quantitative module features most relevant to biological function and developing simple design rules to predictably modify these features. This modeling study delineates how features such as signal amplification, input potency and dynamic range of output may be tuned by manipulating chief module components. Importantly, the model construction identifies a metric of resistance to signal activation that quantitatively predicts module features and design trade-offs for broad perturbations in kinase and phosphatase expression. Its predictive utility extends to dynamic properties such as signal lifetime, which often dictates MAP kinase effect on cell function. Taken together, we propose that predictably altering MAP kinase signaling by tuning resistance is not only a feasible engineering strategy, but also one exploited by natural systems to allow each MAP kinase to exert pleiotropic effects in a context-dependent manner. External stimuli not only activate kinases, but also alter phosphatase expression and activity, thereby reconfiguring a single module for quantitatively distinct modes of signaling such as transient versus sustained dynamics, each with unique effects on cell function.

Stephen Chapman and Anand R. Asthagiri, *Bioengineering and Biotechnology*, © John Wiley & Sons, Inc, 2004. Reprinted with permission from Wiley-Liss, Inc. a subsidiary of Wiley & Sons, Inc.

## 2. Introduction

The MAP kinase family of serine/threonine protein kinases are found among species ranging from *S. pombe* to *H. sapiens* (Lewis et al., 1998; Pearson et al., 2001). In mammals, MAP kinases have been implicated in regulating cell migration, apoptosis, proliferation and differentiation. Because of its broad influence, establishing strategies to redesign MAP kinase signaling would offer powerful means to engineer cell behavior. Recently, conceptual understanding of how MAP kinase pathways utilize scaffolds to maintain fidelity of stimulus-response relationships was elegantly exploited to engineer an artificial scaffold that converts yeast cell response to  $\alpha$ -factor from the natural mating response to an osmolarity-stress response (Park et al., 2003). Notably, the growing emphasis to transform conceptual description of signaling mechanisms into quantitative, dynamical models (Endy and Brent, 2001) would further expand the design space to include the possibility of quantitatively tuning information flow through signaling networks. This work focuses on early challenges to such quantitative redesign of the ubiquitous MAP kinase signaling module.

Most MAP kinases signal through a well-preserved mechanism, involving serial activation of a cascade of enzymes (Figure II-1). The wide recurrence of this cascade structure has garnered its label as a ‘signaling module’ and has raised interest in the inherent utility of its design. Classically, these cascades have been viewed as signal amplifiers (Pearson et al., 2001). Each active enzyme at the top of the cascade ( $E_1^*$ ) activates several targets ( $E_2$ ); and each of those activated target enzymes ( $E_2^*$ ) would, in

turn, activate its own group of targets ( $E_3$ ). Hence, magnitude amplification has been conjectured as a canonical function for enzyme cascades.

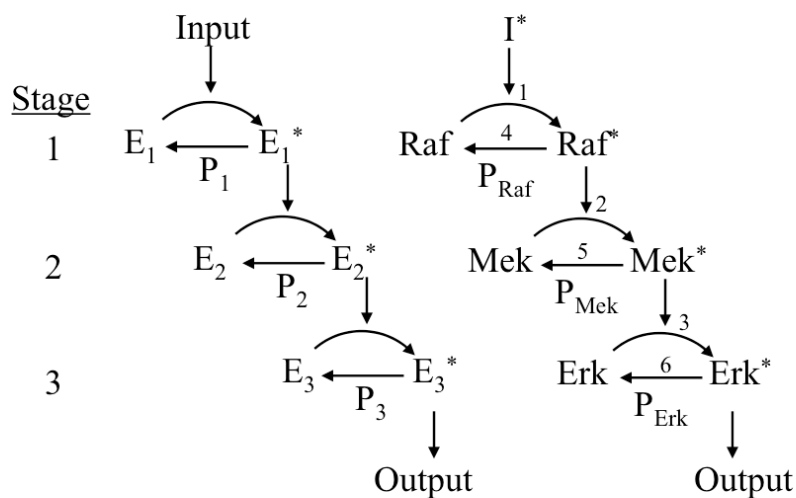


**Figure II-1. Model schematic.**

The MAP kinase module consists of a cascade of three kinases ( $E_i$ ) and their counterpart phosphatases ( $P_i$ ) as illustrated on the left. On the right, an example cascade is depicted: the Erk subfamily of MAP kinases is activated via the Raf-Mek-Erk cascade. An input initiates the cascade by activating the topmost kinase, while the module output is the number of active MAP kinase, in this case Erk. At each stage  $s$ , phosphatases catalyze the deactivation of kinases. More generally, at stage  $s$  an activated, upstream kinase ( $K_{s-1}$ ) converts its substrate ( $K_s$ ) from an inactive to active form. Meanwhile, phosphatases at each stage ( $P_s$ ) deactivate the kinase. Although not depicted, each enzyme(E)-substrate(S) reaction involves the formation of an ES complex:  $E + S \leftrightarrow ES \rightarrow E + P$ .

Computational models offer a framework to examine such issues in a rigorous manner (Tyson et al., 2001). Inferring specific insight into the MAP kinase module from models of large-scale signaling networks is thwarted by the inclusion of numerous

mechanisms external to the cascade (Schoeberl et al., 2002). A complementary approach focuses on the module, typically represented by a cascade of three kinases counterbalanced by constitutive deactivation enzymes (phosphatases) at each level of the cascade (Ferrell, 1996). Such models and congruent experimental work in *Xenopus* oocyte extracts have demonstrated that mechanisms such as distributive, two-step kinase activation confers ultrasensitivity at each step of the cascade (Huang and Ferrell, 1996). Moreover, cascade structure helps to accumulate this ultrasensitivity from each stage, so that module output reveals switch-like, steady-state responses to changes in stimulus concentration (Brown et al., 1997; Ferrell, 1997). In addition, aforementioned scaffolding mechanisms have been analyzed using a similar modular approach, revealing that an optimal, intermediate scaffold concentration may be required for maximal signal (Levchenko et al., 2000).

In addition to delineating signaling properties conferred by cascade structure and its internal mechanisms, computational analysis is necessary to develop strategies to re-engineer this module toward novel performance objectives. In fact, the first challenge is to identify quantitatively the design objectives themselves, with focus on enhancing biological efficacy or altering the information content of this cascade. Here, we delineate how such design goals may be defined in terms of quantitative features of the module, including the threshold amount of input required to trigger the MAP kinase switch. Since signaling via the Erk subfamily of MAP kinases is required for proliferation (Pages et al., 1993), redesigning the Erk module to respond to lower input levels may improve cell sensitivity to a mitogenic factor. Such hyper-responsive, re-engineered cells may help to

reduce costs associated with growth factors necessary for *ex vivo* repopulation of tissue engineering scaffolds. Alternatively, in instances where the MAP kinase of interest, such as JNK, drives apoptosis or programmed cell death (Davis, 2000), it may be desirable to reduce its sensitivity to environmental stresses, with possible implications for cell culture maintenance in bioprocess applications.

Ultimately, even modules with altered sensitivity to stimulus must effectively communicate with downstream targets to elicit cellular response. In some instances, MAP kinase modules perform as a switch, shifting between on- and off-states (Huang and Ferrell, 1996). In order for this switch to impart disparate cellular responses, downstream effectors must clearly distinguish between on- and off-states. Thus, the module must communicate with output intensity of adequate dynamic range.

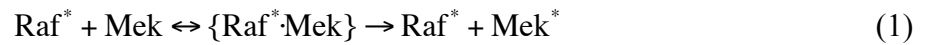
Finally, in addition to optimizing module communication with upstream input and downstream targets, it is desirable to tune the information content of the module itself. This information is often embedded in signal dynamics as in the case of Erk and JNK, whose transient activation has been linked to proliferation and survival, respectively, while sustained activation yields differentiation and apoptosis, respectively (Kao et al., 2001; Marshall, 1995; Roulston et al., 1998). Thus, tuning signal lifetime would offer control over cell fate, with direct implications for rationally designing therapeutic strategies that seek to revert pathological cell behavior. Of particular relevance are those disease states, such as cancer, in which aberrant MAP kinase signaling plays a significant, mechanistic role in leading to hyperproliferation and de-differentiation

(Lewis et al., 1998). This work delineates how these features—responsiveness to stimulus, range of output, and signal lifetime—and other quantitative attributes of the MAP kinase module may be re-engineered by manipulating experimentally-accessible system variables.

Importantly, a second challenge is to guide redesign of these quantitative features of information flow with *a priori* knowledge of potential consequences caused by specific manipulations. Our model construction identifies a metric of resistance to signal activation, which serves as such a predictive tool. Thus, the resistance effectively predicts both steady-state and dynamic features of the module for broad perturbations in kinase and phosphatase expression levels. Notably, these system variables are manipulable using established techniques, such as RNA interference, antisense RNA or exogenous overexpression from mammalian expression vectors, making the proposed redesign strategies practically feasible. Taken together, we propose that predictably altering MAP kinase signaling by tuning resistance is not only a practical engineering strategy, but also one exploited by natural systems to allow each MAP kinase to exert pleiotropic effects on cell behavior.

### 3. Model Development - Schematic and Equations

A first-level representation of the MAP kinase module involves three kinases in series, each activated by its predecessor. A schematic of such a cascade is shown in Figure II-1 for the Erk subfamily of MAP kinases. At each stage ( $s$ ), there are two reactions ( $i = s, s + 3$ ), one catalyzed by the upstream activator, and the other by the counteracting phosphatase. A representative pair ( $i = 2, 5$ ) of reaction mechanisms for the second stage is given below:



where enzyme-substrate complexes are denoted by  $\{\text{ES}\}$ . For Reaction 1, the association of  $\text{Raf}^*$  and  $\text{Mek}$  is governed by the second-order rate constant  $k_{+,2}$ , while the first-order rate constant for dissociation of the complex is given by  $k_{-,2}$ . Finally, the rate of product formation from this enzyme-substrate complex is dictated by the constant  $k_{\text{cat},2}$ . In general, the rate constants of each enzyme-substrate reaction  $i$  is given by  $k_{+,i}$ ,  $k_{-,i}$ , and  $k_{\text{cat},i}$  where  $i = 1 - 6$ .

Taking into account the free ( $I$ ), active ( $I^*$ ) and Raf-associated ( $I^* \cdot \text{Raf}$ ) forms of the input species, there are 17 components of the module. The amount of each of these components per cell were normalized by the total amount of each kinase and each phosphatase present in the system. Normalized, non-dimensional quantities are shown in italics to distinguish them from their dimensional counterparts:

$$\begin{aligned}
I &= \frac{I}{I_T} & I^* &= \frac{I^*}{I_T} \\
\{I^* \cdot Raf\} &= \frac{\{I^* \cdot Raf\}}{I_T} & Raf &= \frac{Raf}{Raf_T} \\
Raf^* &= \frac{Raf^*}{Raf_T} & \{Raf^* \cdot Mek\} &= \frac{\{Raf^* \cdot Mek\}}{Raf_T} \\
Mek &= \frac{Mek}{Mek_T} & Mek^* &= \frac{Mek^*}{Mek_T} \\
\{Mek^* \cdot Erk\} &= \frac{\{Mek^* \cdot Erk\}}{Mek_T} & Erk &= \frac{Erk}{Erk_T} \\
Erk^* &= \frac{Erk^*}{Erk_T} & P_{Rf} &= \frac{P_{Rf}}{P_{Rf,T}} \\
P_{Mk} &= \frac{P_{Mk}}{P_{Mk,T}} & P_{Ek} &= \frac{P_{Ek}}{P_{Ek,T}} \\
\{P_{Rf} \cdot Raf^*\} &= \frac{\{P_{Rf} \cdot Raf^*\}}{P_{Rf,T}} & \{P_{Mk} \cdot Mek^*\} &= \frac{\{P_{Mk} \cdot Mek^*\}}{P_{Mk,T}} \\
\{P_{Ek} \cdot Erk^*\} &= \frac{\{P_{Ek} \cdot Erk^*\}}{P_{Ek,T}} & & 
\end{aligned} \tag{3}$$

Among the 17 non-dimensional variables, the fraction of input species in the active state ( $I^*$ ) is provided as the driving function for the module. The values of the remaining 16 unknown dimensionless variables are determined partly by the following seven mass balances:

$$1 = I + I^* + \{I^* \cdot Raf\} \tag{4}$$

$$1 = Raf + Raf^* + \kappa_1 \{I^* \cdot Raf\} + \{Raf^* \cdot Mek\} + \pi_1 \{P_{Rf} \cdot Raf^*\} \tag{5}$$

$$1 = Mek + Mek^* + \kappa_2 \{Raf^* \cdot Mek\} + \{Mek^* \cdot Erk\} + \pi_2 \{P_{Mk} \cdot Mek^*\} \tag{6}$$

$$1 = Erk + Erk^* + \kappa_3 \{Mek^* \cdot Erk\} + \pi_3 \{P_{Ek} \cdot Erk^*\} \tag{7}$$

$$1 = P_{Rf} + \{P_{Rf} \cdot Raf^*\} \tag{8}$$

$$1 = P_{Mk} + \{P_{Mk} \cdot Mek^*\} \tag{9}$$

$$1 = P_{Ek} + \{P_{Ek} \cdot Erk^*\} \quad (10)$$

In conjunction with above, the following nine differential equations fully specify the behavior of the module:

$$\begin{aligned} \frac{dRaf^*}{d\tau} = & \frac{\kappa_1}{\tau_1} \{I^* \cdot Raf\} - \frac{\alpha_2}{\kappa_1 \kappa_2 \tau_2 \varepsilon_2} Raf^* Mek + \left( \frac{1}{\tau_2 \varepsilon_2} + \frac{1}{\tau_2} \right) \{Raf^* \cdot Mek\} - \dots \\ & \dots - \frac{\alpha_4 \pi_1}{\kappa_1 \tau_4 \varepsilon_4} Raf^* P_{Rf} + \frac{\pi_1}{\tau_4 \varepsilon_4} \{P_{Rf} \cdot Raf^*\} \end{aligned} \quad (11)$$

$$\begin{aligned} \frac{dMek^*}{d\tau} = & \frac{\kappa_2}{\tau_2} \{Raf^* \cdot Mek\} - \frac{\alpha_3}{\kappa_1 \kappa_2 \kappa_3 \tau_3 \varepsilon_3} Mek^* Erk + \left( \frac{1}{\tau_3 \varepsilon_3} + \frac{1}{\tau_3} \right) \{Mek^* \cdot Erk\} - \dots \\ & \dots - \frac{\alpha_5 \pi_2}{\kappa_1 \kappa_2 \tau_5 \varepsilon_5} Mek^* P_{Mk} + \frac{\pi_2}{\tau_5 \varepsilon_5} \{P_{Mk} \cdot Mek^*\} \end{aligned} \quad (12)$$

$$\frac{dErk^*}{d\tau} = \frac{\kappa_3}{\tau_3} \{Mek^* \cdot Erk\} - \frac{\alpha_6 \pi_3}{\kappa_1 \kappa_2 \kappa_3 \tau_6 \varepsilon_6} Mek^* P_{Mk} + \frac{\pi_3}{\tau_3 \varepsilon_3} \{P_{Mk} \cdot Mek^*\} \quad (13)$$

$$\frac{dRaf}{d\tau} = -\frac{\alpha_1}{\tau_1 \varepsilon_1} Raf I^* + \frac{\kappa_1}{\tau_1 \varepsilon_1} \{I^* \cdot Raf\} + \frac{\pi_1}{\tau_4} \{P_{Rf} \cdot Raf^*\} \quad (14)$$

$$\frac{dMek}{d\tau} = -\frac{\alpha_2}{\kappa_1 \tau_2 \varepsilon_2} Mek Raf^* + \frac{\kappa_2}{\tau_2 \varepsilon_2} \{Raf^* \cdot Mek\} + \frac{\pi_2}{\tau_5} \{P_{Mk} \cdot Mek^*\} \quad (15)$$

$$\frac{dErk}{d\tau} = -\frac{\alpha_3}{\kappa_1 \kappa_2 \tau_3 \varepsilon_3} Erk Mek^* + \frac{\kappa_3}{\tau_3 \varepsilon_3} \{Mek^* \cdot Erk\} + \frac{\pi_3}{\tau_6} \{P_{Mk} \cdot Mek^*\} \quad (16)$$

$$\frac{dP_{Rf}}{d\tau} = -\frac{\alpha_4}{\kappa_1 \tau_4 \varepsilon_4} P_{Rf} Raf^* + \left( \frac{1}{\tau_4 \varepsilon_4} + \frac{1}{\tau_4} \right) \{P_{Rf} \cdot Raf^*\} \quad (17)$$

$$\frac{dP_{Mk}}{d\tau} = -\frac{\alpha_5}{\kappa_1 \kappa_2 \tau_5 \varepsilon_5} P_{Mk} Mek^* + \left( \frac{1}{\tau_5 \varepsilon_5} + \frac{1}{\tau_5} \right) \{P_{Mk} \cdot Mek^*\} \quad (18)$$

$$\frac{dP_{Ek}}{d\tau} = -\frac{\alpha_6}{\kappa_1 \kappa_2 \kappa_3 \tau_6 \varepsilon_6} P_{Ek} Erk^* + \left( \frac{1}{\tau_6 \varepsilon_6} + \frac{1}{\tau_6} \right) \{P_{Ek} \cdot Erk^*\} \quad (19)$$

Appearing in Equations 4-19 are five classes of dimensionless parameters:  $\pi_s$ ,  $\kappa_s$ ,  $\alpha_i$ ,  $\varepsilon_i$  and  $\tau_i$ . Their form, significance and range of values are summarized in Table II-1.

Simulations were performed using Matlab v. 6.1 and the *ode23s* and *fsolve* subroutines.

**Table II-1. Five classes of dimensionless parameters specify module attributes.**

| Dimensionless Group   | Significance   | Symbol          | Range of Values |
|-----------------------|--|-----------------|-----------------|
| $P_s/K_s$             | amount of phosphatase relative to kinase at stage $s$  | $\pi_s$         | 0.01-100        |
| $K_{s-1}/K_s$         | amount of upstream kinase relative to kinase at stage $s$  | $\kappa_s$      | 0.3-3           |
| $k_{+,i}I_T/k_{-,i}$  | proportional to affinity for each enzyme-substrate pair $i$  | $\alpha_i$      | 0.1-10*         |
| $k_{cat,i}/k_{-,i}$   | efficiency with which each E'S complex $i$ will form product versus dissociate in a non-productive fashion   | $\varepsilon_i$ | 0.01-1*         |
| $k_{cat,1}/k_{cat,i}$ | characteristic time for product formation from each E'S complex $i$ relative to characteristic time for product formation from $\{I^* \cdot Raf\}$ | $\tau_i$        | 0.1-10*         |

\* Typical values for  $\alpha_i$ ,  $\varepsilon_i$ ,  $\tau_i$  were 0.6, 0.2 and 1, respectively (Asthagiri and Lauffenburger, 2001; Ferrell, 1996; Levchenko et al., 2000). For sensitivity analysis (see Appendix), these values were varied over two orders-of-magnitude near their typical value as indicated.

## **4. Results**

### **4.1 Model construction identifies most tangible design opportunities**

Our model construction by dimensional analysis and further parameter grouping reveals five classes of dimensionless parameters, which govern module behavior (Table II-1). Three of these parameter classes ( $\alpha_i$ ,  $\varepsilon_i$ ,  $\tau_i$ ) involve rate constants, whose values are intrinsic properties of the reacting species. While these parameters clearly contribute to the quantitative properties of the module, more tangible design opportunities are offered by two other dimensionless groups. The first ( $\pi_s$ ) represents the amount of phosphatase relative to kinase at each stage of the cascade. The second dimensionless group ( $\kappa_s$ ) compares the expression level of an upstream kinase to the amount of its target at each stage. Thus, the values of these parameters are dictated by the expression levels of kinases and phosphatases, which are particularly attractive from a design perspective, since protein expression levels are readily adjustable in experimental systems using established techniques involving RNA interference, antisense RNA or mammalian expression vectors. Therefore, these two dimensionless groups are the focus of developing a redesign strategy.

### **4.2 Sustained input and steady-state features**

Most mathematical treatments of the MAP kinase cascade utilize a step function for module input, which was initially employed here as well. Upstream components such as Ras, whose active form serves as input, may be expressed at levels as high as  $10^5$

copies per cell (Scheele et al., 1995). Therefore, non-zero values for the fraction of input species in its active state ( $I^*$ ) may range between  $10^{-5} - 10^0$ . The module output is given by the fraction of Erk in its active state ( $Erk^*$ ).

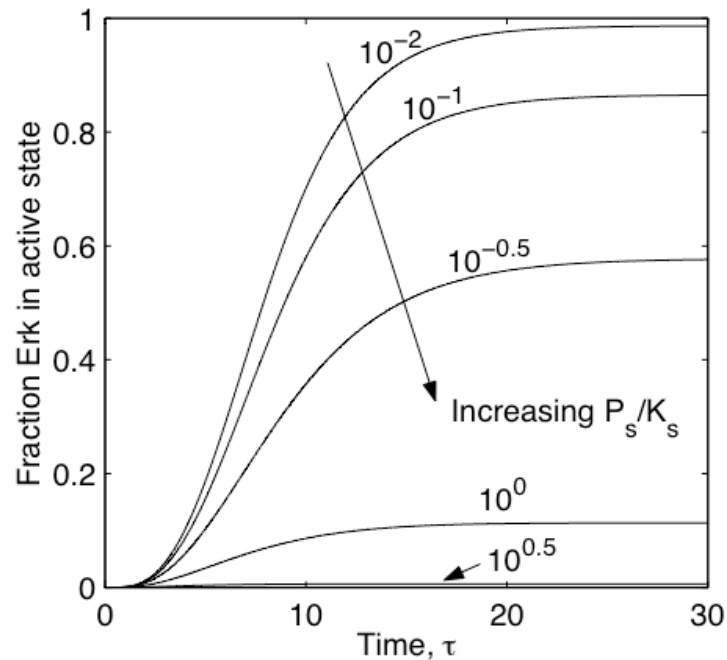


**Figure II-2. Temporal profile of module output in response to a step input: the effect of varying the relative amount of phosphatase versus kinase.**

Module was stimulated with a step input ( $I^* = 10^{-0.5}$ ), and the fraction of Erk in its active state was tracked over time. Simulation was performed for different relative amounts of phosphatases compared to kinases ( $\pi_s = 10^{-2} - 10^{0.5}$ ), while holding the ratio of upstream to downstream components fixed ( $\kappa_s = 1$ ). Constitutive presence of phosphatases does not confer adaptation to a sustained input but affects level of steady-state output.

In the absence of negative feedback, no adaptation is observed in module output (Figure II-2), or among any of the upstream kinases (data not shown). Because signal adaptation does not occur, the steady-state behavior of this module was examined. For

this cascade, the steady-state fraction of Erk in its active state (module output) displays sigmoidal dependence on non-zero input amplitude ( $I^*$ ) as shown in Figure II-3. This sigmoidal dependence has been shown to acquire steeper transition from minimal to maximal output, yielding switch-like behavior when kinase activation involves a two-step, distributive mechanism (Huang and Ferrell, 1996). Here, we consider three other properties—potency, range, and gain—which are crucial measures of this module's ability to propagate signal.

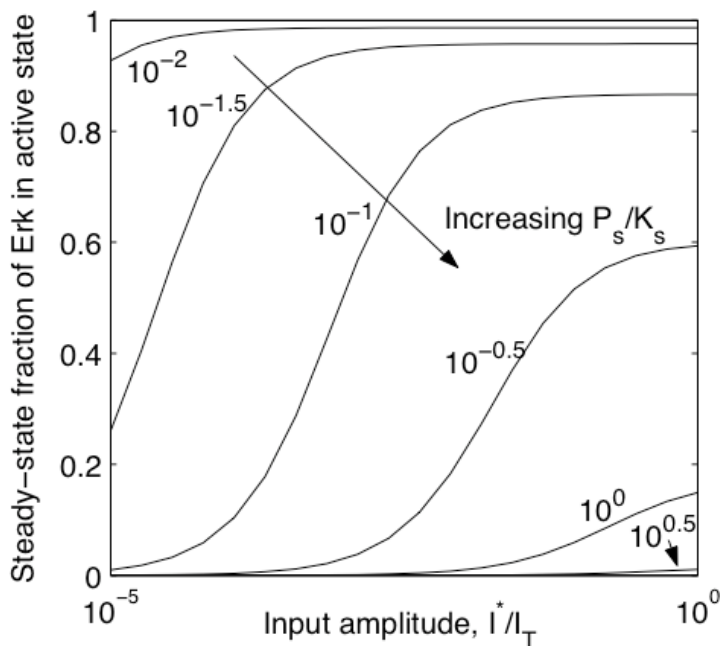


**Figure II-3. Module dose-response to changes in the relative amount of phosphatase versus kinase.**

The steady-state level of output was computed for different, non-zero input amplitudes for  $\kappa_s = 1$ . For intermediate ratios of phosphatase to kinase expression level ( $\pi_s = 10^{-1}$ ), module output is a sigmoidal function of input amplitude. However, if kinases dramatically outnumber phosphatases or vice versa, module becomes insensitive to changes in input. In one extreme ( $\pi_s \rightarrow 0$ ), module output is always maximal, even for minimal input; and, in the other extreme, module output is severely attenuated and unable to respond even complete activation of input species.

#### 4.2-1 Potency

Potency is a measure of how much input is required to elicit efficient module response. In experimental terms, stimulus potency is inversely related to the  $EC_{50}$ , which is the effective concentration of stimulus (typically, a ligand) required to attain half-maximal response (e.g., cell proliferation). By direct analogy, the potency of input to the MAPK module is  $1/I_{50}^*$ , where  $I_{50}^*$  is the input amplitude which promotes medium level of output. Module configurations that yield low values for  $I_{50}^*$  confer high potency to input as they enable low levels of input to efficiently propagate signal. We analyzed the dependence of input potency on module design, particularly focusing on components of the cascade which are most readily tunable experimentally.

The relative expression level of phosphatases to that of kinases ( $P_s/K_s = \pi_s$ ) at each stage  $s$  dramatically affects input potency. This is most clearly revealed in Figure II-3 by the rightward shift in the “dose-response” curves as  $\pi_s$  is increased. In performing these simulations, the value of  $\pi_s$  was assumed to be equal for each stage  $s$ , largely due to the lack of experimental data that would suggest otherwise and in part to remain consistent with previous treatments of the MAP kinase module (Huang and Ferrell, 1996). For high  $\pi_s$  values, more phosphatases are present to deactivate kinases, thereby increasing the threshold amount of input required to elicit module response. Values for potency were calculated from dose-response curves, and its dependence on  $\pi_s$  is portrayed in Figure II-4. Consistent with the dose-response curves, input potency is a

monotonically decreasing function of  $\pi_s$ , with asymptotic upper and lower limits for low and high  $\pi_s$  values, respectively.

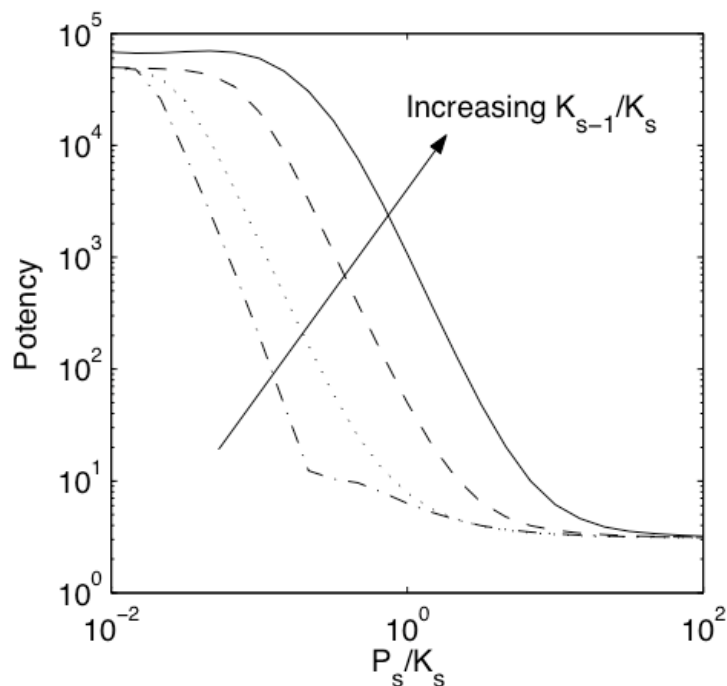


**Figure II-4. Input potency.**

Aspects of the module dose-response (Figure II-3) may be tuned by altering module configuration. The potency of the input is inversely related to the amount of input ( $I_{50}^*$ ) required to attain average module output. For fixed ( $\kappa_s$ ), an increase in the relative amount of phosphatases ( $\pi_s$ ) reduces input potency, since more input is required to elicit half-maximal response. This trend is preserved for all  $\kappa_s = 10^{-0.5}$  ( $-\cdot-$ ),  $10^0$  ( $\cdots$ ),  $10^{0.5}$  ( $--$ ),  $10^1$  ( $-$ ). For fixed  $\pi_s$ , increasing the amount of upstream kinase relative to downstream target increases input potency.

In addition to phosphatase activity, signal generation at each stage of the cascade is determined by competing upstream activators. The net effect on module behavior may be evaluated by considering the  $\pi_s$  value in balance with the expression level of

upstream activators relative to its downstream target ( $K_{s-1}/K_s = \kappa_s$ ). For fixed  $\pi_s$ , input potency is enhanced for higher relative expression levels of upstream activator (Figure II-4). For  $\kappa_s > \pi_s$ , upstream activation outweighs deactivation at each stage, enabling high module output even for low input.

#### 4.2-2 Range of output

A second important attribute of the MAPK module is the range of output produced in response to a spectrum of non-zero input. This range is defined as the difference in output caused by full stimulation (i.e., all input species are active) versus minimal, non-zero input:

$$\text{range} = [Erk_{ss}^*]_{\max \text{ input}} - [Erk_{ss}^*]_{\min \text{ input}} \quad (20)$$

While model results depict output as a continuous function of input, discrete numbers of active Erk molecules serve as physiological module output. Thus, a module whose range of output is large would possess more intermediate values of output with which to convey “higher-grain” information to the next module.

Module range demonstrates biphasic dependence on  $\pi_s$  as shown in Figure II-5. For low  $\pi_s$  values, relatively few phosphatases are present to impede kinase activation. In this case, even minimal non-zero input activates all available kinases, precluding higher output in response to further increments in input. Meanwhile, at high  $\pi_s$ , intense phosphatase activity does not permit signal generation even at maximal stimulation, yielding no difference in output magnitude for low versus high input. Only at an optimal

intermediate  $\pi_s$  value, balanced phosphatase and upstream kinase activity enable a large range of output to changes in input stimulation. This balance is affected not only by the dimensionless parameter  $\pi_s$ , but also by the expression level of upstream activators relative to their downstream targets. Since upstream activation is enhanced for higher  $\kappa_s$  values, greater amount of phosphatases relative to kinases is required to balance activation. Thus, the  $\pi_s$  value needed to optimize module range increases for higher  $\kappa_s$  (Figure II-5).

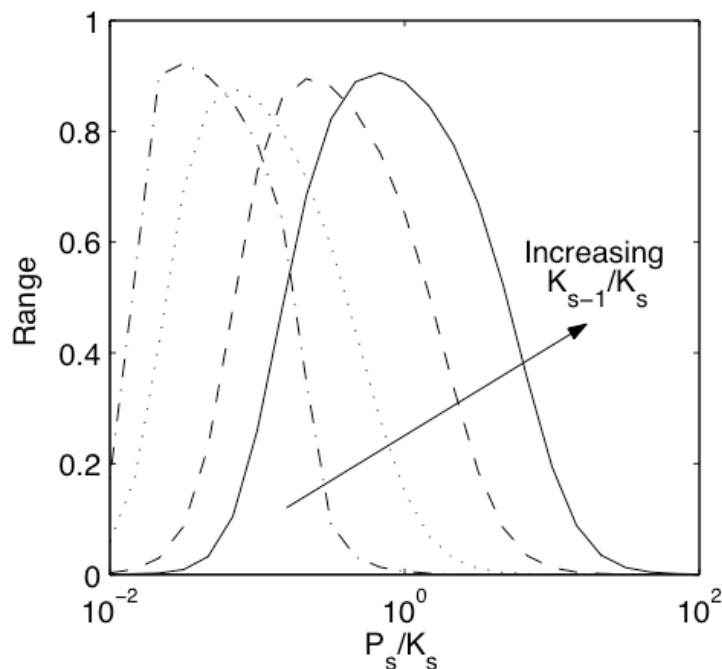


**Figure II-5. Dynamic range of module output.**

The dynamic range of output is the difference in module output in response to maximum input versus minimum, non-zero input. This range is a biphasic function of the ratio of phosphatase to kinase expression level ( $\pi_s$ ) for  $\kappa_s = 10^{-0.5}$  (-·-),  $10^0$  (···),  $10^{0.5}$  (---),  $10^1$  (-). Thus, maximum range of output is achieved at an optimum  $\pi_s$ . An increase in the relative amount of upstream to downstream kinases shifts this optimum  $\pi_s$  value.

### 4.2-3 Signal amplification

While high-range modules “sense” low versus high input by producing maximally disparate output for these two extremes of stimulation, signal amplification quantifies the ability of the module to receive a certain amount of input and respond by generating even greater amount of output. Kinase cascades have been implicated as an optimal configuration to achieve such amplification (Pearson et al., 2001). In fact, amplification has been suggested to require greater amount of downstream kinase than upstream activator (i.e.,  $\kappa_s < 1$ ). Thus, signal transfer from Raf to Mek has been identified as an ideal point for amplification (Pearson et al., 2001) because Mek levels typically far exceed those of Raf (Ferrell, 1996). However, Mek and Erk are expressed typically at equimolar levels (Ferrell, 1996), suggesting that amplification may not be the chief purpose of this part of the cascade (Pearson et al., 2001).

We examined rigorously the dependence of signal amplification on relative expression level of upstream and downstream kinases ( $\kappa_s$ ) and on the relative amount of phosphatases ( $\pi_s$ ). The gain ( $\Gamma$ ) in signal strength from input to output was quantified by the ratio of number of active Erk at steady-state to the level of input:

$$\Gamma = \left( \frac{Erk_{ss}^*}{I^*} \right) \left( \frac{Erk_T}{I_T} \right) \quad (21)$$

where  $Erk_{ss}^*$  and  $I^*$  are the fraction of each enzyme in their active state at steady-state and  $Erk_T$  and  $I_T$  are the total amount of each protein per cell. Thus, the module performs as an amplifier if  $\Gamma > 1$  and as an attenuator if  $\Gamma < 1$ .

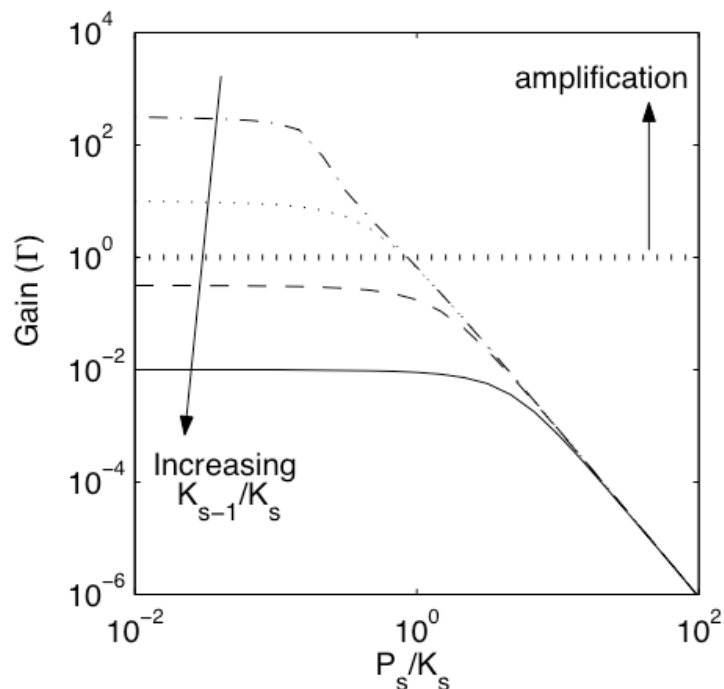


**Figure II-6. Signal amplification versus attenuation.**

For a given amount of input ( $I^* = 10^{-0.5}$ ), the signal gain ( $\Gamma$ ) is quantified as the ratio of number of active Erk species at steady-state to the number of active input species. The horizontal line ( $\Gamma = 1$ ) demarcates regimes yielding signal amplification ( $\Gamma > 1$ ) versus attenuation ( $\Gamma < 1$ ). Even if downstream kinases outnumber upstream activators ( $\kappa_s = 10^{-0.5}$  (---)), signal attenuation occurs for high relative expression of phosphatases. Conversely, at low  $\pi_s$ , amplification may occur even for equimolar expression of upstream and downstream kinases ( $\kappa_s = 10^0$  (...)). If downstream kinases are outnumbered by upstream activators ( $\kappa_s = 10^{0.5}$  (- -),  $10^1$  (-)), the MAPK module serves only as an attenuator, regardless of phosphatase expression levels. Taken together, the module may operate as a signal amplifier or attenuator.

The results from the model demonstrate that the kinase module may operate as both an amplifier and attenuator (Figure II-6). At high values of  $\pi_s$ , the cascade always attenuates signal, even if downstream kinases outnumber upstream activators. Under these conditions, deactivators considerably outnumber activators, and signal production at each stage is strongly inhibited. In turn, low levels of kinase activation at each stage

reduces the driving force for activation in the next stage, thereby diminishing signal strength across the cascade. Hence, even if downstream kinases outnumber upstream activators, amplification is not assured.

In the other extreme, as  $\pi_s \rightarrow 0$ , there is no restraint on kinase activation, and all available enzymes in each stage of the cascade are activated. The fraction of enzymes activated at each stage asymptotes to one (i.e.,  $Erk_{ss}^* \rightarrow 1$ ), and signal gain across the module approaches a value dictated solely by the relative expression levels of kinases and input magnitude:

$$\lim_{\pi_s \rightarrow 0} \Gamma = \frac{Erk_T}{I^* I_T} = \frac{1}{I^*} \left( \frac{Raf_T}{I_T} \right) \left( \frac{Mek_T}{Raf_T} \right) \left( \frac{Erk_T}{Mek_T} \right) \quad (22)$$

In the case of equimolar expression level ( $\kappa_s = 1$ ), the gain asymptotes to  $1/I^*$ . Thus, even for equimolar expression level of kinases, amplification is guaranteed provided all input species are not in their active state (i.e.,  $I^* < 1$ ).

#### 4.2-4 Transient input and module dynamics

The module input represents upstream molecule(s) such as active Ras, which governs Raf activation. In many experimental systems, this upstream component undergoes transient activation and is better represented by a pulse, rather than a step input. To examine module performance to a transient input, a pulse input with lifetime  $\delta$  and amplitude  $I_o$  as follows was utilized:

$$I^* = \begin{cases} I_o, & 0 \leq \tau < \delta \\ 0, & \tau \geq \delta \end{cases} \quad (23)$$

The pulse input is represented by instantaneous activation and deactivation. Furthermore,  $\delta$  is chosen as the time required for the system to reach pseudo-steady state upon receiving input  $I_o$ . Thus, system response to loss of input may be analyzed independent of system response to receiving input.

Upon instantaneous input decay, the fraction of Erk in its active state also decays back to basal level as shown in Figure II-7 for fixed  $\pi_s$  and  $\kappa_s$ . Signal decay requires constitutive expression of phosphatases, since reducing the relative amount of these deactivators by decreasing  $\pi_s$  extends signal duration (Figure II-7, compare solid lines). Notably, signal decay is also retarded if more upstream kinases are present relative to downstream targets. Thus, a two-fold increase in  $\kappa_s$  significantly extends signal lifetime (compare solid and dotted lines).

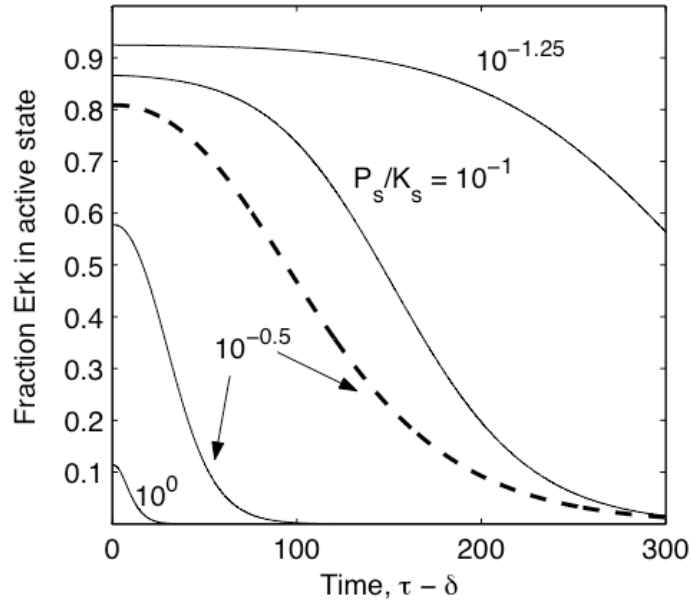


**Figure II-7. Temporal profile of module output following instantaneous loss of input.**

Upon removal of input at time  $\delta$ , the module output decays to a basal level in a two-phase process, involving an initial time-lag during which output does not change dramatically, followed by an active decay phase. For fixed  $\kappa_s = 1$ , reducing the amount of constitutive phosphatases relative to kinases ( $\pi_s = 10^{-1.25}$ ) significantly delays output decay. Thus, instantaneous loss of input enables complete adaptation of module output, provided constitutive phosphatases are expressed. In addition, even for a decay-permissive level of  $\pi_s = 10^{-0.5}$ , doubling the ratio of upstream to downstream kinase expression extends the lifetime of module output (—).

Although a reduction in  $\pi_s$  or an increase in  $\kappa_s$  elevates output lifetime, these parameter changes also increase the level of output from which decay occurs. To determine whether the rate of signal decay is truly affected or whether extended signal lifetime is a byproduct of starting from a higher output, the temporal decay profiles were recast in a semilog plot (Figure II-8). Beyond a time-lag and during the decay phase,  $\log(\text{Erk}^*)$  decreases linearly with time, consistent with a decay rate that is first-order

with respect to fraction of Erk in its active state ( $Erk^*$ ). Importantly, the slope of this output decay, which is the apparent decay rate constant, is directly affected by changes in  $\pi_s$  and  $\kappa_s$ , showing that extended lifetime is not simply a byproduct of starting from a higher output signal.

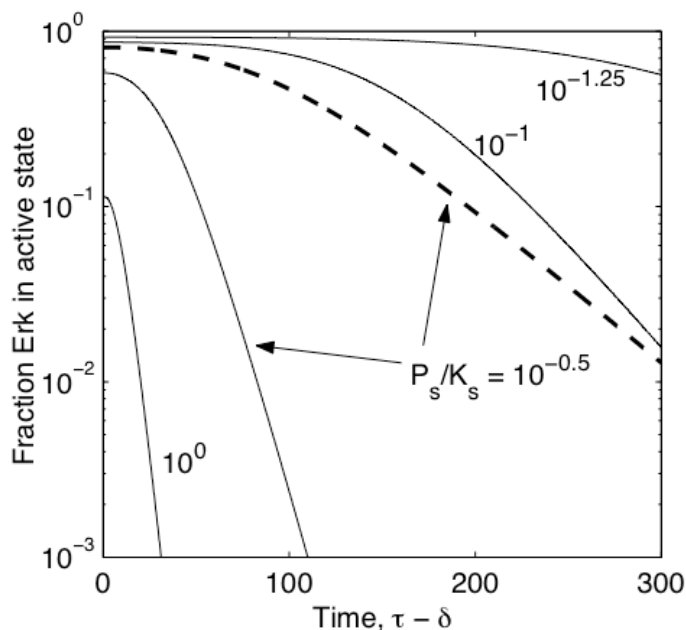


**Figure II-8. Output decay in semi-log format.**

The decay curves from Figure II-7 are shown on a semilog plot. During the active decay phase,  $\log(Erk^*)$  decreases linearly with time, indicating a first-order process with respect to active Erk. Moreover, both  $\pi_s$  and  $\kappa_s$  determine the slope of this linear relationship—the apparent rate constant.

To better understand the relationship between decay rates of input and output, the instantaneous input decay was replaced with an exponential decay characterized by a half-life,  $\tau_{1/2}^{input}$ . In response, the half-life of module output was calculated for different values of  $\pi_s$  and  $\kappa_s$ . Consistent with above results, increasing  $\pi_s$  or decreasing  $\kappa_s$

reduces the half-life of module output (Figure II-9). However, this half-life is bounded by a lower limit, which approaches the half-life of the decaying input, emphasizing that this form of adaptation is fully dependent on loss of input.

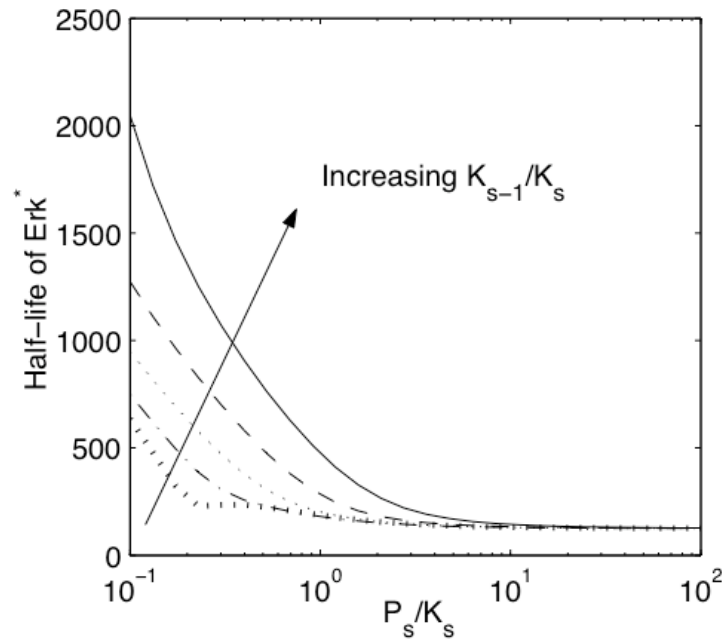


**Figure II-9. Half-life of Erk signal in response to an exponential decay in input.**

Input amplitude ( $I^*$ ) was reduced exponentially with an arbitrary, non-zero half-life,  $\tau_{1/2}^{input} = 100$ . The time for module output to decay to 50% of its initial level was calculated for various  $\pi_s$  and  $\kappa_s$  values. While this half-life of active Erk may be reduced, its lower bound is set by the half-life of input decay.  $\kappa_s = 10^{-0.5}$  (| |),  $10^{-0.25}$  (-.-),  $10^0$  (...),  $10^{0.25}$  (- -),  $10^{0.5}$  (-).

### 4.3 Resistance to activation

It is evident that the dimensionless parameters  $\pi_s$  and  $\kappa_s$  have opposing effects on both steady-state properties and signal dynamics (refer to Figure II-4, Figure II-5, Figure II-6, and Figure II-9). These two ratios capture the competing effects that

phosphatases and upstream activators exert on kinase activity at each stage of the cascade. To determine if a single parameter accurately integrates these opposing effects, we defined a combined parameter as follows:

$$\Omega_s = (P_s/K_s)/(K_{s-1}/K_s) = \pi_s/\kappa_s. \quad (24)$$

This parameter represents the expression level of phosphatase ( $P_s$ ) relative to the total amount of upstream kinase ( $K_{s-1}$ ), offering a net measure of resistance to signal activation at each stage of the cascade. The present treatment maintains that all stages have the same resistance, allowing overall module resistance to be equated to resistance at each stage.

To determine if this metric of resistance accurately predicts module behavior, the dependence of signal half-life on  $\Omega_s$  was examined. The half-life of output in response to an exponential decay in input was presented for independent variations in  $\kappa_s$  and  $\pi_s$  in Figure II-9. These data collapse into a single dependence on resistance to activation (Figure II-10), indicating that effects of changing  $\kappa_s$  and  $\pi_s$  may be predicted by the correlating parameter,  $\Omega_s$ . As resistance to activation increases, module output is more easily diminished, thereby reducing the half-life of signal. In fact, the predictive utility of this metric of resistance is robust. Thus, for values of the rate constant-embedded dimensionless groups ( $\alpha_i$ ,  $\varepsilon_i$ ,  $\kappa_i$ ) that span a range of two orders of magnitude, the resistance quantitatively predicts signal half-life in response to changes in  $\kappa_s$  and  $\pi_s$  (see Appendix).

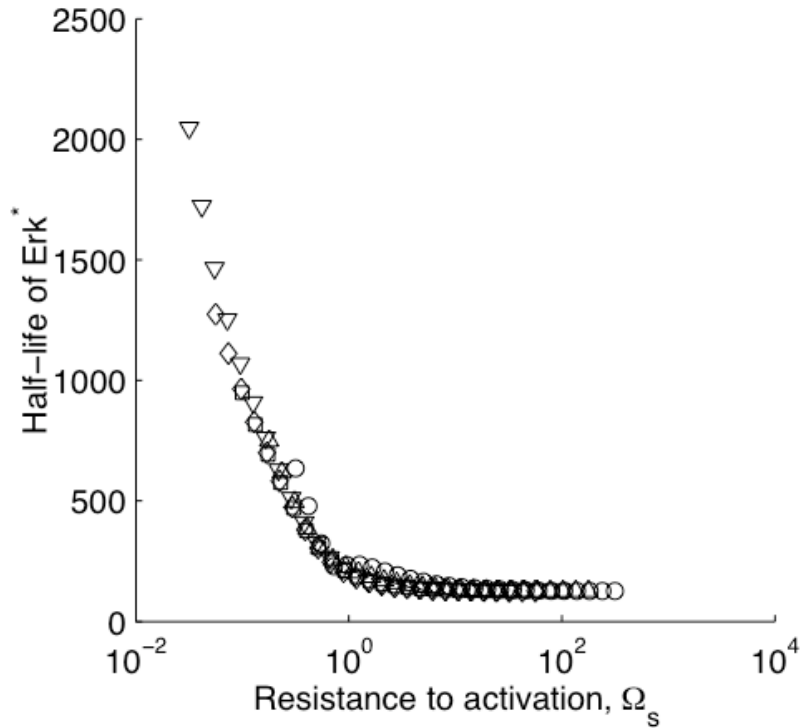


**Figure II-10. The dependence of half-life of Erk signal on the resistance to activation for wide range of perturbations in  $\pi_s$  and  $\kappa_s$ .**

The half-life of module output depicted in Figure II-9 for  $\pi_s = 10^{-1} - 10^2$  and  $\kappa_s = 10^{-0.5}$  (O),  $10^{-0.25}$  ( $\Delta$ ),  $10^0$  ( $\square$ ),  $10^{0.25}$  ( $\diamond$ ),  $10^{0.5}$  ( $\nabla$ ) have been plotted as a function of module resistance,  $\Omega_s = \pi_s / \kappa_s$ . A single relationship is revealed between half-life of active Erk and resistance, encompassing all changes in  $\pi_s$  and  $\kappa_s$ .

Additionally, the resistance to activation accurately predicts steady-state features such as module range and input potency. As shown in Figure II-11, at low resistance, even the smallest input produces maximum output, limiting module range. Conversely, high resistance to deactivation impedes signal production even at maximum input. Only at an intermediate resistance, the opposing effects of upstream activators and phosphatases are balanced to yield maximum range of module output. However, at a

resistance ( $\Omega_s \approx 10^{-1}$ ) that is optimal for output range, the input potency is reduced by approximately 1.5 orders of magnitude (Figure II-12).

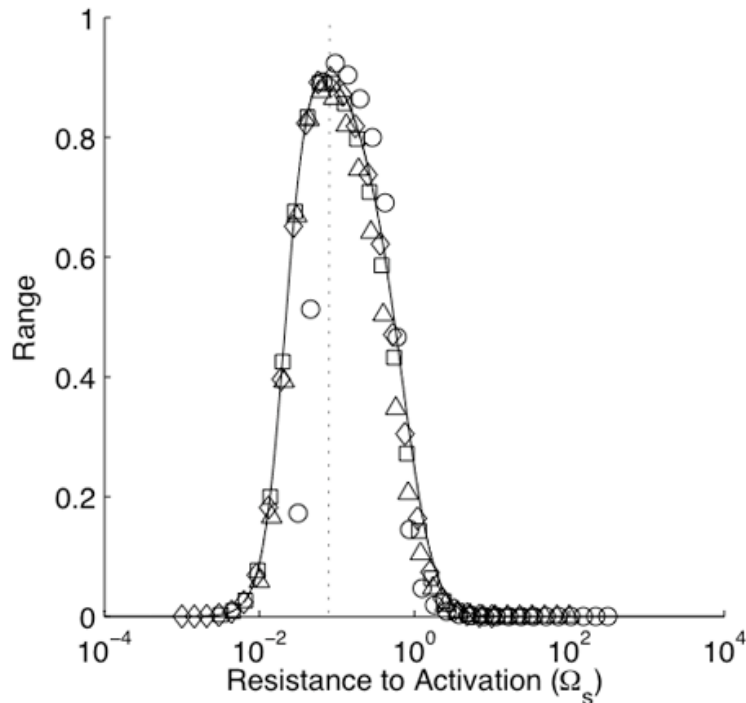


**Figure II-11. The dependence of dynamic range of module output on resistance to activation for wide range of perturbations in  $\pi_s$  and  $\kappa_s$ .**

Output range, which was depicted in Figure II-5 for  $\pi_s = 10^{-2} - 10^2$  and  $\kappa_s = 10^{-0.5}$  (O),  $10^0$  ( $\Delta$ ),  $10^{0.5}$  ( $\square$ ),  $10^1$  ( $\diamond$ ), shows a single, biphasic relationship to resistance to activation. Thus, maximum range may be obtained by adjusting either  $\pi_s$  or  $\kappa_s$  to net a resistance  $\Omega_s \approx 10^{-1}$  (dotted line). The solid black line shows the analytic solution of the range for a three stage cascade.

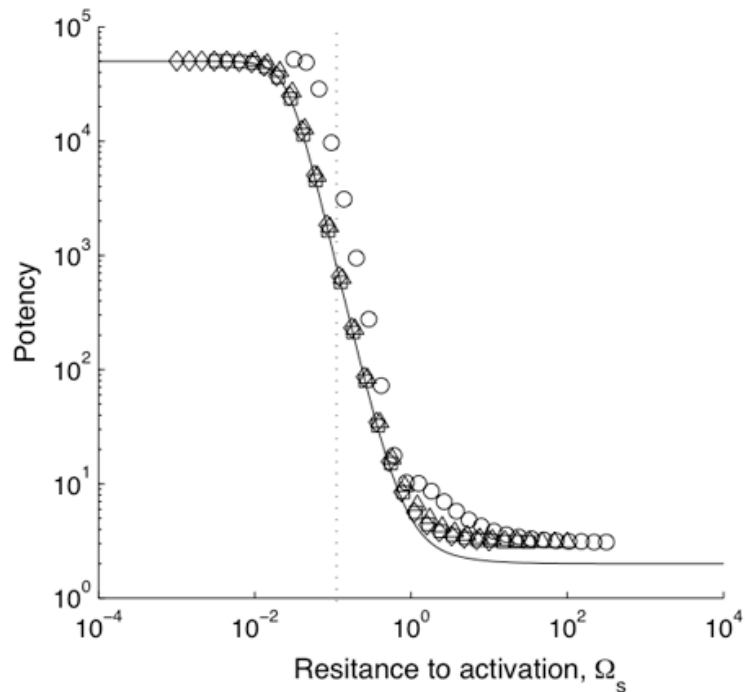


**Figure II-12. The dependence of input potency on resistance to activation for wide range of perturbations in  $\pi_s$  and  $\kappa_s$ .**

Input potency, which was depicted in Figure II-4 for  $\pi_s = 10^{-2} - 10^2$  and  $\kappa_s = 10^{-0.5}$  (O),  $10^0$  ( $\Delta$ ),  $10^{0.5}$  ( $\square$ ),  $10^1$  ( $\diamond$ ), shows a single, monotonically decreasing relationship to resistance to activation. At an intermediate resistance that optimizes module range (dotted line), input potency is at least one order of magnitude below its maximum. The solid black line shows the analytic solution of the potency for a three stage cascade.

#### **4.4 Relaxation of resistance parameters**

The previous results were subject to the constraint that a single resistance ( $\Omega_s$ ) was uniformly applied to all stages of the MAP kinase module. We relaxed this constraint to allow unequal stage resistances ( $\omega_1, \omega_2, \omega_3$ ). To describe the behavior of the MAP kinase cascade with variable stage resistances, we first focused analytically on the performance of a single stage in isolation. (For consistent nomenclature, we used Raf activation in isolation from the rest of the cascade to illustrate our derivation of single

stage resistance.) Previous work by Goldbeter and Koshland appropriately described the steady-state behavior of such a single stage system (Goldbeter and Koshland, 1981). To arrive at their solution, the authors made two key assumptions. First, they neglected the contribution of  $\{I^* \cdot Raf\}$  and  $\{P_{Rf} \cdot Raf^*\}$  to the species balance of the substrate, Raf. Second, they assumed that the converter enzymes,  $I^*$  and  $P_{Rf}$ , operate in the first order regime, or that

$$Raf_T \ll \frac{k_{-1} + k_{cat,1}}{k_{+1}} \text{ and } Raf_T \ll \frac{k_{-4} + k_{cat,4}}{k_{+4}} \quad (25)$$

The following analytical expression describes the steady-state activation of the modified substrate ( $Raf_{ss}^*$ ) as a function of the rate constants and the total concentrations of the model components, where we have recast the equation using our dimensionless groups:

$\pi_s$ ,  $\kappa_s$ ,  $\alpha_i$ ,  $\varepsilon_i$  and  $\tau_i$ .

$$Raf_{ss}^* = \frac{1}{1 + \omega_1 \frac{K_{M,1}}{K_{M,4}} \left( \frac{1}{I^*} \right)}, \text{ where } K_{M,i} = \frac{\tau_i(1 + \varepsilon_i)}{\alpha_i/\kappa_s} \text{ and } \omega_s = \frac{\pi_s}{\kappa_s} \quad (26)$$

Note that the single stage resistance,  $\omega_1$ , falls cleanly out of the above equation, as suggested from our prior computational results. Generalizing this result to the second and third stages of the cascade, we obtain the following equations:

$$Mek_{ss}^* = \frac{1}{1 + \omega_2 \frac{K_{M,2}}{K_{M,5}} \left( \frac{1}{Raf^*} \right)} \quad (27)$$

$$Erk_{ss}^* = \frac{1}{1 + \omega_3 \frac{K_{M,3}}{K_{M,6}} \left( \frac{1}{Mek^*} \right)} \quad (28)$$

Now, to reconstruct an n-stage cascade using the above equations, it must further be assumed that there are no upstream interactions, i.e., the parameters and potential behavior of stage  $s + 1$  does not influence the behavior of stage  $s$ . Then, the above equation can be iteratively substituted into itself to obtain a steady-state dose-response expression for any n-stage cascade. Following are the first three iterations:

$$Raf_{ss}^* = \frac{1}{1 + \omega_1 \frac{K_{M,1}}{K_{M,4}} \left( \frac{1}{I^*} \right)} \quad (29)$$

$$Mek_{ss}^* = \frac{1}{1 + \omega_2 \frac{K_{M,2}}{K_{M,5}} \left( 1 + \omega_1 \frac{K_{M,1}}{K_{M,4}} \left( \frac{1}{I^*} \right) \right)} \quad (30)$$

$$Erk_{ss}^* = \frac{1}{1 + \omega_3 \frac{K_{M,3}}{K_{M,6}} \left( 1 + \omega_2 \frac{K_{M,2}}{K_{M,5}} \left( 1 + \omega_1 \frac{K_{M,1}}{K_{M,4}} \left( \frac{1}{I^*} \right) \right) \right)} \quad (31)$$

The above dose-response curves can now be used to quantitatively predict any steady-state property of the cascade, including the dynamic range and potency. The dynamic range can be obtained in a straightforward manner by substituting Equation 30 or 31 into Equation 20. Below are the analytic equations for the range of a 2-stage and a 3-stage cascade:

$$\text{range}_{s=2} = \frac{1}{1 + \omega_2 \frac{K_{M,2}}{K_{M,5}} \left( 1 + \omega_1 \frac{K_{M,1}}{K_{M,4}} \left( \frac{1}{I_{\max}^*} \right) \right)} - \frac{1}{1 + \omega_2 \frac{K_{M,2}}{K_{M,5}} \left( 1 + \omega_1 \frac{K_{M,1}}{K_{M,4}} \left( \frac{1}{I_{\min}^*} \right) \right)} \quad (32)$$

$$\begin{aligned} \text{range}_{s=3} = & \frac{1}{1 + \omega_3 \frac{K_{M,3}}{K_{M,6}} \left( 1 + \omega_2 \frac{K_{M,2}}{K_{M,5}} \left( 1 + \omega_1 \frac{K_{M,1}}{K_{M,4}} \left( \frac{1}{I_{\max}^*} \right) \right) \right)} - \dots \\ & \dots - \frac{1}{1 + \omega_3 \frac{K_{M,3}}{K_{M,6}} \left( 1 + \omega_2 \frac{K_{M,2}}{K_{M,5}} \left( 1 + \omega_1 \frac{K_{M,1}}{K_{M,4}} \left( \frac{1}{I_{\min}^*} \right) \right) \right)} \end{aligned} \quad (33)$$

Equation 33 precisely recapitulates the results from our numerical simulations for the same values of  $\pi_s$  and  $\kappa_s$  (Figure II-11). Using Equation 32 for a 2-stage cascade, we computed the dynamic range where  $\omega_1$  and  $\omega_2$  vary independently of each other (Figure II-13). We chose to show this result for a 2-stage cascade so that the results could be displayed graphically. The model predicted that the dynamic range will depend on both  $\omega_1$  and  $\omega_2$  and that there is a region in the  $\omega_1, \omega_2$  plane for which the range is biologically significant (i.e., where the range is near 1).

Likewise, the potency can be described by an analytic expression derived from Equations 30 and 31. Given a certain dynamic range determined by  $I_{min}$  and  $I_{max}$ , the potency is equal to the  $I/I^*$  that gives half-maximal response within the dynamic range; the potency is therefore a function of  $I_{min}$ ,  $I_{max}$ ,  $\omega_s$ , and  $K_{M,i}$ . The potency has been derived for a 2-stage and a 3-stage cascade as follows:

$$potency_{s=2} = \frac{1}{2} \left( \frac{1}{I_{max}} + \frac{1}{I_{min}} \right) \frac{\left( 1 + \omega_2 \frac{K_{M,2}}{K_{M,5}} \left( 1 + \omega_1 \frac{K_{M,1}}{K_{M,4}} \left( \frac{2}{I_{max} + I_{min}} \right) \right) \right)}{\left( 1 + \omega_2 \frac{K_{M,2}}{K_{M,5}} \left( 1 + \omega_1 \frac{K_{M,1}}{K_{M,4}} \frac{1}{2} \left( \frac{1}{I_{max}} + \frac{1}{I_{min}} \right) \right) \right)} \quad (34)$$

$$potency_{s=3} = \frac{1}{2} \left( \frac{1}{I_{max}} + \frac{1}{I_{min}} \right) \frac{\left( 1 + \omega_3 \frac{K_{M,3}}{K_{M,6}} \left( 1 + \omega_2 \frac{K_{M,2}}{K_{M,5}} \left( 1 + \omega_1 \frac{K_{M,1}}{K_{M,4}} \left( \frac{2}{I_{max} + I_{min}} \right) \right) \right) \right)}{\left( 1 + \omega_3 \frac{K_{M,3}}{K_{M,6}} \left( 1 + \omega_2 \frac{K_{M,2}}{K_{M,5}} \left( 1 + \omega_1 \frac{K_{M,1}}{K_{M,4}} \frac{1}{2} \left( \frac{1}{I_{max}} + \frac{1}{I_{min}} \right) \right) \right) \right)} \quad (35)$$

Equation 35 is plotted in Figure II-12, and accurately recapitulates the results from our numerical simulations. To characterize the variation of the potency with single stage resistance, we plotted Equation 34 as a function of both  $\omega_1$  and  $\omega_2$  (Figure II-14). As

anticipated, the potency is maximized when both  $\omega_1$  and  $\omega_2$  are small. Comparing both the range and the potency for a 2-stage cascade, we observe that both properties cannot be simultaneously optimized by altering the resistance vector,  $(\omega_1, \omega_2)$ . Rather, a balance must be achieved that permits an appropriately large dynamic range to communicate with downstream modules, while having an adequate potency to sense the input.

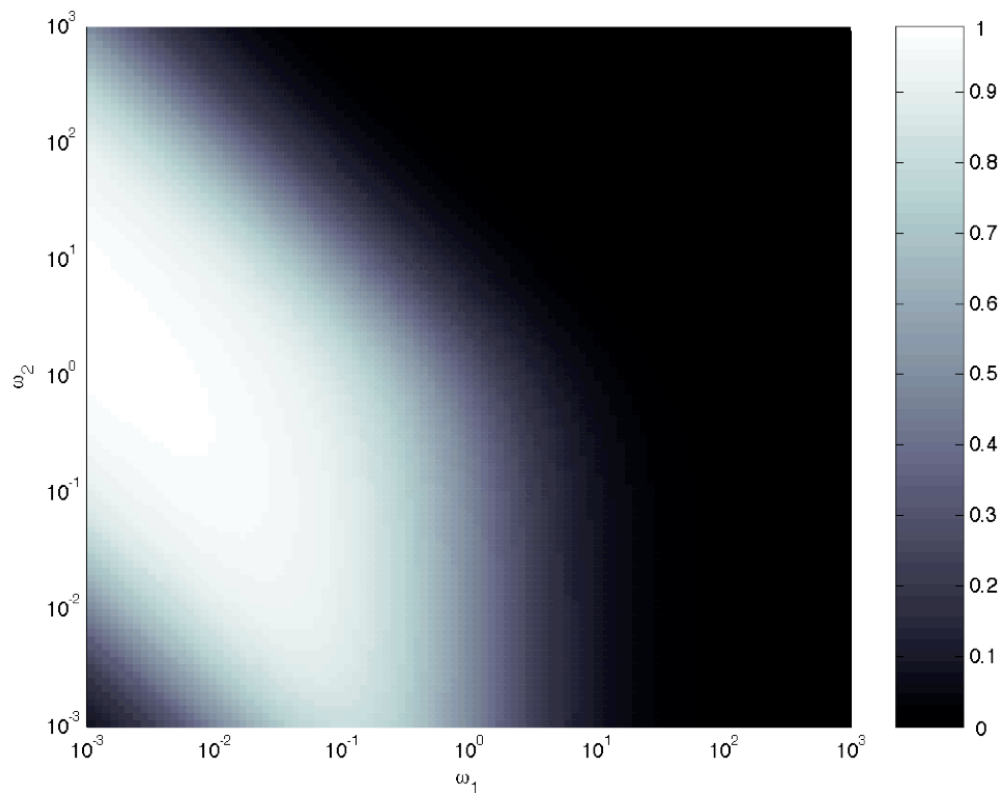


**Figure II-13. Dynamic range as a function of single stage resistances.**

The analytic solution to the dynamic range for a 2-stage cascade (Equation 32) is plotted as a function of independent resistances,  $\omega_1$  and  $\omega_2$ . The color intensity indicates the value of the range.

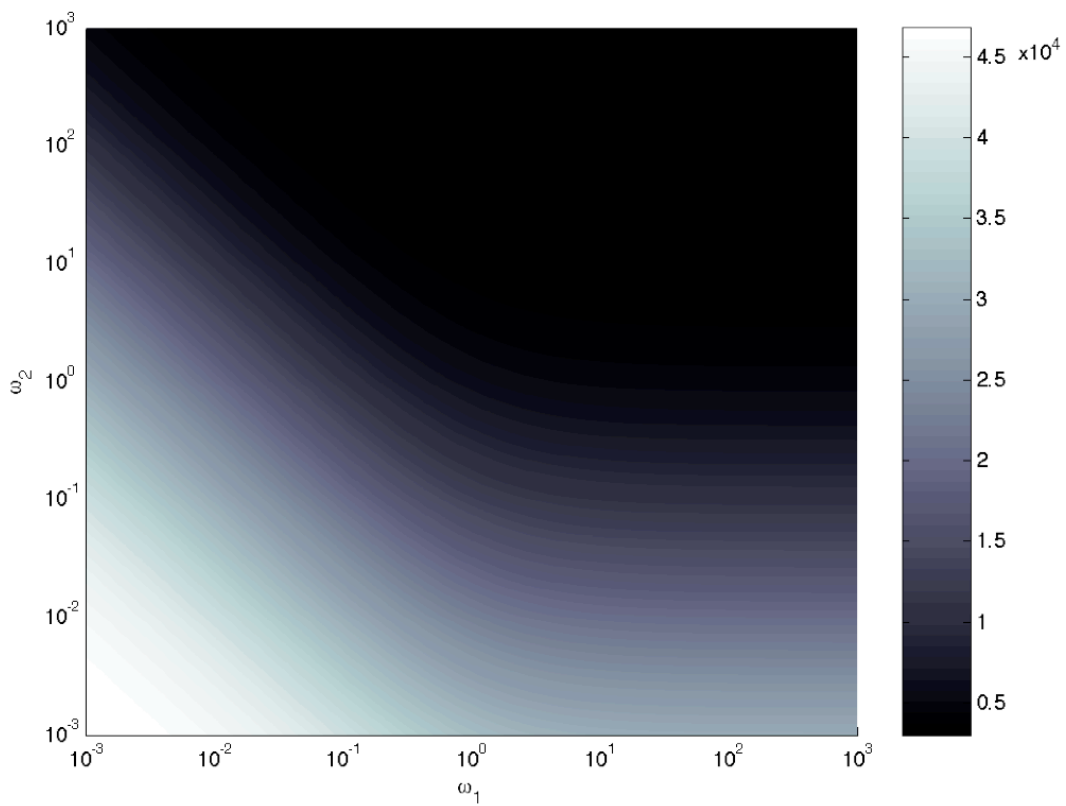


**Figure II-14. Potency as a function of single stage resistances.**

The analytic solution to the input postency for a 2-stage cascade (Equation 34) is plotted as a function of independent resistances,  $\omega_1$  and  $\omega_2$ . The color intensity indicates the value of the potency.

## 5. *Discussion*

The MAP kinase module is a recurring mode of signal transduction utilized in natural systems to regulate cell proliferation, differentiation, migration and gene expression (Lewis et al., 1998; Pearson et al., 2001). Therefore, re-engineering this module's quantitative signaling properties would offer powerful means to control a range of cell behaviors. Two important issues emerge when developing strategies to re-engineer signaling networks. First, the quantitative features most attractive to redesign must be identified. Second, an understanding as to how these features depend on parts of the circuit that are most amenable to manipulation in experimental systems must be developed. The computational analysis presented here delineates how features of the MAP kinase module such as signal amplification, range of output and signal lifetime depend on experimentally adjustable components—kinase and phosphatase expression level. Moreover, it is illustrated that the effect of perturbing the expression level of these constituents on the MAP kinase circuit may be accurately predicted through a parameter that gauges resistance to signal activation.

Signal amplification has been viewed classically as a chief function of kinase cascades, especially under conditions where downstream target outnumber upstream kinase as in the case of Raf-Mek signal exchange (Pearson et al., 2001). Model analysis suggests that this sufficiency criteria for amplification represents only a limiting condition in which the amount of kinases greatly exceed phosphatases. In this scenario, even the smallest, non-zero input triggers complete activation of all kinases in the cascade. Thus, output is assured to be greater than input, since the downstream

component is expressed at higher level. However, phosphatases such as HePTP, PP1 and PP2A, which deactivate module kinases, are expressed constitutively in many cell systems (Keyse, 2000; Saxena and Mustelin, 2000; Tamura et al., 2002). In their presence, the model predicts that even modules with greater downstream components than upstream activators may perform as attenuators. This is consistent with measurements in both yeast and mammalian cells in which signal gain is often orders-of-magnitude lower than that predicted by knowledge of relative kinase expression level alone (Ferrell, 1996). Therefore, the important parameter is not only the relative amount of upstream to downstream factors ( $\kappa_s$ ), but also the amount of phosphatase relative to kinase ( $\pi_s$ ) at each stage  $s$  of the cascade.

Integrating the contributions from these two parameters, the resistance to signal activation at each stage ( $\Omega_s$ ) effectively gauges module capacity to transduce signal. Large values for  $\Omega_s$  represent greater resistance to signal activation, impeding module response to input. One gauge of input effectiveness is its potency, which measures the amount of input required to induce half-maximal response. A single, monotonically decreasing function describes the dependence of input potency on resistance to signal activation, despite independently varying the ratio of upstream to downstream kinase amount or relative level of phosphatases and kinases. At low resistance, efficient output is produced even for small input values, thereby conferring high potency to the input.

This result would suggest that a module design with kinases and relatively minimal phosphatases would offer the strongest response to input. However, while input

potency may be enhanced by reducing resistance to activation, there is a design trade-off involving another feature—the range of output with which the module communicates to potential downstream effectors. A discrete number of active Erk molecules serve as module output. If output is a graded function of input amount, the range represents intermediate amounts of active MAP kinase with which the module may relay higher-grain information to downstream targets. Alternatively, the MAP kinase cascade may function as a switch, toggling between an on- and off-state (Huang and Ferrell, 1996). In this case, maximum range is desirable, since it dictates the ease with which downstream effectors resolve between on- and off-states. Unlike input potency, module range is a biphasic function of resistance to activation. At low and high resistances, module output is either too easily stimulated to maximum or too difficult to activate beyond near-zero response, respectively. To maximize range, an intermediate resistance to activation is required, but at the cost of input potency. Importantly, the resistance to signal activation offers predictive value in assessing this design trade-off between enhancing communication with input (input potency) versus downstream effectors (range).

In addition to steady-state features, module resistance to activation serves as a predictive tool for redesigning signal dynamics. Since transient MAP kinase signals elicit different cell behaviors than sustained signals (Marshall, 1995; Roulston et al., 1998), tuning signal lifetime has direct implications for engineering cell behavior. Model analysis indicates two regimes of control over signal lifetime. In the first regime, resistance to activation is high, ensuring rapid signal decay. In this case, input and output decay with similar kinetics, and further increasing resistance will not reduce signal

lifetime. This prediction of input-dictated control of signal lifetime is consistent with regulatory schemes employed in natural systems. In PC12 cells, EGF transiently activates Erk and promotes proliferation, while NGF-mediated sustained Erk activation leads to differentiation (Marshall, 1995). Underlying this difference, EGF drives Erk activation via an unstable protein complex including Crk, C3G and Rap1, while NGF-mediated input to the Erk module involves a stable form of the same complex (Kao et al., 2001). Hence, regulating input stability has been proposed to mediate differences in module output dynamics. Model predictions would further suggest an important role for constitutive phosphatase activity in such systems, since module resistance to signal activation is required for transient input to produce transient output.

The second regime of control over dynamics occurs at low or intermediate resistances at which input decays more rapidly than output. In this case, the time-scale of MAP kinase signal decay will be sensitive to an increase in module resistance to activation. Similar to other signaling systems in which signal adapts despite continued presence of input (Alon et al., 1999; Barkai and Leibler, 1997; Yi et al., 2000), decay of this module's output in response to a transient input is a robust property, but the time to achieve complete decay is not. In fact, this flexibility is likely exploited by natural systems, in which external stimuli not only activate kinases, but also alter phosphatase expression and/or their enzymatic activity (Keyse, 2000; Saxena and Mustelin, 2000; Tamura et al., 2002). Model results indicate that such changes would modify the resistance to signal propagation, altering signal lifetime based on environmental context. Since choice of cell behavior has been linked to MAP kinase signal dynamics, this offers

an adaptable platform to produce quantitatively distinct signals with disparate functional outcomes using a single signaling module. Such flexibility is consistent with the pleiotropic effects that individual MAP kinases exert on cell function. Furthermore, similar phosphatase-mediated flexibility has been reported in a larger scale network, which includes pathways extrinsic to the MAP kinase module involving Erk-mediated negative and positive feedback (AsthaGiri and Lauffenburger, 2001; Bhalla et al., 2002).

In summary, this work delineates features of the MAP kinase module that are attractive targets for engineering design. Moreover, it is proposed that these features may be tuned in a predictable fashion by considering a single metric—the resistance to activation. Future work will focus not only on implementing these design strategies in experimental systems, but also to exploit the modular character of our model, which focuses on mechanisms intrinsic to the MAP kinase cascade. Such modular models are an important first-step in a hierarchical strategy to represent large signal networks through interconnected modules in a manner analogous to the construction of a circuit board of interconnected integrated chips (AsthaGiri and Lauffenburger, 2000). To be effective, hierarchical models require that the mechanistic, detailed description of individual modules be substituted with computationally less intensive, yet quantitative, “operating rules.” This computational work offers such a description for the MAP kinase module by reducing the combined contributions of kinases and phosphatases into a single metric, which gauges resistance to signal activation and accurately predicts several quantitative module features. Interconnecting such analog rules for information processing, along with Boolean operations characteristic of other biochemical networks (Arkin and Ross,

1994), may help to form a quantitative basis for model reduction of large signaling networks.

## 6. Appendix

The resistance to activation accurately predicts signal half-life over a wide range of values for  $\pi_s$  and  $\kappa_s$  (see Figure II-10). Here, we examined the robustness of this predictive capability to changes in the dimensionless groups that involve rate constants, namely  $\alpha_i$ ,  $\varepsilon_i$ ,  $\tau_i$ . Sensitivity to each parameter was performed by varying its value over two orders of magnitude around its reference value (see Table II-1).

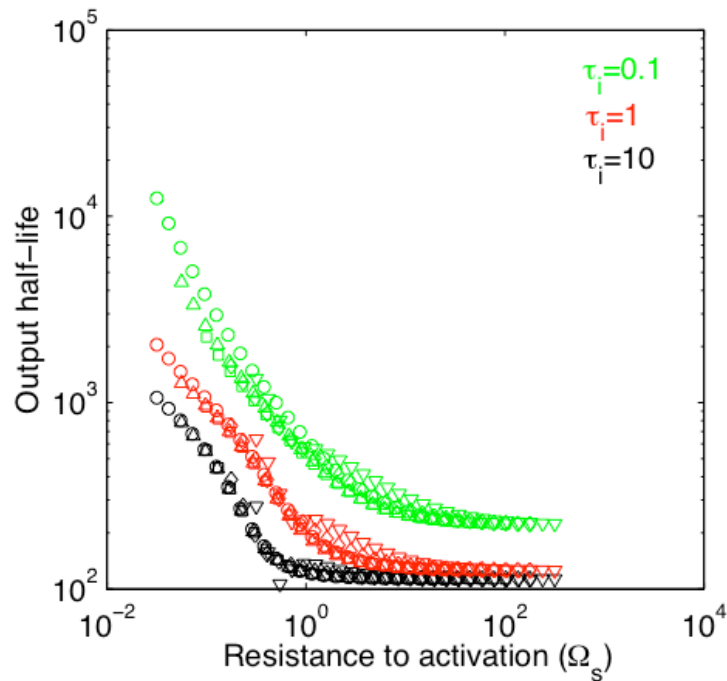


**Figure II-15. Sensitivity analysis of the ability of module resistance to predict half-life due to changes in  $\pi_s$  and  $\kappa_s$  for perturbations in  $\tau_i$ .**

The value of  $\tau_i$  was varied among 0.1 (green), 1 (red) and 10 (black). The parameters  $\pi_s$  and  $\kappa_s$  were varied over the same range as in Figure II-10, i.e.,  $\pi_s = 10^{-1} - 10^2$  and  $\kappa_s = 10^{-0.5}$  ( $\nabla$ ),  $10^{-0.25}$  ( $\diamond$ ),  $10^0$  ( $\square$ ),  $10^{0.25}$  ( $\Delta$ ),  $10^{0.5}$  (O).

As expected, for fixed  $\pi_s$  and  $\kappa_s$ , decreasing  $\tau_i$  changes the half-life of output signal (Figure II-15). Notably, for each value of  $\tau_i$  (0.1, 1 and 10 with each grouped by color), module resistance accurately predicts half-life for wide perturbations in the potential design variables— $\pi_s$  and  $\kappa_s$ . Similar robustness in the ability of module resistance to predict signal half-life for changes in  $\pi_s$  and  $\kappa_s$  is observed for perturbations in  $\varepsilon_i$  and  $\alpha_i$  (Figure II-16 and Figure II-17, respectively).

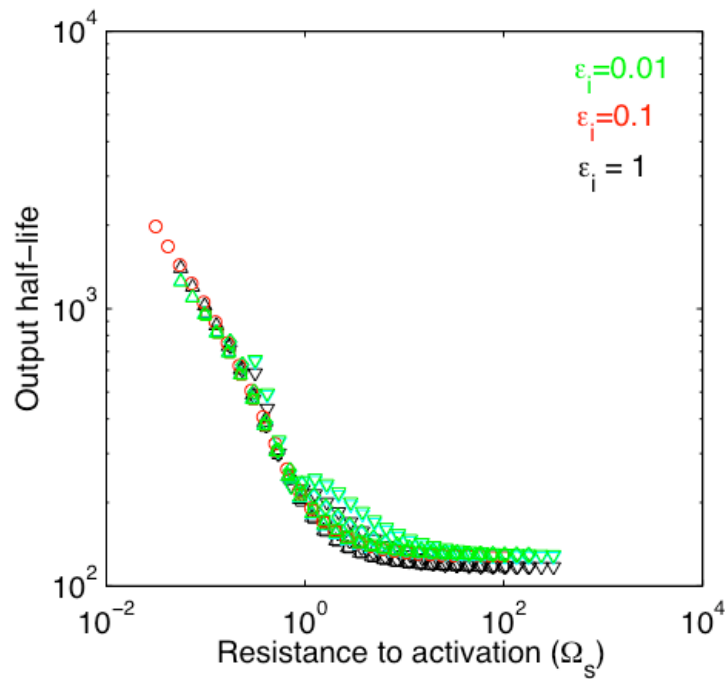


**Figure II-16. Sensitivity analysis of the ability of module resistance to predict half-life due to changes in  $\pi_s$  and  $\kappa_s$  for perturbations in  $\varepsilon_i$ .**

The value of  $\varepsilon_i$  was varied among 0.01 (green), 0.1 (red) and 1 (black). The parameters  $\pi_s$  and  $\kappa_s$  were varied over the same range as in Figure II-10, i.e.,  $\pi_s = 10^{-1} - 10^2$  and  $\kappa_s = 10^{-0.5} (\nabla)$ ,  $10^{-0.25} (\diamond)$ ,  $10^0 (\square)$ ,  $10^{0.25} (\Delta)$ ,  $10^{0.5} (O)$ .

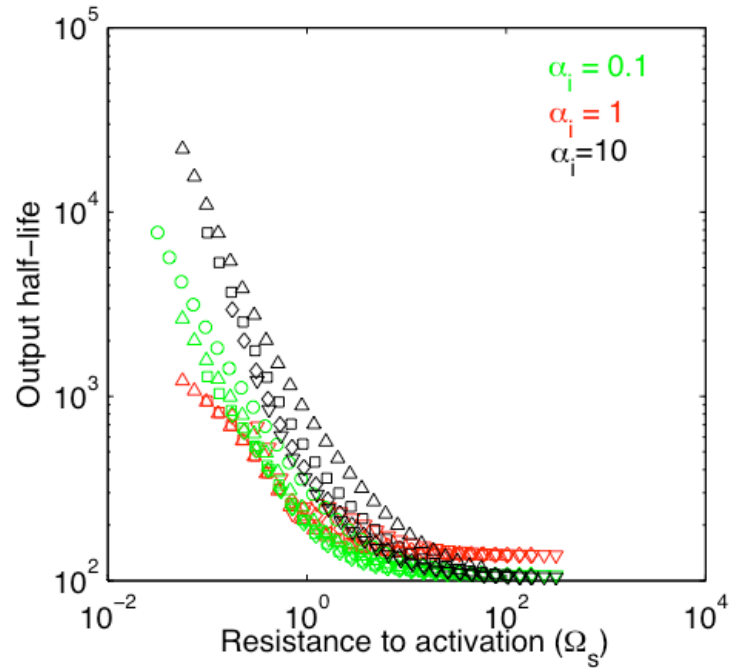


**Figure II-17. Sensitivity analysis of the ability of module resistance to predict half-life due to changes in  $\pi_s$  and  $\kappa_s$  for perturbations in  $\alpha_i$ .**

The value of  $\alpha_i$  was varied among 0.1 (green), 1 (red) and 10 (black). The parameters  $\pi_s$  and  $\kappa_s$  were varied over the same range as in Figure II-10, i.e.,  $\pi_s = 10^{-1} - 10^2$  and  $\kappa_s = 10^{-0.5}$  ( $\nabla$ ),  $10^{-0.25}$  ( $\diamond$ ),  $10^0$  ( $\square$ ),  $10^{0.25}$  ( $\Delta$ ),  $10^{0.5}$  ( $\circ$ ).

## ***7. Acknowledgements***

The authors thank M. Davis and P. Sternberg for critical review of the manuscript. Financial support was provided by the California Institute of Technology and the Institute for Collaborative Biotechnologies through grant DAAD 19-13-D-0004 from the U.S. Army Research Office.

## 8. References

- Alon, U., M.G. Surette, N. Barkai, and S. Leibler. 1999. Robustness in bacterial chemotaxis. *Nature*. 397:168-71.
- Arkin, A., and J. Ross. 1994. Computational functions in biochemical reaction networks. *Biophys J*. 67:560-78.
- Asthagiri, A.R., and D.A. Lauffenburger. 2000. Bioengineering models of cell signaling. *Annu Rev Biomed Eng*. 2:31-53.
- Asthagiri, A.R., and D.A. Lauffenburger. 2001. A computational study of feedback effects on signal dynamics in a mitogen-activated protein kinase (MAPK) pathway model. *Biotechnol Prog*. 17:227-39.
- Barkai, N., and S. Leibler. 1997. Robustness in simple biochemical networks. *Nature*. 387:913-7.
- Bhalla, U.S., P.T. Ram, and R. Iyengar. 2002. MAP kinase phosphatase as a locus of flexibility in a mitogen-activated protein kinase signaling network. *Science*. 297:1018-23.
- Brown, G.C., J.B. Hoek, and B.N. Kholodenko. 1997. Why do protein kinase cascades have more than one level? *Trends Biochem Sci*. 22:288.
- Davis, R.J. 2000. Signal transduction by the JNK group of MAP kinases. *Cell*. 103:239-52.
- Endy, D., and R. Brent. 2001. Modelling cellular behaviour. *Nature*. 409:391-5.
- Ferrell, J.E., Jr. 1996. Tripping the switch fantastic: how a protein kinase cascade can convert graded inputs into switch-like outputs. *Trends Biochem Sci*. 21:460-6.

- Ferrell, J.E., Jr. 1997. How responses get more switch-like as you move down a protein kinase cascade. *Trends Biochem Sci.* 22:288-9.
- Goldbeter, A., and D.E. Koshland, Jr. 1981. An amplified sensitivity arising from covalent modification in biological systems. *Proc Natl Acad Sci U S A.* 78:6840-4.
- Huang, C.Y., and J.E. Ferrell, Jr. 1996. Ultrasensitivity in the mitogen-activated protein kinase cascade. *Proc Natl Acad Sci U S A.* 93:10078-83.
- Kao, S., R.K. Jaiswal, W. Kolch, and G.E. Landreth. 2001. Identification of the mechanisms regulating the differential activation of the mapk cascade by epidermal growth factor and nerve growth factor in PC12 cells. *J Biol Chem.* 276:18169-77.
- Keyse, S.M. 2000. Protein phosphatases and the regulation of mitogen-activated protein kinase signalling. *Curr Opin Cell Biol.* 12:186-92.
- Levchenko, A., J. Bruck, and P.W. Sternberg. 2000. Scaffold proteins may biphasically affect the levels of mitogen-activated protein kinase signaling and reduce its threshold properties. *Proc Natl Acad Sci U S A.* 97:5818-23.
- Lewis, T.S., P.S. Shapiro, and N.G. Ahn. 1998. Signal transduction through MAP kinase cascades. *Adv Cancer Res.* 74:49-139.
- Marshall, C.J. 1995. Specificity of receptor tyrosine kinase signaling: transient versus sustained extracellular signal-regulated kinase activation. *Cell.* 80:179-85.
- Pages, G., P. Lenormand, G. L'Allemain, J.C. Chambard, S. Meloche, and J. Pouyssegur. 1993. Mitogen-activated protein kinases p42mapk and p44mapk are required for fibroblast proliferation. *Proc Natl Acad Sci U S A.* 90:8319-23.

- Park, S.H., A. Zarrinpar, and W.A. Lim. 2003. Rewiring MAP kinase pathways using alternative scaffold assembly mechanisms. *Science*. 299:1061-4.
- Pearson, G., F. Robinson, T. Gibson, B.-E. Xu, M. Karandikar, K. Berman, and M. Cobb. 2001. Mitogen-activated protein (MAP) kinase pathways: Regulation and physiological functions. *Endocrine Reviews*. 22:153-183.
- Roulston, A., C. Reinhard, P. Amiri, and L.T. Williams. 1998. Early activation of c-Jun N-terminal kinase and p38 kinase regulate cell survival in response to tumor necrosis factor alpha. *J Biol Chem*. 273:10232-9.
- Saxena, M., and T. Mustelin. 2000. Extracellular signals and sources of phosphatases: all roads lead to MAP kinase. *Semin Immunol*. 12:387-96.
- Scheele, J.S., J.M. Rhee, and G.R. Boss. 1995. Determination of absolute amounts of GDP and GTP bound to Ras in mammalian cells: comparison of parental and Ras-overproducing NIH 3T3 fibroblasts. *Proc Natl Acad Sci U S A*. 92:1097-100.
- Schoeberl, B., C. Eichler-Jonsson, E.D. Gilles, and G. Muller. 2002. Computational modeling of the dynamics of the MAP kinase cascade activated by surface and internalized EGF receptors. *Nat Biotechnol*. 20:370-5.
- Tamura, S., M. Hanada, M. Ohnishi, K. Katsura, M. Sasaki, and T. Kobayashi. 2002. Regulation of stress-activated protein kinase signaling pathways by protein phosphatases. *Eur J Biochem*. 269:1060-6.
- Tyson, J.J., K. Chen, and B. Novak. 2001. Network dynamics and cell physiology. *Nat Rev Mol Cell Biol*. 2:908-16.

Yi, T.M., Y. Huang, M.I. Simon, and J. Doyle. 2000. Robust perfect adaptation in bacterial chemotaxis through integral feedback control. *Proc Natl Acad Sci U S A.* 97:4649-53.

## CHAPTER III. QUANTITATIVE EFFECT OF SCAFFOLD ABUNDANCE ON SIGNAL PROPAGATION

### *1. Abstract*

Protein scaffolds bring together multiple components of a signaling pathway, thereby promoting signal propagation along a common physical “backbone.” Scaffolds play a prominent role in natural signaling pathways and are emerging as a promising platform for synthetic circuits. To better understand how scaffolding quantitatively affects signal transmission, we conducted an *in vivo* experimental sensitivity analysis of the yeast mating pathway to a broad range of perturbations in Ste5 abundance. Our results demonstrate that the expression level of Ste5 significantly affects several quantitative aspects of signal propagation, including signal throughput, pathway ultrasensitivity and baseline leakage. Some of these effects, such as changes in pathway responsiveness to pheromone stimulation, impact the ultimate physiological response of yeast cells. In contrast, other effects, such as the baseline leakage in MAP kinase signaling at higher expression levels of Ste5, remain buffered and do not propagate downstream. Our quantitative measurements reveal performance tradeoffs in scaffold-based modules and help to define engineering challenges for implementing molecular scaffolds in synthetic regulatory versus metabolic pathways.

## ***2. Introduction***

Protein scaffolds bind concomitantly to multiple components of a signaling pathway, thereby organizing signal transmission onto a common physical backbone (Bhattacharyya et al., 2006b). Scaffold-based modules are broadly used to propagate signals that regulate cell cycle, proliferation, differentiation and motility in species ranging from yeast to human (Pawson and Scott, 1997). Scaffolds are also emerging as a promising platform for engineering synthetic signaling modules. Molecular redesign of scaffolds has been used to alter the repertoire of scaffold binding partners, thereby redirecting signal flow (Park et al., 2003) and altering signal dynamics (Bashor et al., 2008).

In addition to the molecular design of the scaffold, the quantitative performance of scaffold-based modules will depend on the expression level of the scaffold and its binding partners. Computational models have been used to examine how the expression levels of module constituents may contribute to signal throughput (Levchenko et al., 2000). These models predict that scaffolds may not always promote signal propagation. When scaffold concentration exceeds an optimal level, enzymes and substrates are predicted to bind to distinct scaffolds rather than onto a single backbone, thereby inhibiting signal transmission via combinatorial inhibition.

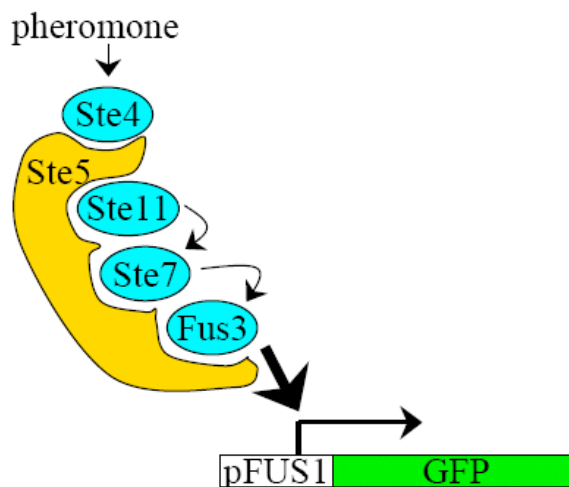


**Figure III-1. The Ste5 scaffold and the pheromone MAP kinase pathway in *S. cerevisiae*.**

Ste5 has independent binding sites for Ste4, Ste11, Ste7 and the MAP kinase, Fus3. Another MAP kinase, Kss1 (not depicted for clarity), also binds Ste5, albeit with lower affinity than Fus3, and is also activated by Ste7. Upon pheromone stimulation, Ste5 facilitates signal transmission from Ste4 to Fus3/Kss1. Active Fus3 and Kss1 trigger the transcription of *FUS1*, cell cycle arrest, and ultimately mating.

These and other model predictions, however, are based on idealized mathematical representations of scaffold-based signaling. In contrast, scaffold-mediated signaling *in vivo* is often far more intricate as exemplified for the prototypical scaffold Ste5 in yeast cells (Figure III-1). Some of the binding partners of Ste5 (e.g., Ste7 and Fus3) dock with each other independent of the scaffold (Bardwell et al., 1996). This scaffold-independent interaction may compete with scaffold-mediated signaling, rendering scaffold-based signaling ‘brittle’ to variations in the expression levels of critical components (Ferrell 2000). Furthermore, dimerization of Ste5 and other scaffolds is a critical step in signal transmission (Yablonski et al., 1996) and may contribute to apparent cooperativity

(Ferrell 2000). In addition, Ste5 translocates between different subcellular compartments (Pryciak and Huntress, 1998; van Drogen et al., 2001), is regulated by Fus3-mediated negative feedback (Bhattacharyya et al., 2006a) and binds competitively to multiple proteins (Fus3 and Kss1) with different affinities (Kusari et al., 2004). This complex array of mechanisms conceals precisely how real scaffolds such as Ste5 quantitatively contribute to signal transmission *in vivo*.

To better understand the quantitative contribution of the Ste5 scaffold to signal transmission, we conducted an *in vivo* experimental sensitivity analysis of the mating pathway to a broad range of perturbations in Ste5 abundance. Our results demonstrate that perturbations in scaffold abundance have significant effects on several quantitative aspects of signal propagation, including signal throughput, baseline drift and pathway ultrasensitivity.

### 3. Results and Discussion

#### 3.1 Modulation of scaffold expression level

To better understand the quantitative effect of scaffold abundance on pheromone-mediated MAP kinase signaling, we engineered a panel of yeast strains that express Ste5 at different levels. Starting with a *ste5Δ* null parent strain, we introduced a C-terminal, myc-tagged version of *STE5* under the regulation of various constitutive promoters (Mumberg et al., 1995) and measured the relative expression level of Ste5 in the different strains by a quantitative immunoblot procedure (see Materials and Methods and Figure III-8 in Supplementary Data). Ste5 expression in this panel of yeast strains spanned nearly two orders of magnitude (Figure III-2). The highest level of expression was 50-fold greater than that supported by the wild-type *STE5* promoter.

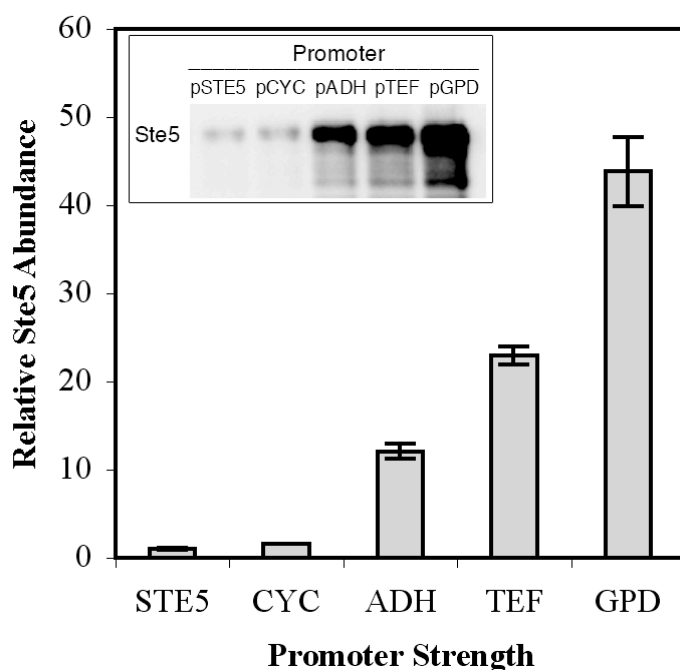


**Figure III-2. Modulating the expression level of the scaffold Ste5.**

Myc-tagged Ste5 was expressed behind an array of constitutive promoters (pCYC, pADH, pTEF and pGPD), including the wild-type *STE5* promoter (pSTE5). Vectors were transformed into a *ste5Δ* yeast strain, and the relative expression levels of Ste5 were measured by quantitative immunoblot with standard curve. Error bars denote standard error (n=3).

### ***3.2 Effect of scaffold on signal throughput and pathway ultrasensitivity***

To quantify the sensitivity of the mating pathway to Ste5 abundance, we measured the mating transcriptional response over a broad range of  $\alpha$ -factor concentrations in our panel of yeast strains. Variations in scaffold abundance had a significant effect on the transcriptional output of the mating pathway (Figure III-3). At every dose of the  $\alpha$ -factor stimulus, the output was biphasic with respect to the level of Ste5, revealing that an optimum level of Ste5 scaffold is needed to maximize signal throughput. This biphasic relationship is consistent with model predictions (Levchenko et al., 2000) and with previous studies of mammalian scaffolds JIP and KSR (Ferrell, 2000; Levchenko et al., 2000). Past studies involving Ste5 overexpression reported only signal augmentation (Kranz et al., 1994) (Choi et al., 1994; Kranz et al., 1994). Our data shows, however, that this may have been a limitation in the range of Ste5 overexpression explored in those studies rather than a fundamental difference between Ste5 and mammalian scaffolds.

(Section 3.2 continues after Figure III-3.)

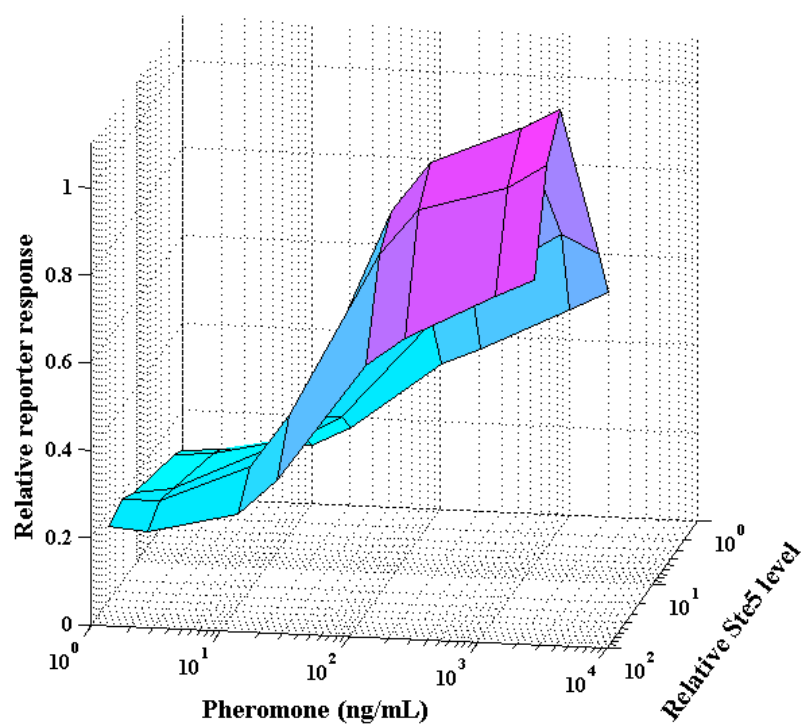
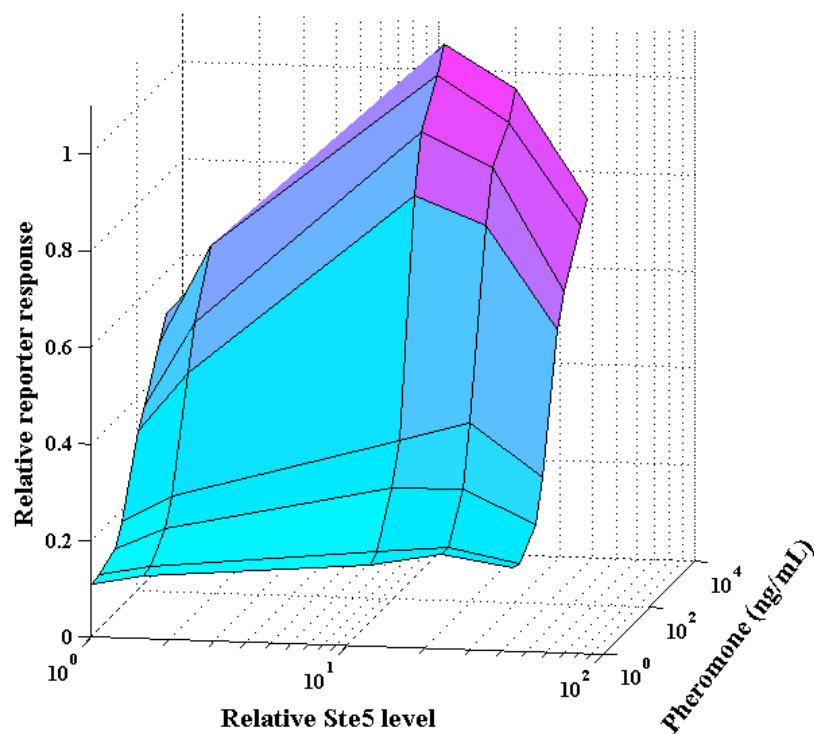


**Figure III-3. Sensitivity analysis of mating pathway response to perturbation in scaffold abundance.**

Yeast cells expressing different levels of Ste5 were induced with  $\alpha$ -factor for 2.5 h. The pFUS1-GFP reporter response was measured by flow cytometry. The relative mean GFP fluorescence is shown for the various Ste5 expression levels and  $\alpha$ -factor doses. Two different views of the surface plot are shown.

In addition to the magnitude of pathway response, Ste5 abundance has a significant effect on the responsiveness of the mating pathway. Fitting the Hill equation to the dose-response curves revealed that both the Hill coefficient ( $n_H$ ) and the pheromone dose at which half-maximal response is achieved ( $EC50_\alpha$ , a widely used biological metric that is inversely related to stimulus potency) are significantly affected by Ste5 expression level (See Supplementary Data, Figure III-9, and Table III-3). At the wild-type level of Ste5, approximately a greater than 100-fold change in pheromone concentration was required to shift from 10% to 90% of maximal response ( $n_H = 0.93$ ); in contrast, at the optimum dose of Ste5, a 25-fold change in pheromone concentration was sufficient to achieve an equivalent shift in reporter output ( $n_H = 1.4$ ). This enhanced cooperativity did not involve a shift from graded to all-or-none response at the single-cell level (Figure III-9). Rather, at the optimum scaffold expression level, the transcriptional output in individual cells was more responsive to changes in pheromone concentration. In addition to a steeper response to pheromone dose, the  $EC50_\alpha$  shifted from 100 ng/mL to 50 ng/mL when Ste5 expression is increased from its wild-type level to its optimum.

These measurements reveal that maximum signal throughput, apparent cooperativity and  $\alpha$ -factor potency occur at approximately the same optimum level of Ste5. To test whether these significant changes in the transcriptional response translate to the ultimate biological response, we assessed the mating response of yeast cells using the halo assay. Here, the pheromone is supplied from a central source and induces cell cycle arrest up to a radius beyond which the pheromone concentration is too low for cells to respond. Since the  $EC50_\alpha$  of the transcriptional response is sensitive to Ste5 level, we

tested whether the radius of the halo exhibits a similar dependence on scaffold expression level. As Ste5 expression was increased from its wild-type level, the size of the mating halo increased until reaching a maximum at an optimal dose of Ste5 (Figure III-4). Increasing Ste5 expression level beyond this optimum reduced the size of the mating halo. The optimum level of Ste5 that maximizes the halo radius precisely correlates with the optimum Ste5 level for transcriptional response.

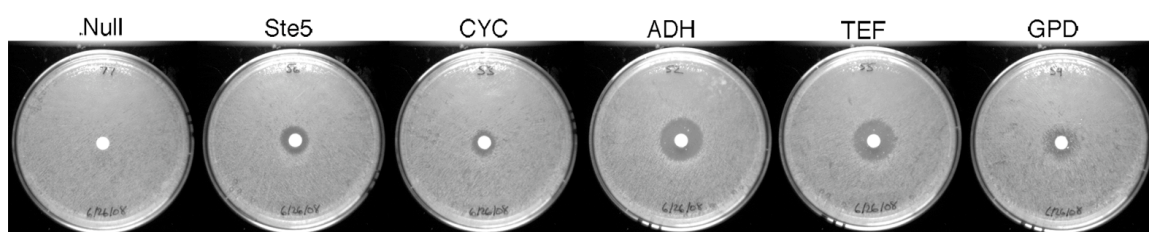


**Figure III-4. Perturbation of scaffold abundance quantitatively alters phenotypic response.**

The mating halo assay was performed in cells expressing different levels of Ste5. Results from a single representative out of two independent trials are shown.

### *3.3 Closer examination of the Ste5 module*

Transcriptional response and cell-cycle arrest are several steps downstream of the direct MAP kinase outputs of the Ste5 scaffold. To confirm that the effect of Ste5 perturbations on the mating pathway truly emanates from the direct outputs of the Ste5 module, we measured the phosphorylation of the mating MAP kinases, Fus3 and Kss1, by quantitative Western blotting. At the saturating dose of 2  $\mu\text{g/mL}$   $\alpha$ -factor, the levels of both phospho-Fus3 and phospho-Kss1 exhibit a biphasic dependence on Ste5 abundance (Figure III-5). Furthermore, the biphasic dependence of MAP kinase signaling on

scaffold abundance closely matches the trend in the transcriptional output (Figure III-6).

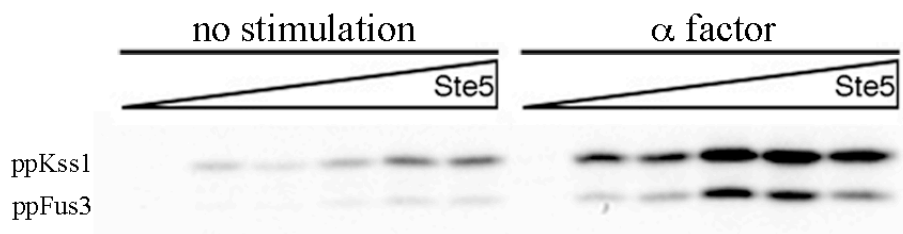


**Figure III-5. Phospho-MAPK response to perturbation in Ste5 expression.**

Yeast cells were induced with  $\alpha$ -factor or left unstimulated for 15 minutes and phospho-Fus3 and phospho-Kss1 were analyzed by immunoblot.

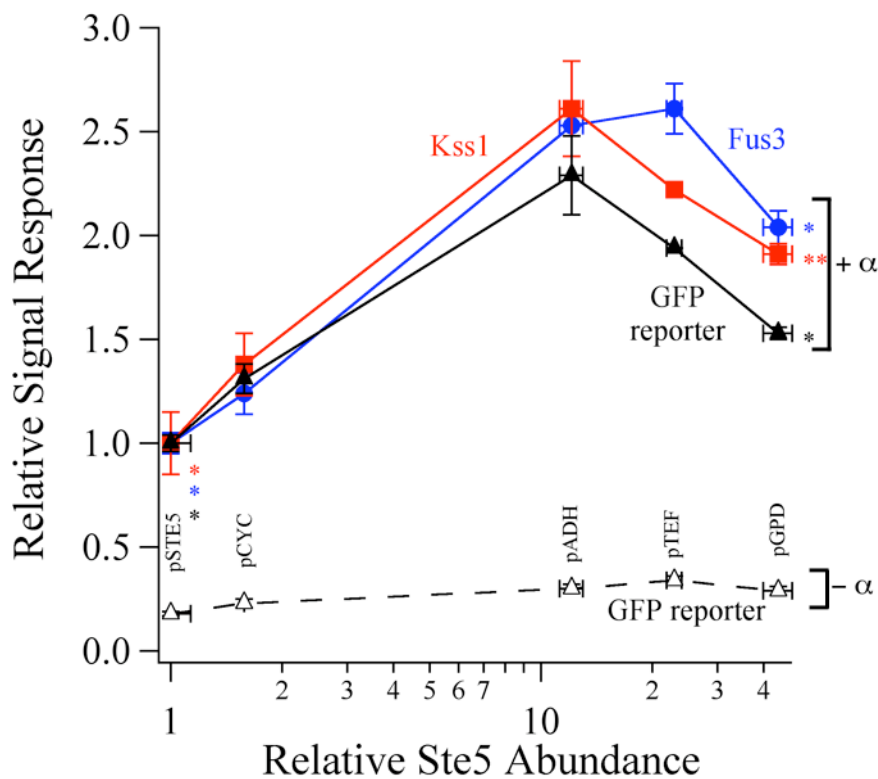


**Figure III-6. Quantitative measurements of phospho-MAP kinase and pFUS1-GFP responses.**

The levels of the phospho-MAP kinases were normalized by their respective total protein expression. Error bars denote standard error ( $n=3$ ). The *asterisks* indicate the  $p$ -value between the marked data point and the maximum data point for a given curve: \*,  $p < 0.01$  and \*\*,  $p < 0.05$  (Student's  $t$  test).

These measurements also revealed that both phospho-Fus3 and phospho-Kss1 exhibit a similar biphasic dependence on Ste5 abundance, suggesting that a common upstream factor, such as Ste7, may be the limiting component. To test this hypothesis, we overexpressed HA-tagged Ste7 in our panel of yeast strains that express Ste5 at different levels (Figure III-7). In parallel, we constructed a control panel of yeast strains that carries an empty control vector. At low scaffold abundance, overexpression of Ste7 did not appreciably alter the mating reporter response relative to control cells carrying the empty vector (Figure III-7). However, at higher scaffold concentrations, overexpression of Ste7 significantly increased the reporter response and eliminated the downturn in signal throughput.

These results demonstrate a scaffold-limited and Ste7-limited regime of signaling. When the scaffold is the limiting factor to signal throughput (for scaffold doses below the optimum), increasing the expression of Ste7 had no effect on signal throughput. However, past the optimum dose of scaffold, signal throughput was limited by Ste7. Overexpression of Ste7 eliminated the biphasic dependence of signal throughput on scaffold amount, at least within the range of Ste5 expression explored. We reason that the optimum Ste5 dose has shifted to a level higher than that captured by our panel of yeast strains. These results demonstrate quantitatively that the abundance of scaffold and its binding partners together shape the biphasic dependence of signal throughput and determine the optimum dose of scaffold.

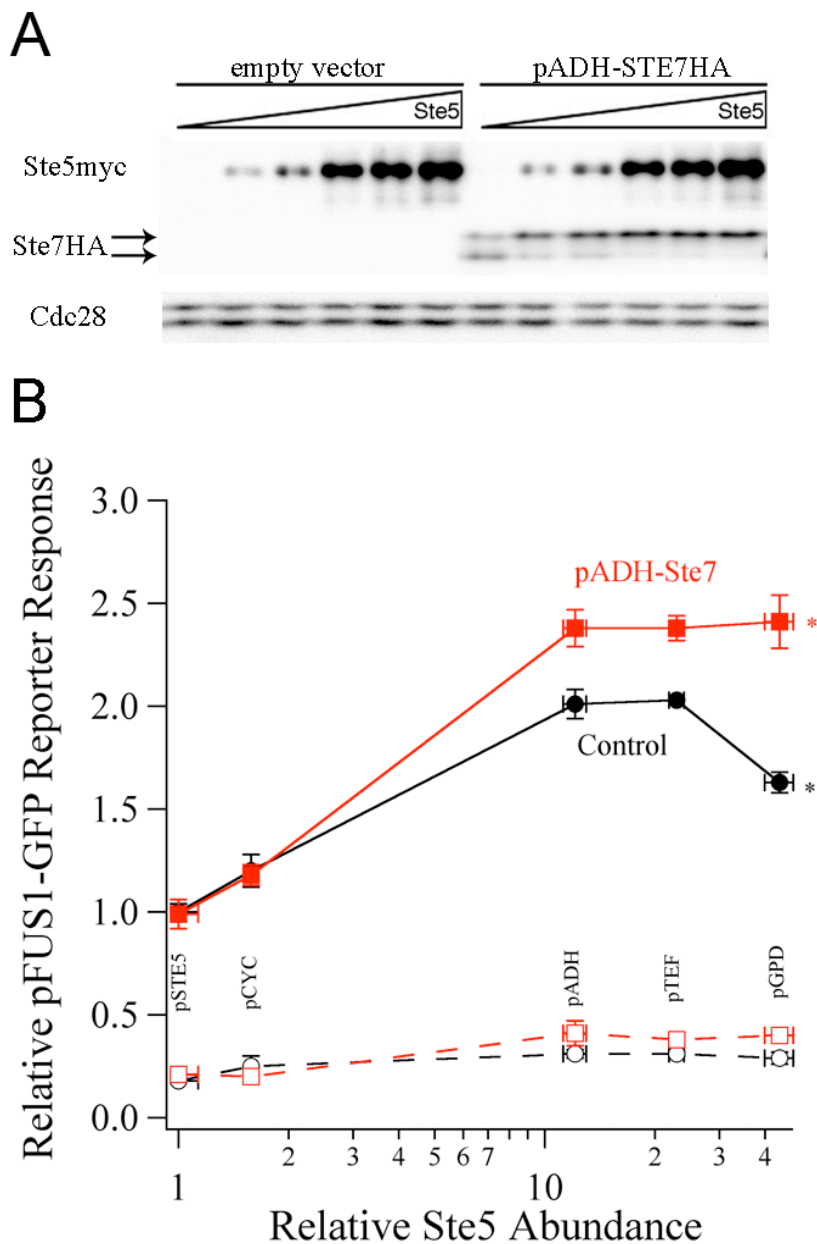


**Figure III-7. Scaffold-limited and Ste7-limited regimes of signaling.**

(A) Yeast strains expressing different levels of Ste5 were transformed with either an empty vector control or a vector encoding HA-tagged Ste7 downstream of an ADH promoter. The expression of Ste5myc and Ste7HA were confirmed by immunoblot. (B) Yeast overexpressing Ste7 or not were stimulated with  $\alpha$ -factor for 2.5 h, and the pFUS1-GFP reporter response was quantified by flow cytometry. Error bars denote standard error (n=4). The *asterisks* indicate the *p*-value between the marked data points: \*,  $p < 0.01$  (Student's *t* test).

### ***3.4 Sensitivity of signal quality to scaffold abundance***

Our data demonstrate that the optimum dose of Ste5 provides a number of improvements to signal transmission and raises the question of whether there are tradeoffs in other metrics of pathway performance. Scaffolds play an important role in maintaining the fidelity of stimulus-response relationships between pathways that use a common pool of signaling intermediates. We tested whether changes in Ste5 expression level affect cross-activation between two closely related pathways, the pheromone and the high-osmolarity MAP kinases pathways (see Supplementary Data and Figure III-10). Pheromone stimulation activated only the mating MAP kinases and did not stimulate phosphorylation of Hog1, the high-osmolarity MAP kinase. Meanwhile, stimulation with sorbitol appropriately activated Hog1 with no cross-activation into the pheromone pathway. Thus, across nearly 50-fold change in Ste5 expression level, signal fidelity is maintained.

Another important metric of the performance of signaling modules is the signal-to-noise ratio. High-quality signal transmission involves maintaining a low baseline signal in the absence of stimulation, while responding with a strong signal when the stimulus is present. To investigate the effect of increased scaffold abundance on baseline signaling, we examined the phosphorylation of Fus3 and Kss1 in the absence of pheromone. Our measurements show that increasing Ste5 expression elevates the basal activities of Fus3 and Kss1 (Figure III-5). In fact, the baseline level of phosphorylated Fus3/Kss1 among cells expressing high levels of scaffold was equal to the pheromone-induced response in cells expressing wild-type levels of Ste5. Interestingly, this

significant baseline leakage in Fus3/Kss1 signaling is not propagated to the downstream transcriptional response. The baseline pFUS1-GFP response exhibited little change across a 50-fold change in Ste5 expression (Figure III-6). Thus, although baseline activation of the immediate outputs of the Ste5 module is compromised, the downstream transcriptional mating response is buffered and maintains a normal baseline level at all expression levels of Ste5.

### ***3.5 Potential implications for natural and synthetic scaffold-based modules***

Our results reveal that the wild-type expression level of Ste5 is not set for optimum throughput and responsiveness (Figure III-3) and suggest potential reasons for this sub-optimal configuration. The most straightforward explanation is that operating at half-maximal throughput permits regulatory flexibility to tune up or down module performance. Indeed, our data show that such modulation of throughput would have quantitative effects on the ultimate biological response. Furthermore, operating in the Ste5-limited regime permits the tuning of pathway performance solely by tuning altering Ste5 expression level and makes the module less sensitive to perturbations in other module components. Finally, our measurements suggest that there may be a penalty for operating at the optimum level of Ste5. Baseline activation of Fus3/Kss1 significantly increases; while this baseline leakage does not affect the quality of the mating response, other cellular activities regulated by these kinases may be adversely affected.

Molecular scaffolds offer a promising platform for engineering synthetic regulatory and metabolic circuits. Our results suggest that baseline leakage may be a

potential design constraint for scaffold-based synthetic regulatory circuits, an issue that the natural mating pathway has circumvented. Baseline leakage, however, is not a critical drawback for metabolic scaffold-based pathway, since by definition, as these pathways require an input molecule on which molecular transformations would be carried out. In addition to baseline performance, our data suggests that shifting to an optimal dose of scaffold provides only a 2-3 fold improve in signal throughput. In regulatory circuits, such quantitative changes have important implications for downstream response as we have demonstrated for pheromone-mediated cell cycle arrest. In addition, it has recently been demonstrated that even a mild change in the strength of Fus3 signaling has significant qualitative effects on the phenotypic response to pheromone stimulation (Hao et al., 2008). In other biological contexts, small differences in signals lead to drastic switch-like responses in cell decisions (Ferrell, 1996). Thus, scaffold-mediated contributions to signal flux could play a significant role in synthetic circuits. However, in metabolic circuits, improving product yield by 2-3 fold may not provide significant process advantages. Thus, our results suggest both promising opportunities and potential engineering challenges for the utilization of scaffolds in regulatory versus metabolic synthetic circuits. By quantitatively delineating these tradeoffs, our results help to define the engineering challenges that must be addressed to effectively implement scaffolds in synthetic circuits.

## 4. Materials and Methods

### 4.1 Strains

The strains used in this study are listed in Table III–1 and were kindly provided by Elaine Elion of Harvard University and by Wendell Lim of UCSF.

**Table III–1. Yeast strains used in this study.**

| Strain              | Description  |
|---------------------|--|
| CB011 <sup>1</sup>  | W303 <i>MATa</i> , <i>ste5::KanR</i> , <i>bar1::NatR</i> , <i>far1Δ</i> , <i>mfa2::pFus1-GFP</i> , <i>his3</i> , <i>trp1</i> , <i>leu2</i> , <i>ura3</i> |
| EY1775 <sup>2</sup> | W303 <i>MATa</i> , <i>ste5::TRP1</i> , <i>bar1Δ</i> , <i>his3</i> , <i>trp1</i> , <i>leu2</i> , <i>ura3</i> , <i>ade2</i> , <i>can1</i>                  |

<sup>1</sup> Strain kindly provided by Wendell Lim at UCSF (Bhattacharyya et al., 2006a).

<sup>2</sup> Strain kindly provided by Elaine Elion at Harvard (Flotho et al., 2004).

### 4.2 Plasmid constructs

The plasmids used in this study are listed in Table III–2. Vectors containing the *STE5* allele, the *STE7* allele, the 13Myc and 3HA epitope tags, and the ADH/CYC1/GPD/TEF promoters that were kindly provided by Elaine Elion (Harvard University), Christina Smolke (Caltech), Ray Deshaies (Caltech) and David Chan (Caltech), respectively. The *STE5* allele was sub-cloned by PCR from plasmid pSKM12 (Table III–2) and was ligated into the base shuttle vector pRS416 (low-copy CEN/ARS, URA3). The *STE7* allele was sub-cloned from plasmid pVS10 (Table III–2) and was ligated into the base shuttle vector pRS415 (low-copy CEN/ARS, LEU2). The 13Myc and 3HA epitope tags were subcloned from plasmids pFA6a-13Myc-His3MX6 and pFA6a-3HA-His3MX6 (Table III–2), respectively, and were fused to the C-terminus of the gene of interest in the base shuttle vectors. The various constitutive promoters were

sub-cloned from the following vectors: p416ADH, p416CYC1, p416GPD, and p416TEF (Table III–2). The native *STE5* promoter was cloned from W303 genomic DNA by PCR, encompassing a sequence 800 bp upstream to the start codon. All promoters were inserted into the base shuttle vector immediately upstream of the start codon of the gene of interest.

**Table III–2. Plasmids used in this study.**

| Name    | Parent Vector | Promoter <sup>1</sup> | Description             |
|---------|---------------|-----------------------|-------------------------|
| pSC6-G  | pRS416        | GPD                   | Empty vector            |
| pSC7-A  | pRS416        | ADH                   | STE5-13Myc <sup>2</sup> |
| pSC7-C  | pRS416        | CYC1                  | STE5-13Myc              |
| pSC7-G  | pRS416        | GPD                   | STE5-13Myc              |
| pSC7-T  | pRS416        | TEF                   | STE5-13Myc              |
| pSC7-P  | pRS416        | STE5                  | STE5-13Myc              |
| pSC10-G | pRS415        | GPD                   | Empty vector            |
| pSC11-A | pRS415        | ADH                   | STE7-3HA <sup>3</sup>   |

<sup>1</sup> All promoters listed (except the native *STE5* promoter) are from (Mumberg et al., 1995).

<sup>2</sup> The *STE5* allele is from pSKM12 (Flotho et al., 2004). The 13Myc epitope tag is from pFA6a-13Myc-His3MX6 (Longtine et al., 1998).

<sup>3</sup> The *STE7* allele is from pVS10 (van Drogen et al., 2001). The 3HA epitope tag from pFA6a-3HA-His3MX6 (Longtine et al., 1998).

### 4.3 Western blot

#### 4.3-1 Cell growth and lysis

Yeast cells grown on selective media at mid-log phase growth (OD ~ 1.0, 1.3e7 cells/mL) were induced with 1.2μM α-factor or 1M sorbitol and incubated for 15 minutes at 30°C. TCA was added to 8mL cells at a final concentration of 20%, and incubated on ice for 5 minutes. Cells were then collected and washed 3x with 1mL Tris-HCl pH = 8.0 by centrifugation to ensure good solubility of protein. SDS-urea buffer [50μL water and

100 $\mu$ L of 125 mM Tris-HCl pH = 7.5, 8M urea, 4% (wt g/vol mL) SDS, 2% (vol/vol)  $\beta$ -mercaptoethanol, 0.02% (wt g/vol mL) bromophenol blue] was added with ~50 $\mu$ L acid-washed glass beads (425-600 $\mu$ m). Cells were homogenized using Fast Prep (Bio101 Savant) at speed 6.5 for 45 seconds, and then whole cell lysate was incubated at 42°C for 15 minutes to promote protein solubilization. After centrifugation for 15 minutes at max speed in a tabletop centrifuge, 50 $\mu$ L lysate was recovered and diluted by SDS-loading buffer [300 $\mu$ L of 50mM Tris-HCl pH = 6.8, 12% (vol/vol) glycerol, 2% (wt g/vol mL) SDS, 1% DTT, 0.01% (wt g/vol mL) bromophenol blue].

#### ***4.3-2 SDS-PAGE – quantitative Western blots only***

To obtain quantitative data, many modifications to the standard Western blot protocol were made. To validate the linear comparison of samples within a gel, a standard curve consisting of ~7 data points was included with each gel as an internal control. To minimize variability of quantification, samples to be compared in a given gel were loaded in quadruplicate. Figure III-8 displays a typical quantitative Western blot for Ste5myc measurement. This approach requires the concomitant analysis of multiple samples on a single gel; thus, all quantitative gels were run using a wide-gel apparatus (TV-200YK from Topac) that accommodated 30 lanes in a single gel.

The dynamic range of the Western blot protocol is limited. To successfully detect all samples within a common dynamic range (as defined by the standard curve), samples were diluted as required in whole cell lysate of equivalent protein concentration but lacking the antigenic protein of interest. (Finding the proper dilutions for each blot was

accomplished through an iterative procedure.) We loaded lanes, whenever possible, with an equivalent lysate volume and protein concentration. This was done to mitigate pipetting error during gel loading, and to prevent horizontal band dispersion during electrophoresis (this effect complicates the box-drawing step of quantitation).

#### ***4.3-3 Immuno-blotting***

Blots were transferred to nitrocellulose (Biorad) and were blocked for 1 hour in 3% milk TBST solution. Primary antibody incubation was conducted in blocking buffer overnight at 4°C. Primary antibodies and dilutions used in this study were as follows: anti-myc for detection of Ste5myc, 1:10,000 (9e10 Covance); anti-Cdc28 for equal loading control, 1:10,000 (sc-53 Santa Cruz Biotechnologies); anti-phospho-p44/42 MAPK for activity of both Fus3 and Kss1, 1:1,000 (9101 Cell Signaling Technology); anti-Fus3 for total Fus3, 1:1,000 (sc-6773 Santa Cruz Biotechnologies); anti-Kss1 for total Kss1, 1:500 (sc-28547 Santa Cruz Biotechnologies); anti-HA for detection of Ste7HA, 1:10,000 (MMS-101R Covance); and anti-phospho-p38 MAPK for phospho-Hog1, 1:1,000 (9211 Cell Signaling Technology). HRP-conjugated secondary antibodies (Biorad) were used at dilution 1:10,000. Blots were treated with Supersignal West Pico or Femto substrate (Pierce) and images were recorded using the Versa-Doc 3000 imager (Biorad).

#### ***4.3-4 Analysis – quantitative Western blots only***

Signal intensities were quantified using the Volume tool in Quantity1 software. For each blot, equivalently sized, rectangular boxes were drawn around each band. A global background measurement was taken and was subtracted from all band intensities.

For each blot, a standard curve was constructed via linear regression. The signal intensities for experimental samples were averaged and then interpolated using the standard curve (Figure III-8). The interpolated values were then adjusted for the differential volumes used during loading by dividing by the respective volume loaded. The output of this calculation yields the final data from a single quantitative Western blot.

Data from anti-myc Ste5, anti-phospho-Fus3, and anti-phospho-Kss1 blots were subsequently normalized by the following equal loading controls: total Cdc28, total Fus3, and total Kss1, respectively. Signal intensities for the equal loading controls were determined through the same quantitative procedure described above.

#### ***4.4 Flow cytometry***

Yeast cells grown on selective media at mid-log phase growth (OD ~ 0.1-1.0) were induced with 1.2 $\mu$ M  $\alpha$ -factor or 1M sorbitol and incubated for 2.5 hours at 30°C. One mL ice cold TE buffer was added to 0.5mL cells. Cells were spun at 2000rcf in a tabletop centrifuge and were resuspended in 1mL cold TE buffer. Cells were briefly

vortexed to break up cell clumps, and Fus1-GFP was detected using the Cell Lab Quanta SC flow cytometer from Beckman Coulter.

Data was analyzed as described previously with the following modifications (Bhattacharyya et al., 2006a). Electronic volume, a rough measurement of cell size, was used instead of forward scatter. Cells were first gated on a side scatter versus electronic volume plot, and then cells were gated on a GFP versus side scatter plot to quantify fluorescence.

#### ***4.5 Halo assays for $\alpha$ -factor sensitivity***

Halo assays were performed as previously described except that assays were performed on normal selective media with neutral pH (Sprague, 1991).

## ***5. Acknowledgements***

The authors thank members of the Asthagiri and Deshaies labs for helpful discussions and guidance with experiments, D. Chan, R. Deshaies, C. Smolke, E. Elion and W. Lim for reagents, and E. Davidson, R. Deshaies and P. Sternberg for comments on the manuscript. This work was supported by the Institute for Collaborative Biotechnologies through grant DAAD19-03-D-0004 from the U.S. Army Research Office. S. Chapman was supported by the NIH Molecular Cell Biology Training Grant (NIH/NRSA 5T32GM07616).

## 6. Supplementary Data

### 6.1 Quantitative Western blot analysis

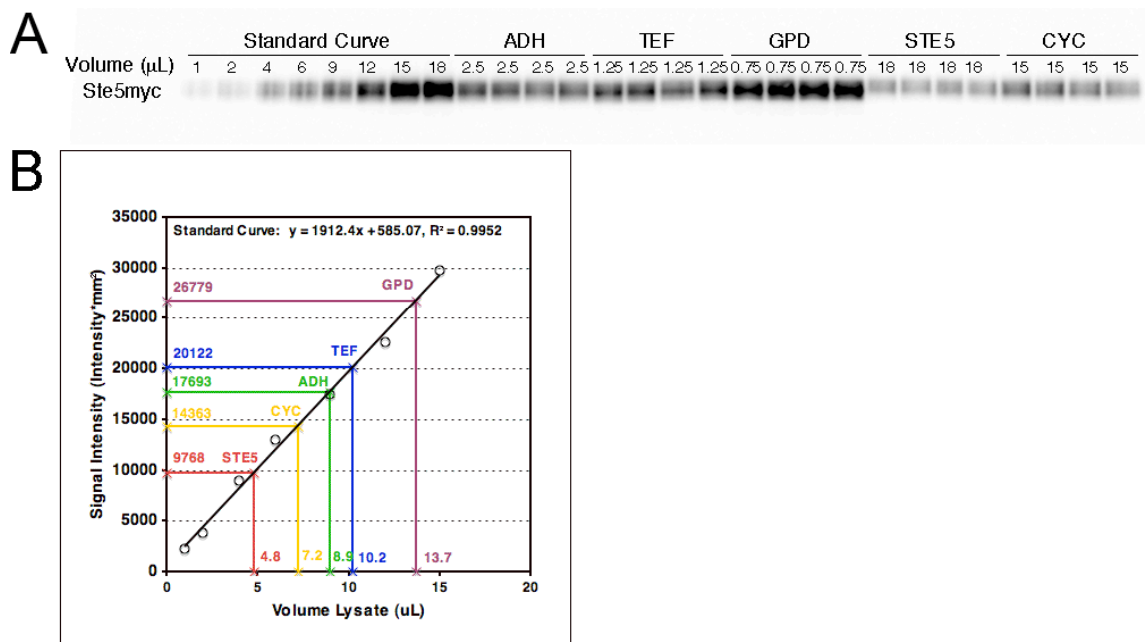


**Figure III-8. Quantitative Western blot of Ste5myc abundance.**

(A) Lysates of yeast expressing varying levels of Ste5myc were loaded in quadruplicate along with a standard curve in a single gel. Samples were differentially loaded by the volume indicated in order that all signals fall within the dynamic range of the standard curve. All lanes were loaded with a minimum of 15  $\mu\text{L}$  total lysate using a filler lysate that lacked the antigenic protein of interest. Using Quantity1 software, boxes were drawn around the bands to obtain signal intensities (not shown). (B) Interpolation of quantitative Ste5 data from standard curve. The standard curve corresponding to the blot in part A was plotted and a linear fit was determined by regression. Mean signal intensities for the five yeast strains expressing varying amounts of Ste5 are displayed on the y-axis. The signal intensities were used to interpolate a corresponding volume of lysate from the standard curve. The interpolated values are indicated on the x-axis.

## 6.2 Dose-response properties as a function of *Ste5* abundance

For each expression level of *Ste5*, the dose-response data displayed in Figure III-3 and Figure III-9 were fit to the Hill equation of the following form:

$$y - y_{\min} = y_{\max} \cdot \frac{x^{n_H}}{EC50_{\alpha}^{n_H} + x^{n_H}}$$

where  $y$  is the predicted pFUS1-GFP response and  $x$  is the  $\alpha$ -factor dose. The parameters determined by non-linear regression were  $y_{\min}$  (the pFUS1-GFP fluorescence corresponding to 0  $\mu\text{g/mL}$  pheromone),  $y_{\max}$  (the pFUS1-GFP fluorescence corresponding to 2  $\mu\text{g/mL}$ ),  $EC50_{\alpha}$  (the dose of  $\alpha$ -factor that elicits half-maximal response), and  $n_H$  (the Hill coefficient). Hill coefficients,  $EC90_{\alpha}/EC10_{\alpha}$  (computed as  $81^{1/n_H}$ ) and  $EC50_{\alpha}$  values are listed in Table III-3.

**Table III-3. Quantitative characteristics of dose-response profiles.**

| Promoter of <i>Ste5</i> | $n_H$ | $EC90_{\alpha}/EC10_{\alpha}$ | $EC50_{\alpha}$ (ng/mL) |
|-------------------------|-------|-------------------------------|-------------------------|
| STE5                    | 0.93  | 110                           | 97                      |
| CYC                     | 1.2   | 40                            | 67                      |
| ADH                     | 1.4   | 26                            | 48                      |
| TEF                     | 1.3   | 30                            | 43                      |
| GPD                     | 1.1   | 46                            | 60                      |

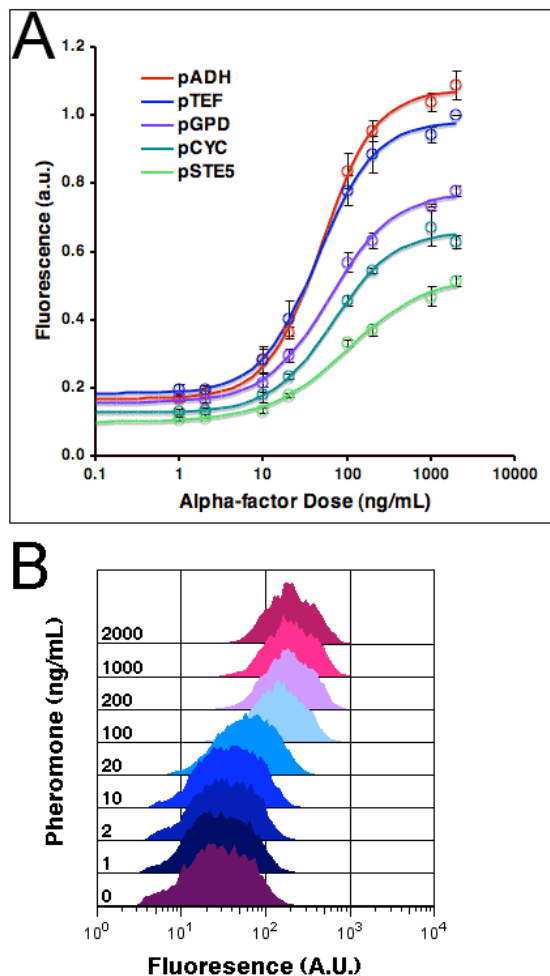


**Figure III-9. Dose-response curves of pFUS1-GFP as a function of Ste5 abundance.**

(A) Dose-response curves fit to Hill equation. Open circles are pFUS1-GFP data points and solid lines represent the fit to the Hill equation. Error bars on the data points denote standard error ( $n=3$ ). See Supplementary text for more details. (B) Yeast cells expressing Ste5 from an *ADH* promoter were induced with  $\alpha$ -factor for 2.5 h. The pFUS1-GFP reporter response was measured by flow cytometry. Histograms of GFP fluorescence are shown for various  $\alpha$ -factor doses.

### ***6.3 Signal fidelity is robust to perturbation in Ste5 expression***

Signal crosstalk between the pheromone and high-osmolarity pathways is minimized in part through the use of two distinct scaffolds (Ste5 versus Pbs2, respectively). In addition, this scaffold-mediated fidelity is reinforced by mutual inhibition of pathway output (Figure III-10) (Bardwell, 2006; Bardwell et al., 2007; Hall et al., 1996; McClean et al., 2007; O'Rourke and Herskowitz, 1998). While mutual inhibition sharpens cell commitment to the proper response in the presence of a stimulus, our results raise the possibility that the baseline activation of Fus3/Kss1 in the absence of pheromone may inappropriately hamper the responsiveness of the high-osmolarity pathway.

To determine whether the basal activities of Fus3/Kss1 impede the high-osmolarity pathway, we measured sorbitol-mediated phosphorylation of Hog1, the high-osmolarity MAP kinase, in cells expressing different levels of Ste5. Our data show that the Hog1 signaling remains robust for all expression levels of Ste5 (Figure III-10, sorbitol). Thus, basal activation of Fus3/Kss1 does not inhibit the high-osmolarity pathway. Furthermore, this data shows that elevating Ste5 expression does not deplete the cellular pool of Ste11, allowing this upstream factor to remain available for the high-osmolarity response pathway. In fact, modulating the Ste5 expression level does not induce any inappropriate crosstalk between the pheromone and high osmolarity pathway: sorbitol treatment failed to activate pFUS1-GFP reporter above baseline levels and appropriately triggered Hog1 phosphorylation (Figure III-10). Meanwhile, pheromone stimulation did not activate Hog1, but did appropriately stimulate Fus3 and Kss1

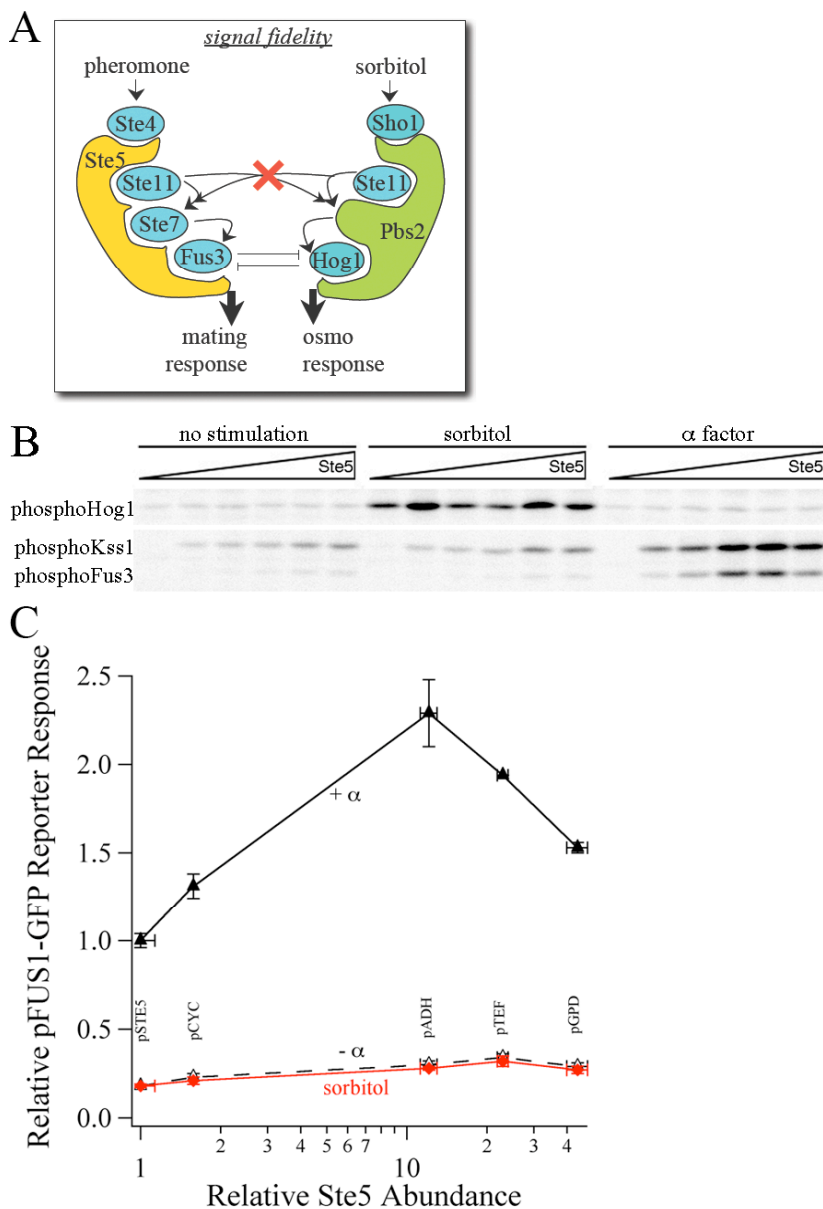
activation (Figure III-10). Thus, across nearly 50-fold change in Ste5 expression level, signal fidelity is maintained.

**Figure III-10. Signal fidelity is robust to perturbations in Ste5 abundance.**

(A) The fidelity of input-output response may be compromised by the presence of excess Ste5. Ste11 is a common component of the high-osmolarity pathway (right) and the mating pathway (left). Inappropriate exchange of Ste11 may cause high-osmolarity to trigger mating signals, or vice versa. Mutual inhibitory mechanisms between the two pathways prevent co-activation due to upstream leakiness.

(B) Baseline and induction of MAP kinase signaling. Yeast expressing varying levels of Ste5 were left unstimulated or stimulated with sorbitol or  $\alpha$ -factor for 15 minutes. The phosphorylation of Hog1, Kss1, and Fus3 were monitored by Western blot. Blots are indicative of two independent trials.

(C) Baseline and induction of the mating transcriptional reporter. Yeast expressing varying levels of Ste5 were left unstimulated (gray) or stimulated with sorbitol (black) or  $\alpha$ -factor (green) for 2.5 hours. The pFUS1-GFP reporter response was measured by flow cytometry. Error bars denote standard error (n=3).



## 7. *References*

- Bardwell, L. 2006. Mechanisms of MAPK signalling specificity. *Biochem Soc Trans.* 34:837-41.
- Bardwell, L., J.G. Cook, E.C. Chang, B.R. Cairns, and J. Thorner. 1996. Signaling in the yeast pheromone response pathway: specific and high-affinity interaction of the mitogen-activated protein (MAP) kinases Kss1 and Fus3 with the upstream MAP kinase kinase Ste7. *Mol Cell Biol.* 16:3637-50.
- Bardwell, L., X. Zou, Q. Nie, and N.L. Komarova. 2007. Mathematical models of specificity in cell signaling. *Biophys J.* 92:3425-41.
- Bashor, C.J., N.C. Helman, S. Yan, and W.A. Lim. 2008. Using engineered scaffold interactions to reshape MAP kinase pathway signaling dynamics. *Science.* 319:1539-43.
- Bhattacharyya, R.P., A. Remenyi, M.C. Good, C.J. Bashor, A.M. Falick, and W.A. Lim. 2006a. The Ste5 scaffold allosterically modulates signaling output of the yeast mating pathway. *Science.* 311:822-6.
- Bhattacharyya, R.P., A. Remenyi, B.J. Yeh, and W.A. Lim. 2006b. Domains, motifs, and scaffolds: the role of modular interactions in the evolution and wiring of cell signaling circuits. *Annu Rev Biochem.* 75:655-80.
- Ferrell, J.E., Jr. 1996. Tripping the switch fantastic: how a protein kinase cascade can convert graded inputs into switch-like outputs. *Trends Biochem Sci.* 21:460-6.
- Ferrell, J.E., Jr. 2000. What do scaffold proteins really do? *Sci STKE.* 2000:PE1.

- Choi, K.Y., B. Satterberg, D.M. Lyons, and E.A. Elion. 1994. Ste5 tethers multiple protein kinases in the MAP kinase cascade required for mating in *S. cerevisiae*. *Cell*. 78:499-512.
- Flotho, A., D.M. Simpson, M. Qi, and E.A. Elion. 2004. Localized feedback phosphorylation of Ste5p scaffold by associated MAPK cascade. *J Biol Chem*. 279:47391-401.
- Hall, J.P., V. Cherkasova, E. Elion, M.C. Gustin, and E. Winter. 1996. The osmoregulatory pathway represses mating pathway activity in *Saccharomyces cerevisiae*: isolation of a FUS3 mutant that is insensitive to the repression mechanism. *Mol Cell Biol*. 16:6715-23.
- Hao, N., S. Nayak, M. Behar, R.H. Shanks, M.J. Nagiec, B. Errede, J. Hasty, T.C. Elston, and H.G. Dohlman. 2008. Regulation of cell signaling dynamics by the protein kinase-scaffold Ste5. *Mol Cell*. 30:649-56.
- Kranz, J.E., B. Satterberg, and E.A. Elion. 1994. The MAP kinase Fus3 associates with and phosphorylates the upstream signaling component Ste5. *Genes Dev*. 8:313-27.
- Kusari, A.B., D.M. Molina, W. Sabbagh, Jr., C.S. Lau, and L. Bardwell. 2004. A conserved protein interaction network involving the yeast MAP kinases Fus3 and Kss1. *J Cell Biol*. 164:267-77.
- Levchenko, A., J. Bruck, and P.W. Sternberg. 2000. Scaffold proteins may biphasically affect the levels of mitogen-activated protein kinase signaling and reduce its threshold properties. *Proc Natl Acad Sci U S A*. 97:5818-23.
- Longtine, M.S., A. McKenzie, 3rd, D.J. Demarini, N.G. Shah, A. Wach, A. Brachat, P. Philippsen, and J.R. Pringle. 1998. Additional modules for versatile and

- economical PCR-based gene deletion and modification in *Saccharomyces cerevisiae*. *Yeast*. 14:953-61.
- McClellan, M.N., A. Mody, J.R. Broach, and S. Ramanathan. 2007. Cross-talk and decision making in MAP kinase pathways. *Nat Genet*. 39:409-14.
- Mumberg, D., R. Muller, and M. Funk. 1995. Yeast vectors for the controlled expression of heterologous proteins in different genetic backgrounds. *Gene*. 156:119-22.
- O'Rourke, S.M., and I. Herskowitz. 1998. The Hog1 MAPK prevents cross talk between the HOG and pheromone response MAPK pathways in *Saccharomyces cerevisiae*. *Genes Dev*. 12:2874-86.
- Park, S.H., A. Zarrinpar, and W.A. Lim. 2003. Rewiring MAP kinase pathways using alternative scaffold assembly mechanisms. *Science*. 299:1061-4.
- Pawson, T., and J.D. Scott. 1997. Signaling through scaffold, anchoring, and adaptor proteins. *Science*. 278:2075-80.
- Pryciak, P.M., and F.A. Huntress. 1998. Membrane recruitment of the kinase cascade scaffold protein Ste5 by the Gbetagamma complex underlies activation of the yeast pheromone response pathway. *Genes Dev*. 12:2684-97.
- Sprague, G. 1991. Assay of Yeast Mating Reaction. *Methods in Enzymology*. 194:77-93.
- van Drogen, F., V.M. Stucke, G. Jorritsma, and M. Peter. 2001. MAP kinase dynamics in response to pheromones in budding yeast. *Nat Cell Biol*. 3:1051-9.
- Yablonski, D., I. Marbach, and A. Levitzki. 1996. Dimerization of Ste5, a mitogen-activated protein kinase cascade scaffold protein, is required for signal transduction. *Proc Natl Acad Sci U S A*. 93:13864-9.

## CHAPTER IV. FUTURE WORK

In this study, we elucidated how the expression level of network constituents—kinases, phosphatases, and scaffolds—affects the quantitative performance of the MAP kinase module. In Chapter II, we presented a model that focuses on the three stages of the cascade and established a simple metric—the resistance to activation—to quantitatively gauge module performance. In Chapter III, our experimental results of the effect of scaffold abundance on the mating MAPK response revealed that many module properties quantitatively depend on scaffold abundance, including pathway ultrasensitivity, maximum signal throughput, and baseline leakage. These findings provide new quantitative insights and lay a foundation for intriguing future directions that are outlined below.

### ***1. Experimental sensitivity analysis of scaffold perturbation in the HOG pathway***

Through the systematic variation of Ste5 expression, we demonstrated that various signaling properties of the mating MAP kinase pathway, such as pathway ultrasensitivity, maximum signal throughput, and baseline leakage, all varied biphasically with respect to scaffold abundance. However, the quantitative role of Ste5 in the mating pathway may not be representative of scaffolds in general. It would be intriguing to use the experimental platform that we have developed to quantify the role of other scaffolds in signal propagation.

In yeast, scaffold-mediated MAP kinase signaling plays a critical role in both the mating and the HOG pathways (Elion, 2001; Gustin et al., 1998; Hohmann, 2002). These two pathways control very different phenotypic responses: the mating pathway induces the cell to grow chemotropically in the direction of the pheromone gradient and ultimately facilitates cell fusion, while the HOG pathway monitors and responds to pressure changes in the cell's osmolar environment. Given that these MAP kinase pathways govern such diverse responses, these pathways offer a compelling context to compare and contrast the quantitative role of scaffolds in signal propagation. Such studies would begin to address how general the quantitative relationship between scaffold abundance and MAP kinase signal response may be.

This new study centered on the osmolarity pathway would involve systematically varying the HOG scaffold, Pbs2, using the same vector-based expression system that was described in Chapter III. Wild-type yeast cells have two signaling pathways that regulate the response to high osmolarity (Hohmann, 2002). To properly study the HOG MAP kinase pathway in isolation, an *ssk2Δ ssk22Δ* strain that ablates the non-MAP kinase signaling must first be obtained (Park et al., 2003). Then, the osmolarity pathway output can be assessed by quantifying the level of phospho-Hog1 via Western blot. However, this method is time consuming and low-throughput. Therefore, as a supplement to phospho-Hog1 detection, it may be effective to use a Hog1-reporter level readout such as pSTL1-RFP (McClellan et al., 2007).

## ***2. The effect of scaffold abundance on signal dynamics in the MAP kinase mating pathway***

Scaffold abundance may not only affect steady-state throughput of signal activation, but may also be a key factor in determining its duration. Recently, Monte Carlo simulations of scaffold-based MAP kinase signaling predicted that scaffolds may influence signal dynamics by broadening the distribution of time scales for kinase activation (Locasale and Chakraborty, 2008). The model predicted that an optimal scaffold concentration would maximize signal duration.

The dependence of signal duration on scaffold abundance can be tested using our panel of yeast strains that express different levels of Ste5. The pheromone-induced response can be monitored by Western blot of the phospho-MAPKs. Once the most appropriate time points have been selected, the duration of the MAP kinase signal as a function of Ste5 abundance can be quantified. The physiological time scale for mating is approximately four hours and is consistent with the duration in phospho-MAPK signals that has been reported (Sabbagh et al., 2001). In our yeast strains that express Ste5 at wild-type levels, preliminary results indicate that the activation of the mating MAPKs, Fus3 and Kss1, persists for two hours with peak activation at 15 minutes (data not shown).

Recently, an experimental protocol was reported that uses the pFUS1-GFP transcriptional response to measure the signaling dynamics of the mating pathway (Bashor et al., 2008). While Western blot detection of phospho-MAP kinase signals is

straightforward, monitoring pathway output by FACS analysis of the pFUS1-GFP transcriptional response would permit more rapid, higher throughput quantitation of the MAP kinase pathway. Ultimately, this procedure would provide the easiest platform by which to generate high resolution time-course data of MAP kinase signal activation.

### ***3. Extension of resistance metric to a scaffold-based MAP kinase cascade***

The MAP kinase model presented in Chapter II defines a metric, the resistance to activation, which predicts salient features of module performance. The resistance captures the opposing contributions of pathway activators (kinases) and deactivators (phosphatases) that represent the players in this network. A meaningful extension of this model would be to incorporate the effect of scaffolding and to develop a new resistance metric that can predict module performance in the context of a scaffold.

To construct the model, we would generate a system of ODE's similar to our previous model. Restriction of the new model to 2-stages would reduce the number of additional scaffold species; a 2-stage cascade would introduce 9 new molecular species, while a 3-stage cascade would introduce 27. By non-dimensionalization of model variables, groups containing the total expression of the kinases, phosphatases, and scaffold can be scrutinized.

#### ***4. Investigation of MAP kinase design properties that result from scaffold dimerization***

A prominent feature of scaffolds is its ability to bind concomitantly to multiple components of a signaling pathway, localizing them onto a single molecular backbone. The close proximity of scaffold-bound kinases facilitates signal transfer, although the precise mechanism of signal propagation is not well understood. Most representations of scaffolds tacitly assume a monomeric, *cis*-phosphorylation mechanism, whereby the signaling kinases bound to the same scaffold activate one another (Figure IV-1). However, an often-overlooked alternative mechanism involves dimerization. Scaffold dimerization has been demonstrated by ample experimental evidence for Ste5 and JIP (Inouye et al., 1997; Yablonski et al., 1996; Yasuda et al., 1999). In a genetics study, two mutants alleles of Ste5, one unable to bind Ste11 and the other unable to bind Ste7, display interallelic complementation (Inouye et al., 1997). While each mutant Ste5 allele alone was unable to promote mating, when co-expressed the mating phenotype was restored. Furthermore, in a pull-down assay of co-expressed myc-tagged Ste5 and GST-tagged Ste5, detection of GST-tagged Ste5 was possible after immunoprecipitation of the myc-tagged Ste5 (Yablonski et al., 1996). Thus, the differentially tagged versions of Ste5 can dimerize *in vivo*.

Dimerization may challenge basic assumptions about how scaffolds influence the quantitative properties of MAP kinase signaling networks. For example, scaffolds are thought to attenuate the ultrasensitivity of the MAP kinase response by promoting a processive rather than distributive mode of kinase activation (Levchenko et al., 2000).

However, our experimental evidence presented in Chapter III shows that shifting Ste5 to its optimal scaffold abundance *increases* the ultrasensitivity of the MAP kinase response. Interestingly, if signal activation were to require the dimerization of assembled scaffolds, then scaffolding would *generate* an ultrasensitive response (Ferrell, 2000).

An investigation of scaffold dimerization would provide an extension of the mechanistic insights that scaffolds confer to the quantitative performance of the MAP kinase cascade. To our knowledge, no scaffold model to date has reported on the effect of dimerization on pathway performance.

#### ***4.1 Robustness to perturbation in scaffold abundance***

In Chapter III, we demonstrated that MAP kinase signal propagation depends biphasically on scaffold abundance. Though perturbation of scaffold abundance quantitatively altered MAP kinase signaling properties and phenotypic response, changes in signal throughput were surprisingly robust. Across a 50-fold change in Ste5 expression level the MAP kinase response varied by a maximum of 2.5-fold. This result was unexpected given that most models predict signal output to be “brittle” with respect to scaffold concentration (Burack and Shaw, 2000; Ferrell, 2000; Levchenko et al., 2000).

Scaffold models that assume a *cis*-phosphorylation mechanism do not intuitively predict robustness to variation in scaffold abundance (Burack and Shaw, 2000). Combinatorial inhibition dictates that as scaffold abundance increases, incomplete scaffold complexes will compete with one another for binding partners and inhibit

signaling. Scaffold dimerization raises the possibility that signal propagation may occur via *trans*-phosphorylation events between the kinases of two distinct scaffolds (Dard and Peter, 2006). Interestingly, a *trans*-phosphorylation scaffold model allows a mechanism by which incomplete scaffold-complexes can dimerize and permit signal propagation (Figure IV-1). A new modeling study directed at exploring the role of *trans*-phosphorylation in scaffold-mediated networks might address the discrepancy in our understanding of scaffolds.

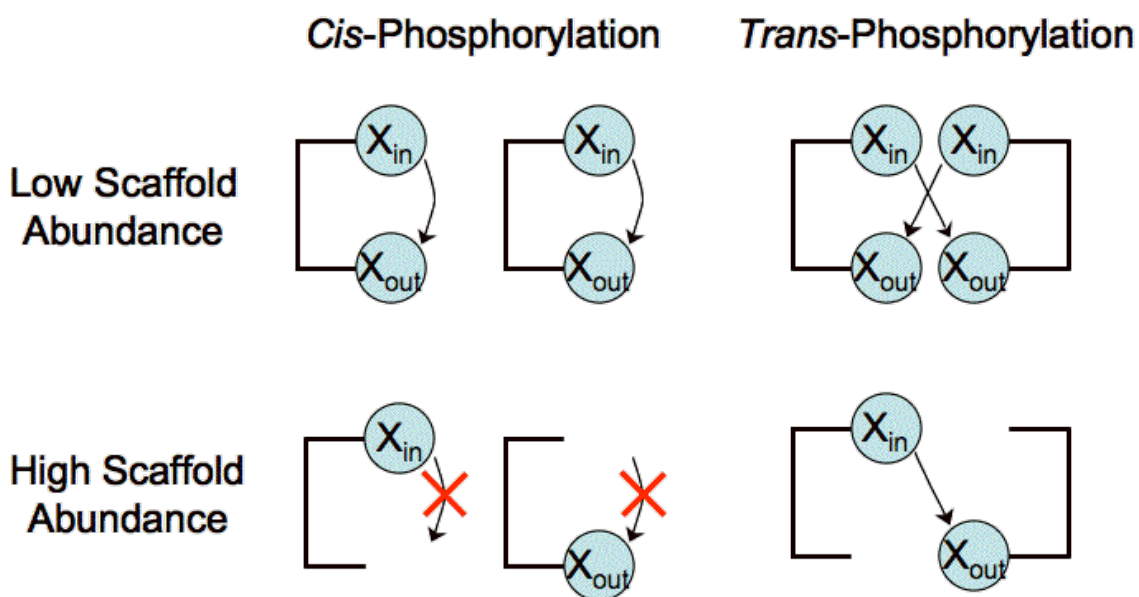


**Figure IV-1. Scaffold dimerization permits signal activation for incompletely bound complexes via *trans*-phosphorylation.**

When in low abundance relative to their binding partners, scaffolds are fully assembled. Signal activation can proceed for both the case of *cis*-acting monomer and *trans*-acting dimer complexes. However, when in high abundance relative to their binding partners, scaffolds are only partially assembled. While signal activation is inhibited via the *cis*-phosphorylation mechanism, the *trans*-phosphorylation mechanism provides a route for partially-assembled complexes to transmit signal.

The new model can use the framework of the Levchenko-Sternberg model, and simply add the trans-phosphorylation mechanism (Levchenko et al., 2000). Dimerization of a two-membered scaffold would introduce 27 dimeric scaffold species in addition to the nine monomeric scaffold species. The omission of off-scaffold mechanisms of signal activation would simplify model construction and analysis. To parse the effect of the *trans*-phosphorylation mechanism on the sensitivity to scaffold abundance, a reference model of *cis*-acting scaffolds (that can also dimerize) would be used for comparison.

#### ***4.2 Dimerization may augment the scaffold's contribution to signal fidelity***

As discussed previously, scaffolds play an important role in signal specificity (see Chapter I-5). However, an overabundance of scaffold may compromise its ability to maintain signal fidelity. Using the yeast mating pathway as an example (Figure IV-2), an overabundance of Ste5 may promote leakage of the mating signal into the adjacent HOG pathway by activating too large a pool of Ste11, a signaling kinase shared by both pathways. Active and unbound Ste11 could then associate with Pbs2 and elicit a HOG response. Conversely, overabundant Ste5 may increase the sensitivity of the mating pathway to activation by leaky signals (Flatauer et al., 2005). Activation of the HOG pathway will lead to Ste11 activation, but an overabundant Ste5 may “soak up” any active and unbound Ste11, thereby activating the mating response.

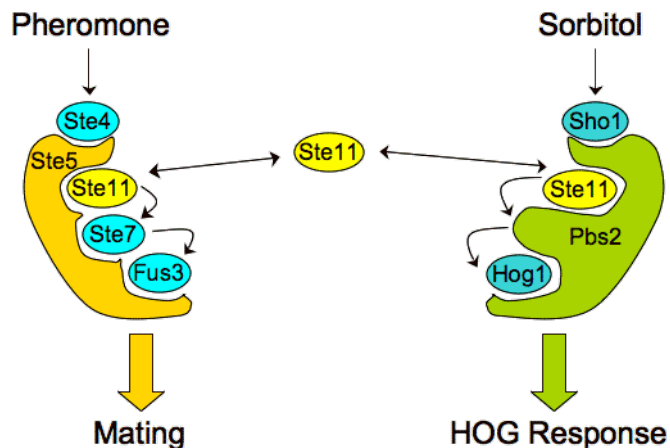


**Figure IV-2. A shared signaling intermediate can facilitate signal leakage.**

The mating and the HOG MAP kinase pathways in yeast have distinct inputs (pheromone and sorbitol, respectively) and distinct outputs (Fus3 and Hog1, respectively). However, they share a common signaling intermediate, Ste11. In each pathway, scaffolding helps maintain signal fidelity.

However, our experimental results show that neither of these scenarios is entirely accurate. In our sensitivity analysis of MAP kinase response to perturbation in Ste5 abundance, pheromone stimulation activated only the mating MAP kinases and did not stimulate phosphorylation of Hog1. Meanwhile, stimulation with sorbitol appropriately activated Hog1 with no cross-activation into the pheromone pathway. Thus, across nearly 50-fold change in Ste5 expression level, signal fidelity is maintained (See Chapter III.6.3).

Previous models have assumed that scaffolds may insulate kinases from deactivation by sterically hindering the access of phosphatases (Levchenko, 2000). In a similar fashion, if dissociation from the dimer-complex is precluded, dimerization may effectively sequester a shared signaling intermediate, thereby preventing leakage (Figure

IV-3). Thus, in addition to binding multiple signaling components, dimerization may be another mechanism by which scaffolds promote signal fidelity.

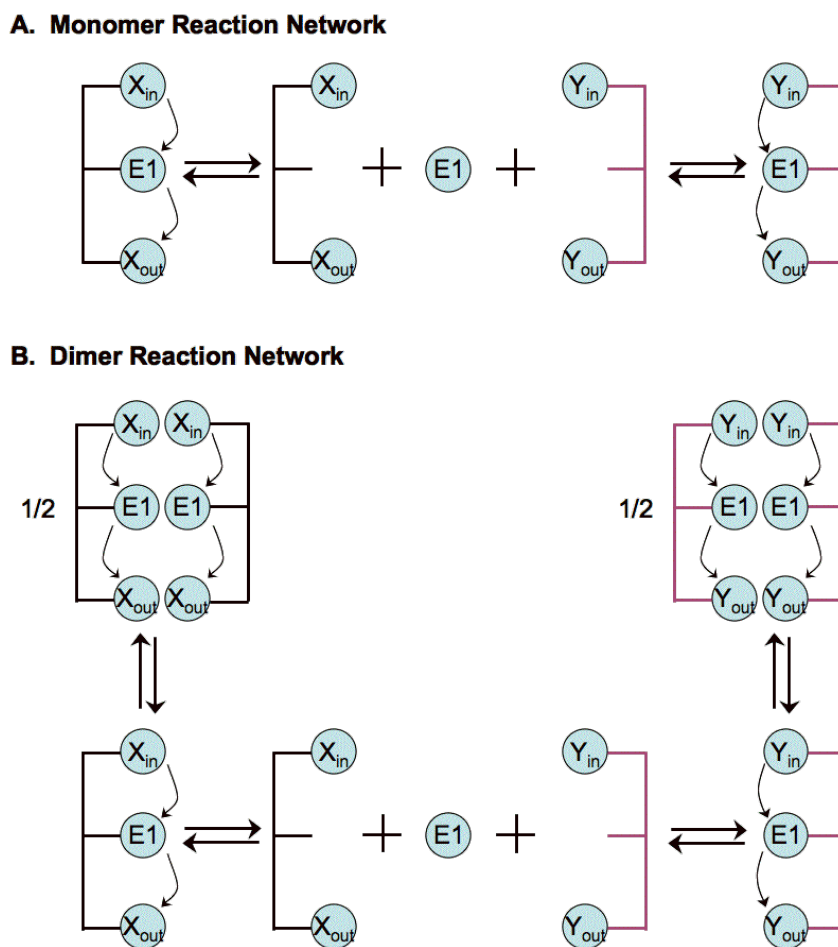


**Figure IV-3. Model schematic of scaffold dimerization with signal crosstalk.**

The mating and the HOG MAP kinase pathways in yeast have distinct inputs (pheromone and sorbitol, respectively) and distinct outputs (Fus3 and Hog1, respectively). However, they share a common signaling intermediate, Ste11. In each pathway, scaffolding helps maintain signal fidelity. **(A)** No Scaffold Dimerization. The E1 kinase can bind to either scaffold. When active E1 dissociates from one scaffold, it can re-associate with another, possibly of an adjacent signaling pathway, thereby facilitating signal leakage. **(B)** Scaffold Dimerization Protects E1 from Dissociation. When scaffolds dimerize, they form a complex that remains signaling competent. However, when dimerized, scaffold-bound components, including E1, cannot dissociate. Thus, scaffold dimerization may serve as a mechanism to sequester a common signaling intermediate and prevent undesirable signal crosstalk.

The effect of dimerization on signal fidelity can be investigated with an ODE model that represents the mass action kinetics of two scaffolds that homodimerize. To distinguish pathway inputs and outputs while permitting a shared signaling intermediate, a three-membered scaffold will be required. In order to monitor the effect of dimerization, a metric to assess the signal fidelity of the two distinct pathways will be required. The following definitions for signal fidelity may suffice (Komarova et al., 2005):

$$S_x = \frac{X_{out}/X_{in}}{Y_{out}/Y_{in}} \text{ and } S_y = \frac{Y_{out}/Y_{in}}{X_{out}/X_{in}}$$

The variables  $X_{in}$  and  $Y_{in}$  represent pre-assigned inputs, while  $X_{out}$  and  $Y_{out}$  represent the terminal outputs for the two pathways. Note that X and Y are versatile representations of the signals, and can manifest as steady-state values or time-integral values of the signals (for dynamic responses).

## 5. References

- Bashor, C.J., N.C. Helman, S. Yan, and W.A. Lim. 2008. Using engineered scaffold interactions to reshape MAP kinase pathway signaling dynamics. *Science*. 319:1539-43.
- Burack, W.R., and A.S. Shaw. 2000. Signal transduction: hanging on a scaffold. *Curr Opin Cell Biol*. 12:211-6.
- Dard, N., and M. Peter. 2006. Scaffold proteins in MAP kinase signaling: more than simple passive activating platforms. *Bioessays*. 28:146-56.
- Elion, E.A. 2001. The Ste5p scaffold. *J Cell Sci*. 114:3967-78.
- Ferrell, J.E., Jr. 2000. What do scaffold proteins really do? *Sci STKE*. 2000:PE1.
- Flatauer, L.J., S.F. Zadeh, and L. Bardwell. 2005. Mitogen-activated protein kinases with distinct requirements for Ste5 scaffolding influence signaling specificity in *Saccharomyces cerevisiae*. *Mol Cell Biol*. 25:1793-803.
- Gustin, M.C., J. Albertyn, M. Alexander, and K. Davenport. 1998. MAP kinase pathways in the yeast *Saccharomyces cerevisiae*. *Microbiol Mol Biol Rev*. 62:1264-300.
- Hohmann, S. 2002. Osmotic stress signaling and osmoadaptation in yeasts. *Microbiol Mol Biol Rev*. 66:300-72.
- Inouye, C., N. Dhillon, and J. Thorner. 1997. Ste5 RING-H2 domain: role in Ste4-promoted oligomerization for yeast pheromone signaling. *Science*. 278:103-6.
- Komarova, N.L., X. Zou, Q. Nie, and L. Bardwell. 2005. A theoretical framework for specificity in cell signaling. *Mol Syst Biol*. 1:2005 0023.

- Levchenko, A., J. Bruck, and P.W. Sternberg. 2000. Scaffold proteins may biphasically affect the levels of mitogen-activated protein kinase signaling and reduce its threshold properties. *Proc Natl Acad Sci U S A.* 97:5818-23.
- Locasale, J.W., and A.K. Chakraborty. 2008. Regulation of signal duration and the statistical dynamics of kinase activation by scaffold proteins. *PLoS Comput Biol.* 4:e1000099.
- McClellan, M.N., A. Mody, J.R. Broach, and S. Ramanathan. 2007. Cross-talk and decision making in MAP kinase pathways. *Nat Genet.* 39:409-14.
- Park, S.H., A. Zarrinpar, and W.A. Lim. 2003. Rewiring MAP kinase pathways using alternative scaffold assembly mechanisms. *Science.* 299:1061-4.
- Sabbagh, W., Jr., L.J. Flatauer, A.J. Bardwell, and L. Bardwell. 2001. Specificity of MAP kinase signaling in yeast differentiation involves transient versus sustained MAPK activation. *Mol Cell.* 8:683-91.
- Yablonski, D., I. Marbach, and A. Levitzki. 1996. Dimerization of Ste5, a mitogen-activated protein kinase cascade scaffold protein, is required for signal transduction. *Proc Natl Acad Sci U S A.* 93:13864-9.
- Yasuda, J., A.J. Whitmarsh, J. Cavanagh, M. Sharma, and R.J. Davis. 1999. The JIP group of mitogen-activated protein kinase scaffold proteins. *Mol Cell Biol.* 19:7245-54.